Novel Delivery and Sample Mixing for Synchrotron Diffraction Experiments using Acoustic Levitation with Multi-Transducer Arrays

Elizabeth R. Dye

A thesis submitted in partial fulfillment of the requirements of Nottingham Trent University for the degree of Doctor of Philosophy

This research programme was carried out in collaboration with Diamond Light Source

24th June 2022

Acknowledgments

"Luck is what happens when preparation meets opportunity" - Seneca

For many years I believed I was incredibly lucky to get to where I am today, and to all those who have walked this journey with me and offered me a helping hand, to you all I am grateful. My journey began as an undergraduate when I received an opportunity to perform research outside of my studies and continued to now as I receive support completing my thesis.

Firstly, I would like to thank Nottingham Trent University (NTU) and Diamond Light Source (DLS) for jointly funding this work. And I would like to express my gratitude towards my supervisory team, composed of Rob Morris (NTU), Pete Docker (DLS) and Mike Newton (NTU). They have all been incredibly supportive throughout my PhD and provided me with very appreciated advice and encouragement. I would also like to thank Pete for initially conceptualising the project, and for proposing it to DLS and NTU to be funded.

There have been a number of people who have helped with the experiments which I performed at Diamond Light Source. A huge thank you to Danny Axford for allowing the experiments to be performed at I24, and for helping me with the modelling of the crystal structures from the diffraction data we acquired. And thank you to John Beale and Agata Butryn for helping me with the preparation of the samples used at Diamond Light Source.

Nottingham Trent has been a wonderful university, in which I have spent just under a third of my life studying and researching. I am privileged to say that I have made countless friends from my time here, both staff and fellow students. This fortune means that I am be unable to name every person who has encouraged me and provided me with support and advice throughout the years, but I would like to mention a few. To Nicasio Geraldi I would like to say a huge thank you for the advice you offered through the development of the SLIPS surfaces. My thanks to Kieran Hall for taking the time to read my work and helping me to describe a cake rather than just listing off the recipe. And finally to Jacob Spear my eternal thanks for listening to my complaints and keeping me the positive and enthusiastic person I have always strived to be.

I would like to close my acknowledgements by thanking my wonderful family, all of them. Thank you for listening to me, supporting me, and for the pride you have shown to me throughout the highs and lows of my life. Your encouragement and empathy knows no limits, it has been this boundless energy that has kept me going throughout the pandemic and the writing of my thesis. Thank you for your passionate belief in me. Thank you for teaching me that "I am a Dye, I am a force of nature and I cannot and will not be stopped". I will take this with me always.

Abstract

Acoustic levitation may utilise standing waves at ultrasonic frequencies to manipulate suspended substances and small objects in a contactless manner. These materials may be levitated in the positions in which the nodes are located, corresponding to positions of low acoustic pressure. In recent years, off the shelf transducer based acoustic levitators have been used for contactless manipulation of liquids. These systems benefit from requiring low power and low-cost components making acoustic levitation more accessible to the masses. Such a system was investigated in this work for presenting protein crystals, within their mother liquor, to the I24 beamline at Diamond light Source for x-ray diffraction experiments. It was found that the crystals tended to sediment toward the bottom of the droplets, which were oblate in shape. The droplets which were levitated often became unstable and fell from their suspended position, or they would not detach from the pipette tip when they were being injected. To rectify this, a coating of silicone oil was added allowing the droplets to remain stable as well as limit the evaporation of the droplet whilst it was manually inserted and the area cleared of personnel before the x-ray beam was engaged. This silicone oil coating is non-crystalline and thus did not invalidate the results collected which showed the lysozyme crystal structure with a resolution of 1.69Å, confirming acoustic levitation as a good sample presentation method for these types of experiments. To remove the requirement for the silicone oil, a bespoke system was created named the DLS-Lev that allowed top-loading of the sample. The droplets of mother liquor which contained protein crystals were easily detached from the pipette tip into the traps within the DLS-Lev system owing to the increased strength of the traps in the modified design. This system, paired with an automated pipette, facilitated sample mixing experiments whilst the x-ray beam was engaged. The further development of the pipetting system was halted due to the COVID-19 pandemic. However, future work should see the permanent installation of these systems at the I24 beamline at Diamond Light Source, as well as additional bespoke acoustic levitators designed for the other beamlines specialising in the research of protein structure via x-ray scattering techniques.

Contents

List of Figures

Chapter 1

Introduction

Proteins are often described as the building blocks of life. They are large molecules which are present within living organisms for the generation of new cells, tissue repair and many other functions. Protein crystallisation is the process which many individual proteins are stacked into a regular repeating structure. Proteins in their crystal state may be investigated through x-ray diffraction experiments to determine their atomic composition and structure.

X-ray diffraction experiments have been performed at synchrotron facilities and synchrotron light sources for many years. However, these experiments are performed on protein crystals which have been removed from the fluid in which they are formed, mounted upon small nylon loops and are often dehydrated or cryogenically frozen before experiments take place. These are not representative of the state that the proteins exist within nature whilst they are performing work within an organism.

Levitation systems may be used to suspend liquid droplets containing the protein crystal and the solution in which they are grown in, the so called mother liquor. There are many different types of levitation techniques including magnetic, electrostatic and optical levitation, however these present with various limitations [14; 15]. Optical levitation requires the sample to be incredibly lightweight and at micrometre length scales, it uses high intensity laser light to achieve levitation and has been used to manipulate protein crystals up to 30μm previously, but prolonged exposure would cause damage to the structure of the protein [16]. Magnetic and electrostatic levitation require the sample to be magnetic or charged respectively which is not ideal as these states are also not representative of how the proteins exist within nature [14].

Acoustic levitation is an ideal suspension system to present the protein crystal to the x-ray beam for experiments. It allows for the levitation of neutral samples and allows for presentation of the crystals suspended within a droplet, bringing the sample as close to its natural states as can be currently achieved. Acoustic levitation in layman's terms is floating a substance using sound, typically this sound is beyond the range of human hearing.

The containerless nature of this sample presentation method allows for additional experiment opportunities which are not available through traditional methods. Specifically, by presenting

protein crystal samples within a solution, additional substances may be added during the experiment to observe mixing and depending on the substance added the x-ray diffraction results could show the interaction of a compound with a protein or structural changes within the protein related to its function.

This work explores the use of acoustic levitation systems to present protein crystals within their mother liquor to the x-ray beam at Diamond Light Source for x-ray diffraction experiments. The literature review provides the knowledge and background to this thesis. The fundamental principles of acoustic levitation is covered as well as the different bespoke acoustic levitation devices that have been published and the behaviour of droplets whilst they are being suspended with sound. A brief overview of the formation of protein crystals is presented and the x-ray diffraction techniques used to identify their structure are described. And finally, the facilities in which a compatible bespoke acoustic levitation would be used are described and presented, including the Diamond Light Source synchrotron and its current sample presentation methods.

This work begins with the construction, verification and use of an existing acoustic levitation device for proof of concept experiments at Diamond Light Source. It investigates the stability of droplets suspended in this system as well as the volumes of droplet which may be levitated at varying operating voltages of the device. Silicone oil encapsulation is used to improve the droplet stability of liquids with surface tension which is too high or too low and allows them to be suspended. A silicone oil encapsulated droplet containing mother liquor and a lysozyme protein crystal was levitated at the I24 beamline at Diamond Light Source. X-ray diffraction experiments were used to determine the suitability of acoustic levitation as a sample presentation method.

Following this, a bespoke acoustic levitator is simulated and constructed, this system was specifically designed to allow for a droplet to be suspended at the I24 beamline without the need for silicone oil encapsulation in order to levitate the mother liquor. Similarly to the previous acoustic levitation device, volume and stability of the suspended droplets at varying operating voltages is investigated to find the devices suitability for experimentation at Diamond Light Source.

In order to fully utilise the designed levitation device, a compatible sample delivery system must be developed. Firstly, SLIPS surfaces were investigated to allow for the encapsulation of the sample with silicone oil. Following this, an automated pipetting system was designed in order to allow for direct deposition into the levitation device to facilitate sample mixing when installed on the I24 beamline. The samples mixed in beam are lysozyme and a ligand that would

be hydrolysed by the enzyme. These experiments and results then informed the design of a subsequent prototype sample delivery system.

This work aims to realise acoustic levitation as a sample presentation method for x-ray diffraction experiments, and allow for sample delivery and mixing utilising a protein sample which is more representative of the crystal's natural environment rather than the frozen or dehydrated crystals which are presented to the beamline currently.

Chapter 2

Literature Review

2.1 Acoustic Levitation

The manipulation of materials has been performed for many years within air and liquid environments via levitation, this creates a simulated micro gravity environment without a container surrounding the substance. There are many forms of levitation including acoustic, magnetic, electrostatic, optical and aerodynamic which use different methods in order to suspend their sample. To suspend a substance against gravity within a magnetic levitator, the sample must be ferromagnetic [17] or, in order to levitate diamagnetic materials, a large magnetic gradient is required, like that which was used to suspend a living frog [18]. Electrostatic levitation utilises an electric field to levitate a sample which is charged in order to suspend samples against gravity [19]. Suspension through optical levitation has only been achieved for very small and lightweight particles by directing a focused laser beam or multiple beams at the sample and relying on the photons transferring momentum to the sample surface. This method is only effective at levitating particles with a higher refractive index than the surrounding medium, limiting the number of effective cases with this technique [20]. Proteins have been optically levitated previously, however this was performed within a liquid environment and were limited to 30 μm diameter samples. Also, prolonged exposure would cause the sample to denature [16]. Finally, high-pressure gas jets are used to suspend the material under investigation in aerodynamic levitation, however this system causes significant agitation to the sample and may cause physical changes to the substance [21].

In contrast, acoustic levitation is effective on a variety of different sample types as there is no requirement for the sample to be ferrous, charged or have a particular refractive index in order to be levitated. These systems use at least one emitter that produce longitudinal waves with frequencies typically above the hearing range of a person. By using reflective surfaces, or by using multiple ultrasound emitters, it is possible to create a position or series of positions in which particles or droplets may be trapped [22].

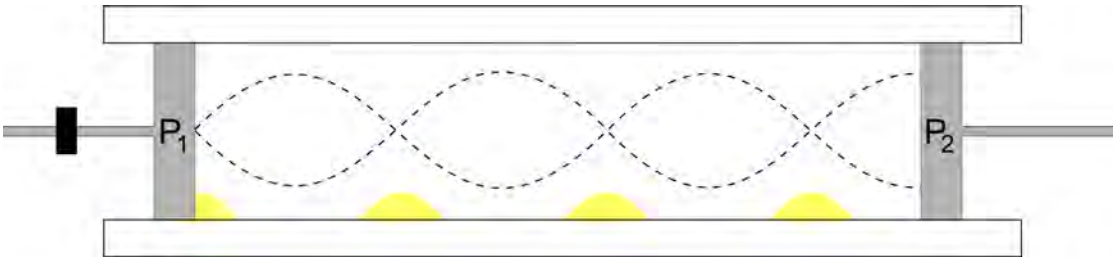

Figure 2.1: *A diagram demonstrating the collection of powder piles within a Kundt's tube. It features a glass tube with two pistons on either end, the piston labelled P_1 is clamped in the middle and driven using a single frequency of sound and the piston labelled P_2 is moveable in order to change the length of the chamber. Air or any desired gas is held between the two pistons and a small amount of lycopodium powder (shown in yellow) is put into the enclosed space. When a standing wave is formed between the pistons from the reflection of the emitted sound wave, the light weight lycopodium powder collects at the node positions of this standing wave. A change in frequency would increase or decrease the number of nodes within the chamber and therefore allow for contactless manipulation of the powder inside.*

This section discusses the physics, hardware and different applications for which this technique has been used.

2.1.1 Kundt's Discovery

In 1866, acoustic levitation was first conceived by Kundt through his development of the Kundt's tube, which was designed to observe the speed of sound through different gases [23]. This tube was transparent and contained a fine powder within it. At one end of the tube, a sound emitter which produced a single frequency was positioned. At the other end of the tube, a moveable piston was used to seal the tube and was moved in order to adjust its length. When the sound emitter was turned on, the piston could be moved until the tube was at resonance, indicated by an increase in sound intensity, the sound waves have formed standing waves in such a case. At the node positions, the air is stationary and the fine powder within the tube collects, there is a distance of $\lambda/2$ (where λ is the wavelength of the emitted sound) between each collected pile of fine powder. This distance and the frequency (f) of the sound can be used to determine the speed of sound (c_s) within the gas in the Kundt's tube as shown in equation 2.1.

$$c_s = \lambda f \tag{2.1}$$

An observation of the Kundt's tube was that particles could be manipulated and moved without the need to introduce additional material into the system. A diagram demonstrating this is shown in figure 2.1. The fine powder used in this experiment is lycopodium and is shown to collect at the node positions of the standing wave.

2.1.2 Fundamental Physics of Acoustic Levitation

Force being exerted due to sound is a phenomenon which everybody is familiar with, but the term for it is the acoustic radiation force. When this force acts on an object, the object is pushed in the direction that the sound was travelling. Acoustic levitation occurs when two opposing radiation forces act upon an object, balancing the forces. This typically occurs when there are two sources of sound or when one source of sound is reflected back, in both cases causing a standing wave. The position in which the object would be stationary due to a balance of forces is the node position within the standing wave. In a system in which gravity is acting down on the object and where the sources of sound for the acoustic levitator are located above and beneath the object, the object will settle just beneath the standing wave node, and therefore the acoustic radiation force acting in an upward direction will counteract the downward pulling force of gravity.

There are relatively few parameters needed to describe the acoustic radiation force. Gor'kov's expression [24] is most commonly used for the evaluation of the levitation of small samples within focal point systems, where the force is estimated upon a spherical particle in an acoustic field which is propagated through an ideal fluid. Gor'kov considers the compressibility of the particle and that it may be set into motion due to the wave incident on its surface. In order to apply the expression, the radius of the spherical particle is assumed to be much smaller than the wavelength of the incident longitudinal wave λ, in which many systems have a wavelength on the order of 1 - 10 mm.

In order to determine the acoustic radiation force of a system, the time-averaged potential U must first be calculated by the use of equation 2.2. In this equation R describes the radius of the spherical particle, $\overline{p_{in}^2}$ and $\overline{v_{in}^2}$ are the mean-square fluctuations of the pressure and the velocity respectively, at the point in which the emitted wave interacts with the particle.

$$U = 2\pi R^3[(\overline{p_{in}^2}/3\rho c^2)f_1 - (\rho\overline{v_{in}^2}/2)f_2], \tag{2.2}$$

f_1 and f_2 are factors which are described by equations 2.3:

$$f_1 = 1 - \rho c^2/\rho_s c_s^2, \qquad f_2 = 2(\rho_s - \rho)/(2\rho_s + \rho), \tag{2.3}$$

in which ρ is the density of the fluid, in most cases ambient air, ρ_s is the density of the particle being levitated, whilst c and c_s are the speeds of sound within the fluid and particle respectively.

The gradient of the potential can be used to then obtain the acoustic radiation force acting upon the particle [24].

However, this approach is not applicable to the levitation of large samples and so an alternative approach is needed to evaluate large arrays. In order to determine the acoustic radiation pressure P *[Pa]* in such cases, equation 2.4 can be used alongside the assumption that the wave is planar. In this equation the ultrasound energy density is represented by E *[Jm^{-3}]*, I *[Wm^{-2}]* is the intensity of sound, v *[ms^{-1}]* is the speed of sound through air, the root-mean-square pressure of the ultrasound is represented by p *[Pa]* and ρ *[kgm^{-3}]* is the density of air. Finally, α is a dimensionless constant within this equation which is a value between 1 and 2 which scales the resultant radiation pressure to account for the reflectivity of the levitated object, a value of 1 represents the complete absorption of the incident sound and a value of 2 represents the complete reflection of sound.

$$P = \alpha E = \alpha \frac{I}{v} = \alpha \frac{p^2}{\rho v^2}, \tag{2.4}$$

This relationship shows that the manipulation of the spatial distribution of ultrasound pressure can cause the control of the acoustic radiation pressure for a provided sample [25].

2.1.3 Ultrasonic Horns

Traditional acoustic levitation systems are typically built around a so called langevin horn, a large single vibrating transducer, and a reflector in order to generate a standing wave capable of levitating materials or droplets. The langevin horn was named after its inventor P. Langevin who was a french physicist best known for conceptualising the Langevin equations [26]. The horn consists of a piezoelectric transducer sandwiched within a metal transmitter, machined into a specific shape leading to a radiating plate. The metal transmitter is specifically machined for the particular transducer and operating frequency, and may be made of various materials such as aluminium [27; 28], stainless steel [28] and lead zirconate titanate (PZT) [29; 28]. The system output power is typically on the order of 100W, but successful acoustic levitation has been achieved with powers as low as 2W [29]. There are four main configurations which are able to achieve levitation using langevin horns: it can be a langevin horn and reflector both with flat faces, a langevin horn and reflector with curved faces or a pair of opposing langevin horns with flat or curved faces.

Langevin horn systems have been shown to be able to levitate liquid droplets in many works [30]. However, the systems themselves are very costly and labour intensive to build and set up, it requires machining the metal transmitters and then measuring the resultant frequency emitted.

If the system features two langevin horns directed to each other, the horns must be frequency matched, this is not easily achieved so many horns must be machined in order to find a pair which matches best. Work completed by Weber [27] saw the production of 10 different horns tested, and a pair of horns selected which were measured to have a 10Hz frequency difference. However, this work also described the need to allow the langevin horns to warm up before operation, because as they heat up the frequency was shown to drift by 4Hz per degree.

Acoustic levitation of samples for presentation to synchrotron diffraction systems has been previously demonstrated using a langevin horn system utilising a ultrasound oscillator with a 38kHz approximate resonant frequency and a concave reflector in order to levitate protein crystals for x-ray diffraction experiments at Swiss Light Source [29]. In this work the langevin horn is approximately 27mm from the reflector and levitated 4 μL of buffer solution and a single protein crystal. However, in order to stably levitate this droplet, the system must be enclosed in a box, with kapton film windows which allowed for the transmission of x-rays.

Since langevin acoustic levitation systems have already been installed on a synchrotron light source, though they needed to be enclosed in order to provide a stable levitated droplet, they are not explored in this work. There are existing alternative acoustic levitation devices which do not require the transducers to be specifically machined and their frequency does not fluctuate with temperature as the sound does not transmit through large blocks of metal. In addition, as the langevin systems require time to warm up, they would have to be installed on the beamline for extended periods of time, which makes them unsuitable for use in modular beamlines with rapid turnaround times between different experiments.

2.1.4 Levitating Polystyrene Spheres using Transducer Array Systems

Acoustic levitation through the use of arrays of transducers either simultaneously or individually controlled is a relatively new development in the field of acoustic levitation, with the technology only beginning to being explored within the past 15 years. A transducer array differs to an ultrasonic horn system, as the piezoelectric element or disk is not mounted onto a large metal transmitter but instead encased and behaves as its own emitter. In order to achieve comparable acoustic radiation forces, arrays of these transducers are required.

The levitation of liquid droplets is challenging owing to droplets being able to easily break apart in poorly set up systems. Due to this, novel techniques are first demonstrated using expanded polystyrene particles and later refined to accommodate droplets.

Development of multi-transducer systems has been traditionally driven not by the desire to levitate samples as in this work but to produce holographic display technologies. An array of ultrasonic transducers that provided tactile feedback without any mechanical contact was developed, allowing for a user to feel virtual objects in air. This prototype consisted an array of 324 ultrasonic transducers operating at 40kHz of which the intensity and phase of each transducer was individually controlled to generate an acoustic force of 16 mN over 20 mm [25]. This system was further developed to design airborne ultrasound focusing devices (AUFD) [31] to use two of these arrays opposing each other to generate a localised standing wave at arbitrary positions utilising the phased-array focusing technique. This generates a focal point at specific positions by calculating the path difference, d_n, between the 0^{th} and n^{th} transducer and using the speed of sound within air, c, to find an appropriate time delay as shown in equation 2.5. By delaying the emission of the square wave signal at the n^{th} transducer by this time delay, the focal point is generated at the specified position.

$$T_n = \frac{d_n}{c}, \tag{2.5}$$

Some advantages have been identified for the airborne ultrasound focusing devices (AUFD):

- The levitated particles may be manipulated in all directions according to the movement of the standing wave controlled by the phase delay of the system.
- This work space is much larger than those in previous studies as the incident ultrasonic wave is focused and therefore can be delivered further.
- The particles are trapped regardless of the axis of the acoustic wave as the system provided a sufficient amplitude of ultrasound.

This work was further expanded upon to allow for the manipulation of expanded polystyrene particles in three dimensions by the use of four arrays facing a centre point as shown in figure 2.2 and operated at 40kHz or 25kHz. The stability of the particle manipulation was quantified by iterating the phase of the transducers in $1/16^{th}$ wavelength steps, causing the particle to accelerate until it was ejected from this levitation system. This experiment was repeated for varying sizes of polystyrene particles and it was found that the smaller 0.6mm particles were confined for accelerations of up to $60ms^{-2}$ corresponding to approximately 500μN of force, whereas the 2mm polystyrene particles maintained entrapment up to $30ms^{-2}$ corresponding to approximately 27mN (both calculated based on Force = mass x acceleration) [1].

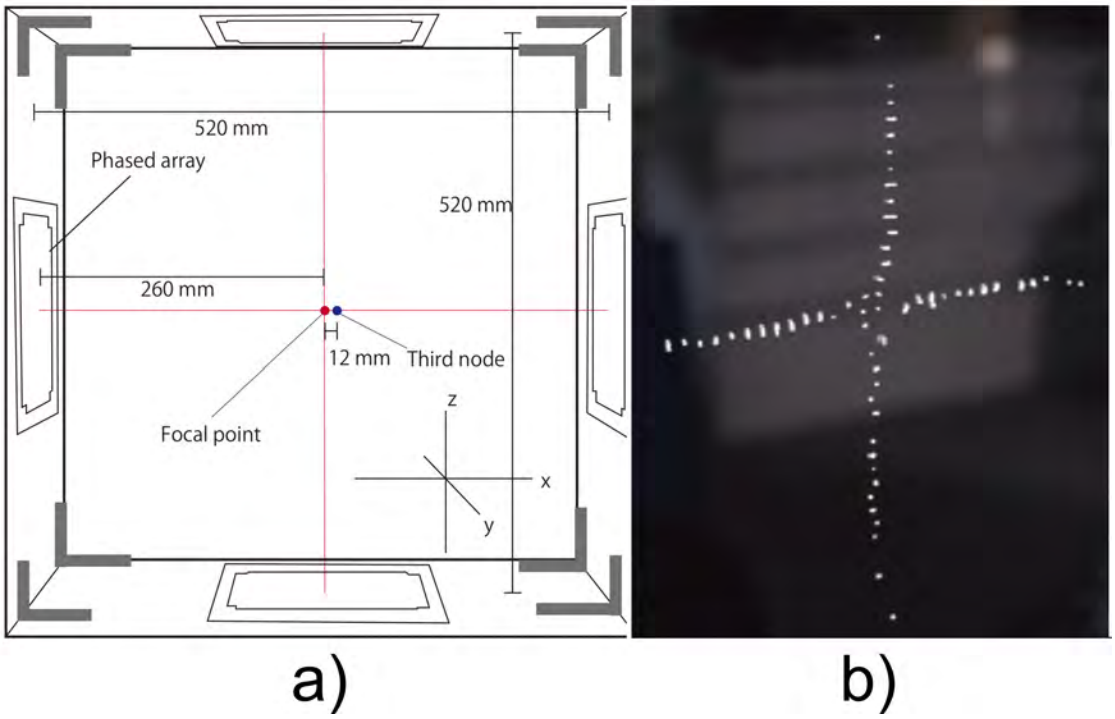

Figure 2.2: *A pair of images showing the three-dimensional control of many 2mm polystyrene balls using four transducer arrays. a) shows the placement of arrays relative to one another. b) demonstrates the suspension of multiple polystyrene spheres using this trapping system. Subfigures reproduced from Ochiai et al. [1] under CC BY 4.0.*

Marzo et al. developed an ultrasonic phased array to show that a single-sided emitter array may be used to translate, rotate and manipulate particles without the need for a reflector. They also introduce a 'holographic acoustic elements framework' that can model and rapidly generate many positions or traps in which a light-weight particle could be situated [32]. This work has been continued and seen the development of a variety of different transducer array structures capable of levitating small polystyrene particles from a single side without a reflector. These systems were termed acoustic tractor beams. They were shown to be capable of holding millimetre sized polymer particles and even fruit-flies [2]. Figure 2.3 shows the different transducer array orientations used to produce these ultrasonic tractor beams as well as the practical realisation of these methods. These systems produce a focal point or trap in which materials may be suspended through four different methods:

- a curved surface in which the transducer array is mounted
- a flat array in which the transducers are mounted at differing heights
- a flat array in which spiralled tubes are embedded above the transducers to vary the path length

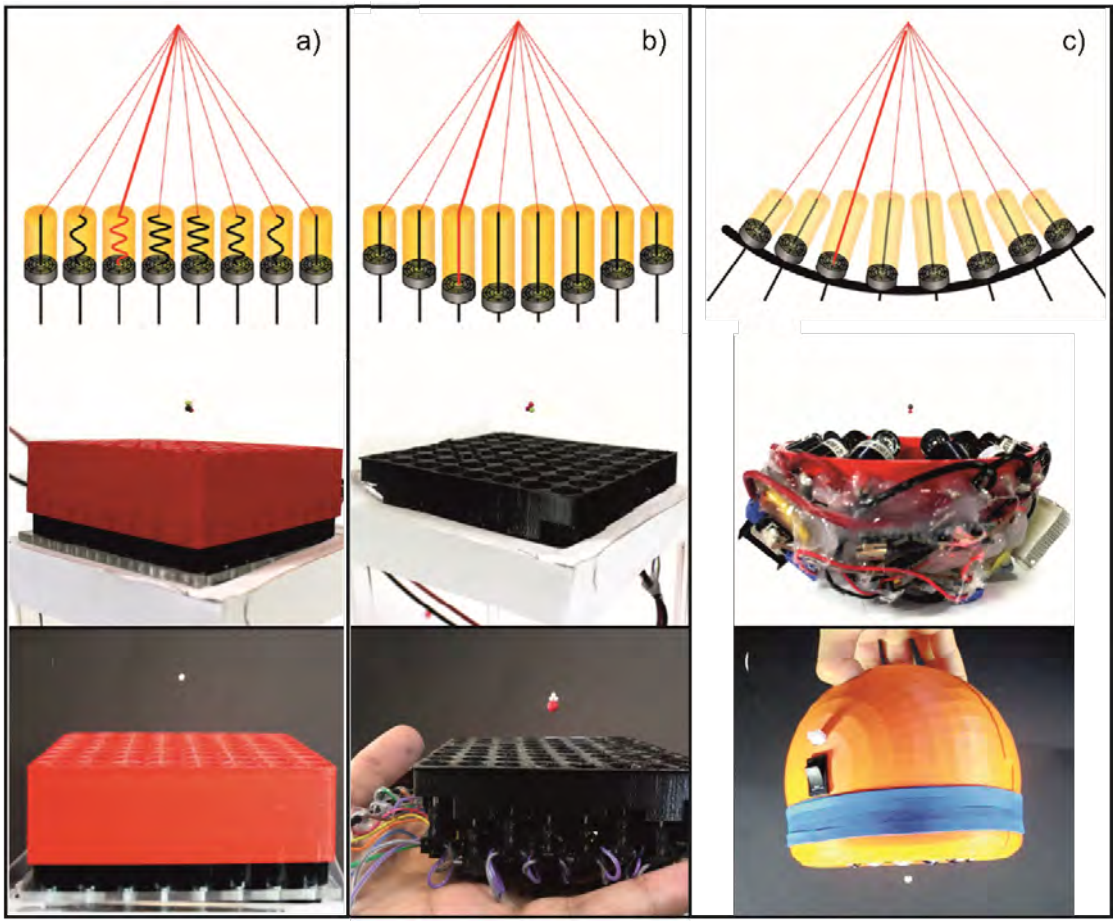

Figure 2.3: *An image depicting various compact and passive single sided acoustic levitation systems which utilise delay lines in order to function. Each of the panels show the schematic for the approach as well as two photographs the devices use. Subfigures a) has coiled tubes above the transducers to extend the path length of the varying positions to provide a phase difference between neighbouring transducers, b) the transducers are embedded at varying depths beneath the surface within this system which provides the phase difference required to levitate polystyrene balls. c) features a sculpted surface on which the transducers are positioned. Subfigures reproduced and rearranged from Marzo et al. [2] under CC BY 4.0.*

- a flat array in which each transducer is mounted parallel to the surface, but the individual phases are electronically controlled

Of these systems, the curved surface array was found to be the most efficient as the transducers all face the region in which a particle will be levitated and therefore there is minimal loses of the ultrasonic emission.

Simulations have been used to showcase a novel method of trap generation in order to form multiple simultaneous acoustic traps used to levitate light-weight spherical particles. These simulations feature a 16 x 16 transducer array operating at 40kHz. They form an acoustic trap at the r_1 position and a quiet zone at position r_2, which is a position that has significantly lower acoustic pressure when compared to the acoustic trap. Following this, an acoustic trap and quiet zone is then superposed on positions r_2 and r_1 respectively, this creates two positions which may trap and suspend lightweight particles. These acoustic traps have very similar strengths and pressure gradients to each other and can be generated at a separation of approximately 10mm [33].

Marzo et al. also explored the effects of orbital angular momentum on the stability of lightweight polystyrene particles when a vortex trapping motion is used within an acoustic levitator. During this work it was found that particles that were larger than the wavelength of the incident ultrasonic sound could be suspended by the driver phases being switched, causing the array to emit two different pressure fields. A 16mm expanded polystyrene ball was the largest of these particles which could be levitated through this method with reasonable stability, this ball had a diameter which was 1.88 times the 8.6mm wavelength of sound used, which overcame the limitation of the trapped particles needing to be significantly smaller than the applied sound wavelength [34].

Trajectory control has also been explored for lightweight polystyrene particles suspended within a two-sided acoustic levitator. This particular levitator consisted of 2 opposing planar arrays of 40 kHz transducers, 30 of these transducers were mounted on each array and powered individually. A square wave with a phase resolution of $\Phi = 2\pi/128$ was used to drive the transducers and allowed for the focal point to be moved. This acoustic levitation configuration was housed within a chamber to limit external air currents and sat upon a passive vibration isolation table to limit external vibrations to the system. The polystyrene particle was tracked as it moved along a circular path in the x-z plane, achieved by altering the phase of the transducers to move the focal point. The comparison between the desired pathway and that the particle travelled showed that they did not match. However, corrections were applied to this pathway

by the comparison between the target position of the particle and the equilibrium position the particle settled into, creating the desired pathway for particles with a velocity below 1cm/s [35].

The capabilities of holographic acoustic tweezers to dynamically manipulate many expanded polystyrene particles simultaneously without interaction with any surface has been explored. An algorithm enabling the control of the emitted field from the transducer arrays is used. These arrays consisted of 256 transducers on either side, each transducer has a 1cm diameter and operates at 40kHz, and these were mounted on two planar surfaces which were opposing and separated by 23cm. The algorithm generates a focal point at the position of the particle before changing the transducers phase in order to move the focal point, and therefore the particle. The minimum distance between levitated polystyrene particles within this system was 1.3cm, when the traps or focal points were generated closer, they merged and the 25 traps which could be generated no longer acted independently. The control of asymmetric particles is performed by the generation of twin traps, however they were insufficient to maintain suspension of the particles thus the rapid switching between twin traps and focal points was used for orientation and suspension of the particles [36].

2.1.5 Example Devices for Droplet Levitation

A major turning point for the accessibility of acoustic levitation and the suspension of liquids was through the publication of TinyLev: A multi-emitter single-axis acoustic levitator [3]. This system built on the curved surface tractor beam system discussed earlier in subsection 2.1.4. However, the TinyLev system utilised two opposing curved surfaces, with transducers mounted on both sides facing inwards. One significant feature of this system, which makes it more accessible, is the use of a low cost Arduino microcontroller, making it possible for anybody with a soldering iron to construct a viable acoustic levitator with help from an Instructable that shared the design and software details in an easy step by step guide [10]. Figure 2.4 shows the TinyLev system and demonstrates that there are multiple positions in which droplets may be levitated.

A more open platform has been presented in ‘Ultraino: An Open Phased-Array System for Narrowband Airborne Ultrasound Transmission’ [37] which has also been described as modular and inexpensive. This platform provides the hardware, software and some example applications aimed to control the transmission of ultrasound through air. This work allows users to use the supplied modelling software to predict an appropriate array configuration to help with the users experiments. This configuration can then be implemented through the use of well-defined hardware building blocks. The feasibility of phased arrays was transformed through the realisation that low-cost off the shelf transducers could be driven by an amplified logic signal

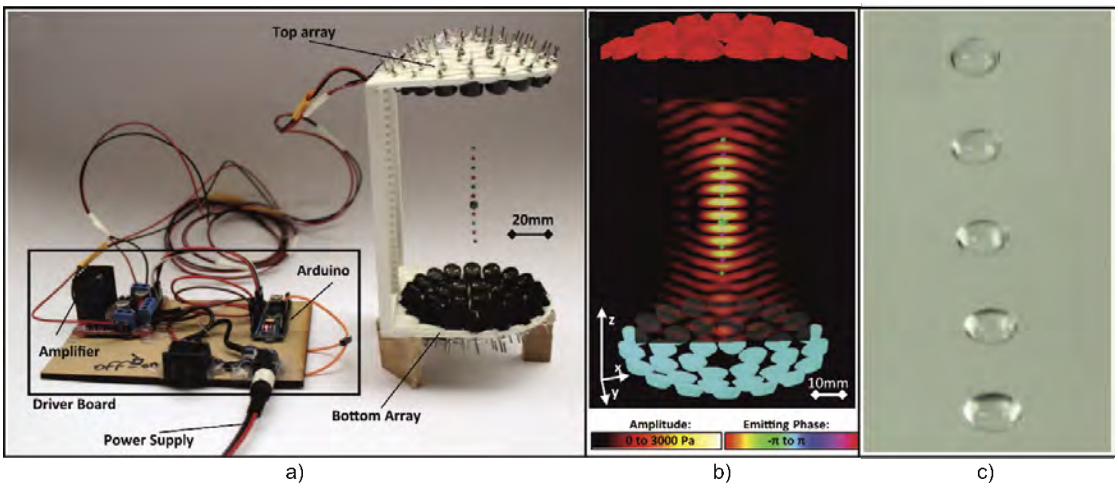

Figure 2.4: *a) TinyLev acoustic levitator which consists of 3D printed structure of which two domes face one another, 72 transducers secured to the structure are driven by a L298N board and Arduino Nano. b) simulated acoustic field of the TinyLev system. c) water droplets suspended in the constructed system. The oblate morphology is of particular note and is due to stronger trapping forces in the vertical direction in comparison to the horizontal direction. Subfigures reproduced from Marzo et al. [3] under CC BY 4.0.*

with a variable phase and duty cycle. It should be noted that liquid levitation was only achieved for two-sided standing wave systems similar to the TinyLev system discussed earlier, the single sided configurations lacked the confinement required to suspend high density samples. Sample spinning is a well known phenomenon which occurs within single axis acoustic levitators, this is often not significant except for in the cases of non-spherical and non-uniform samples such as insects or liquid crystal structures where it is an important factor which must be considered. It occurs as a result of the acoustic forces largely being applied longitudinally to the sample, but the lateral forces applied being significantly weaker meaning the sample may spin on its axis.

In Acoustic Lock: Position and orientation trapping of non-spherical sub-wavelength particles in mid-air using a single-axis acoustic levitator [4], a variation on the single-axis and two sided levitator system was described. In this system each curved surface is divided into two symmetric halves. The transducers on either side of one surface are out of phase with each other which facilitates the generation of both twin traps and vertical standing waves through the Acoustic Lock system. These two states are rapidly switched between, with 100 cycles of the standing wave configuration followed by 50 cycles of the twin-trap configuration. This method of levitation has been shown to stop the rotation of solid objects as well as those which are non-spherical. A 3D model of the Acoustic Lock device is shown in figure 2.5 which depicts the pressure amplitude during each configuration.

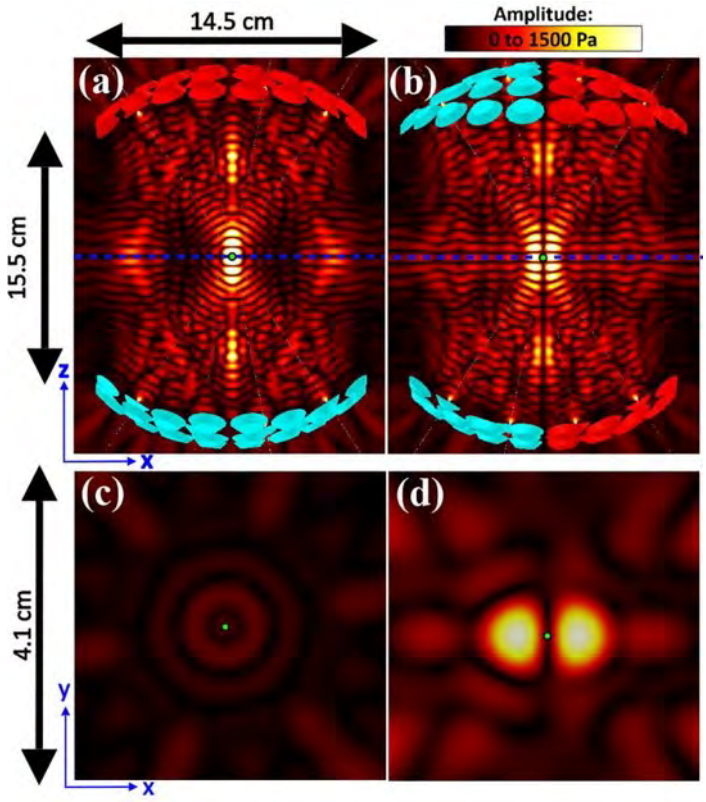

Figure 2.5: *A 3D simulated model of the Acoustic Lock system, showing the two states present. (a) and (c) depicts the standing wave state, (b) and (d) shows the twin-trap state. (a) and (b) are visualisations of the front of the device, (c) and (d) shows the top plane at the position of the blue line in (a) and (c) respectively. The green dot shows the position in which a substance may be levitated. Reproduced from Cox et al. [4] with the permission of AIP Publishing.*

2.1.6 Additional Notable Acoustic Levitators

Acoustic levitator designs have been shown to levitate both solid expanded polystyrene balls and liquid samples, and previous sections discussed the configurations that have achieved this levitation. However, there are some interesting systems that are worth mentioning, in which the droplet dynamics are the focus of the work.

A rectangular phased array of transducers has been combined with a reflector in order to demonstrate mixing and contact-free coalescence of droplets in midair [5]. The array switches between two focal points at 500Hz in order to levitate two droplets simultaneously. The distance between these two focal points was then reduced in order to form a single large standing wave with a single trap, resulting in the coalescence of the droplets within these focal points. Figure 2.6 presents the estimated acoustic potential, the resulting potentials at the pressure nodes and images of the two water droplets over time, moving toward each other due to the movement of the focal points and coalescing. The distance between the transducer array and the reflector however was only 45mm, which is a relatively small separation.

Shen et al. has demonstrated oscillation modes in a single axis acoustic levitator consisting of an emitter and curved reflector and forming a standing wave between them by modulating the amplitude by up to 10%. This work swept the modulation frequency upward in 0.5 Hz increments to observe the different oscillation modes that could be excited. They found that the oscillations occurred in the lateral directions and could be imaged from above the droplets, they caused the shape to change from an oblate droplet to an irregular shape [38]. Watanabe also implemented a similar method in a phased array and was able to find that mode oscillation promotes droplet mixing when the flow within a droplet with mode oscillation is compare to that without. This means this technique is a viable and useful tool for container-less chemistry [5].

In Automatic contactless injection, transportation, merging, and ejection of droplets with a multifocal point acoustic levitator [6], a 16 x 16 array of ultrasonic transducers operating at 40kHz is featured, which is positioned 110mm from a planar reflector in order to form a standing wave with a series of pressure nodes where liquid droplets are trapped and may be moved in two dimensions above the surface of the transducers. The position of the reflector was selected by focusing the transducers to different distances from the array and empirically determining which position provides the greatest pressure amplitude. This system also featured an integrated droplet injector which was inserted into the reflector which included a 1mm diameter nozzle and a piezoelectric buzzer. When a voltage was applied to the buzzer, a droplet of water was injected and trapped within the lowest pressure node of the standing wave. The outlet for droplets was simply a hole within the reflector in which the droplet could be levitated over, at which time the

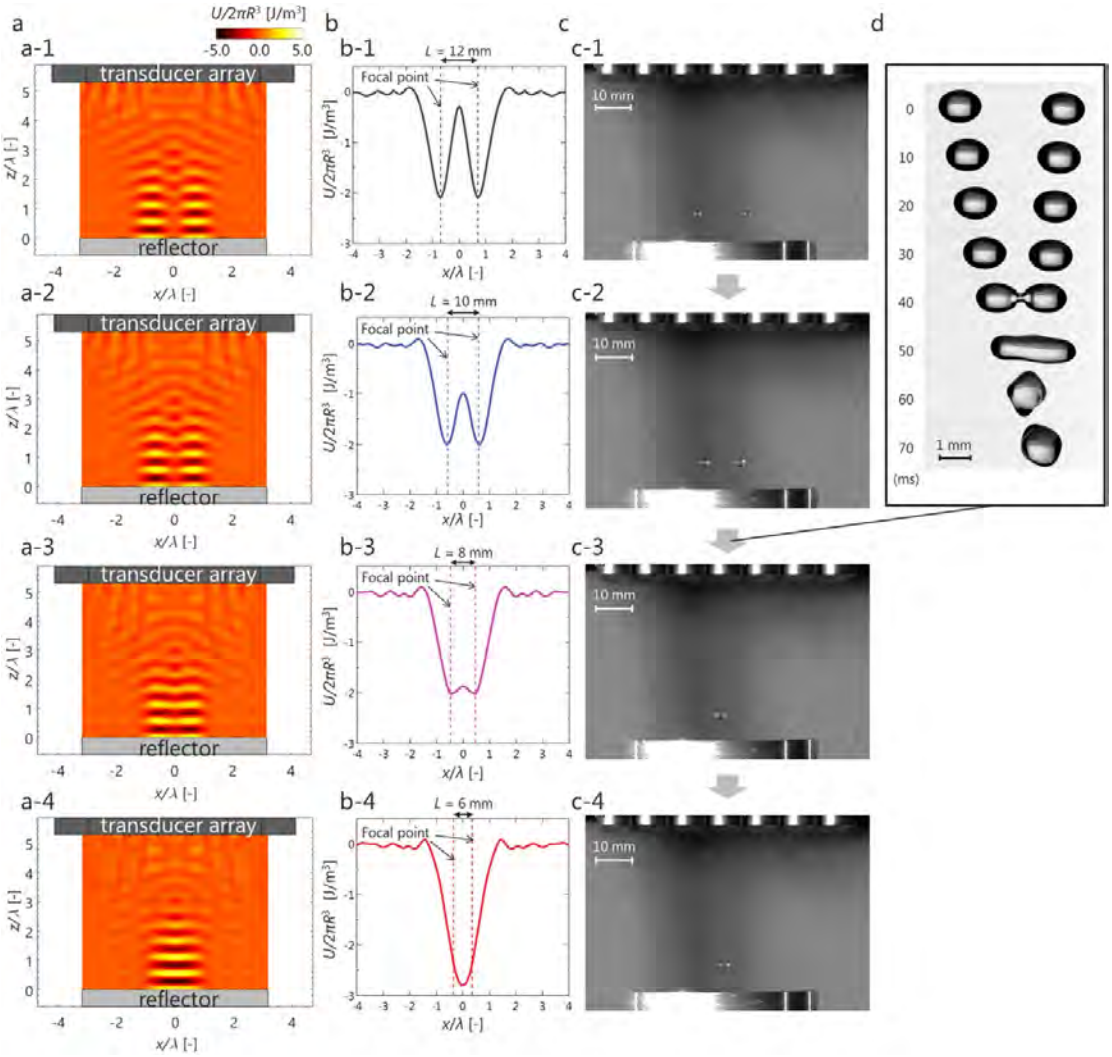

Figure 2.6: *Contactless movement and coalescence which is achieved using acoustic fields which are varied in time. a) shows the acoustic potential of the transducer array with the reflector, b) shows the acoustic potential as a function of lateral space. c) shows photographs of two droplets within the focal points of this system, and d) depicts a the two droplets coalescing over time. This figure demonstrates that droplets within this acoustic levitation system begin to merge when the focal points are separated by approximately 8 - 10mm. Reproduced from Watanabe et al. [5] under CC BY 4.0.*

acoustic field could be turned off causing the droplet to fall through it due to gravity. Figure 2.7 shows the movement of two droplets through the acoustic levitator over time, highlighting the injection and ejection of these droplets throughout this timeframe.

In the published work 'Acoustic Lock: Position and orientation trapping of non-spherical sub-wavelength particles in mid-air using a single-axis acoustic levitator' [4] the supplementary material mentioned the levitation of liquids and made important reference to the shape of the levitated droplet in which it was found the droplet was approximately ovoid but the surface of the droplet appeared less smooth. In the move from the levitation of solids which tend to have a fixed morphology, to fluids of which the shape conforms to the shape of the trap in which it is levitated, the shape of the acoustic field has become much more important. For many experimental systems this is only a feature which limits the droplet size to be confined, however when the system is used for sample presentation this can be vital as it may directly impact the results of any probing to the droplet. For example, the changing morphology of a droplet can be used to infer contamination of the droplet in some cases [39]. Also, when the sample size of a liquid is limited there may not be sufficient sample to perform additional experiments like titrations or NMR spectroscopy.

2.1.7 Droplet Evaporation and Heating

The intention for this work is to acoustically levitate protein crystals within a droplet of their mother liquor. Therefore it is important to have a brief understanding of the evaporation and heating of droplets within acoustic levitators as this may effect the experiments performed on the protein crystal at Diamond Light Source.

Liquids tend to evaporate if the atmosphere surrounding the liquid is not saturated with vapor from the liquid. However there are conditions in which liquids would evaporate despite the surrounding air being saturated with its vapor, such is the case when the liquid is a small droplet as there is an increase of vapor pressure caused by the curvature of the droplets surface [40; 41].

The evaporation of droplets on surfaces has had extensive research, finding applications that directly benefit from the evaporation of droplets on surfaces like inkjet printing [42]. Of particular relevance to this thesis, droplet evaporation has been explored for droplets of water in langevin type systems. For example, in work performed by Schiffter et al. [43] pure water droplets of varying volumes were suspended by a 58kHz langevin horn opposing a reflector contained within a chamber of which the air temperature and relative humidity could be controlled. These droplets were imaged over time as they evaporated and compared to theoretical models for spherical

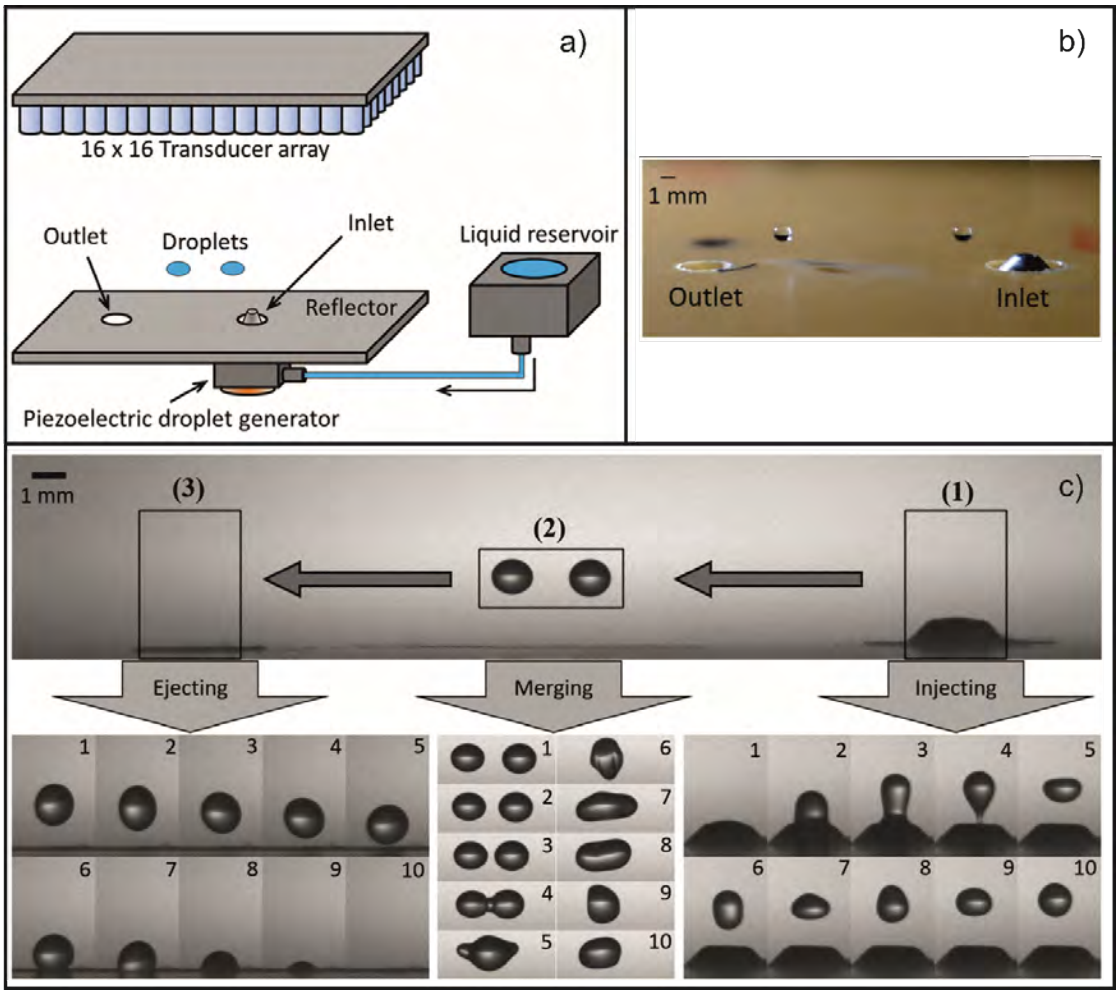

Figure 2.7: *An image depicting the acoustic levitation system. a) shows the schematic of the 16 x 16 transducer array with an opposing planar reflector, substances are drawn from the liquid reservoir and into the system through the piezoelectric droplet generator, and an outlet is positioned on the other side where the levitated droplets may be ejected by turning off the acoustic field. b) shows a photograph of levitated droplets moving toward the outlet within the system. c) clearly depicts a series of images in which droplets are injected in (1), merged together in (2) and ejected from the system in (3). Subfigures reproduced from Andrade et al. [6] with the permission of AIP Publishing.*

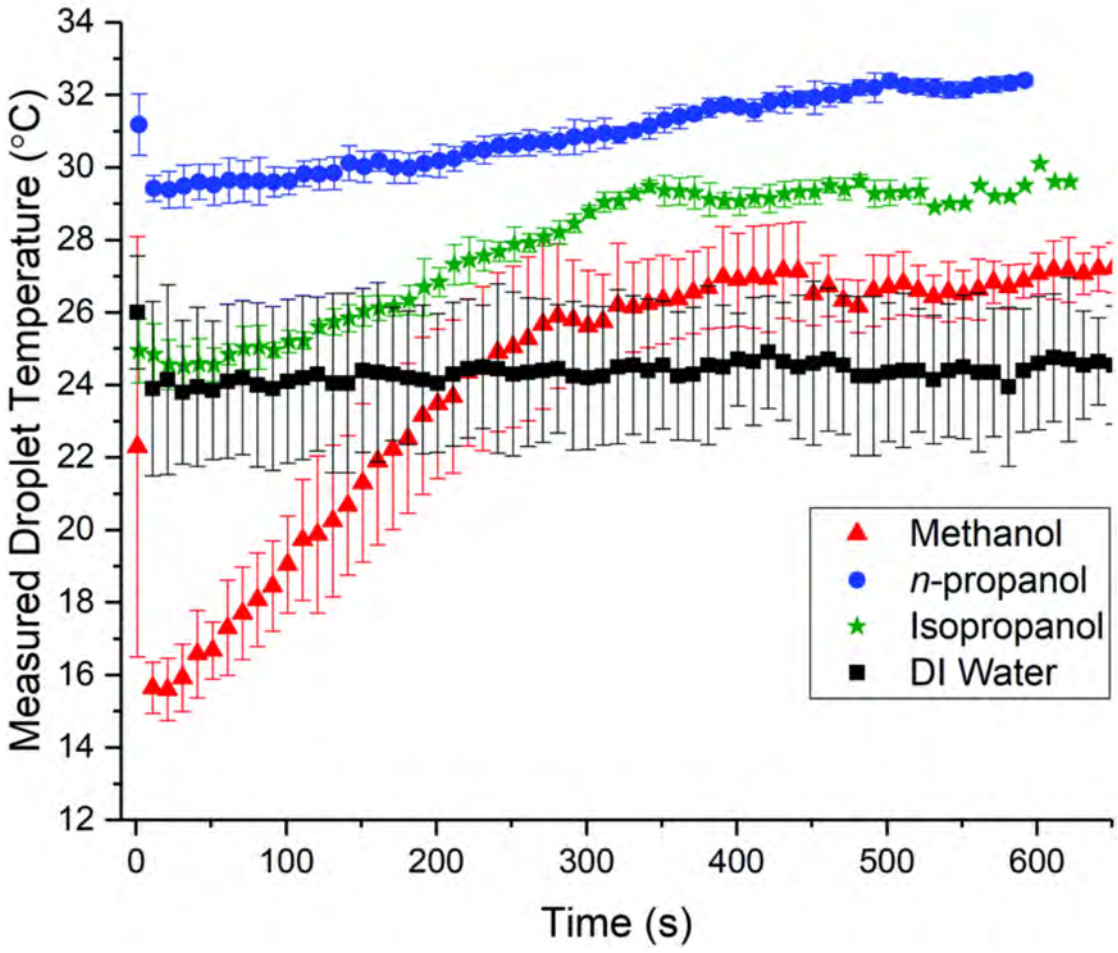

Figure 2.8: *A graph of the temperature of droplets of various acoustically levitated substances over time. The substances studied include methanol, propan-1-ol (n-propanol), propan-2-ol (isopropanol) and deionised (DI) water.The droplet temperature is measured through the use of infrared thermography and so only the surface temperature may be recorded. The deionised water droplet experienced negligible temperature change, where as the methanol droplet experienced a significant temperature increase approximately 11°C throughout the lifetime of the droplet. The temperature appeared to increase linearly with time the droplet spent within the acoustic levitator, until it plateaued [7]. Used with permission of Royal Society of Chemistry, conveyed through Copyright Clearance Center, Inc.*

droplets suspended in stagnant air. It was found that the evaporation rate of the droplet was higher due to the acoustic streaming of the levitation device, which causes the air to flow around the droplet where it is levitated. This allows for any droplet vapour to travel away from the surface of the droplet, meaning the immediate surrounding atmosphere is no longer saturated.

The evaporation and temperature change of levitating droplets of deionised water, methanol, propan-1-ol and propan-2-ol droplets have been studied whilst the droplets are suspended by a TinyLev acoustic levitator [7]. This work featured infrared thermography using a FLIR camera which monitored single droplets until they had evaporated, it found that deionised water increased in temperature at a rate of 1.9 x $10^{-4}°Cs^{-1}$ which means it would have taken approximately 87 minutes to increase the temperature by 1 degree, at which point it had already evaporated, so the temperature increase caused by the TinyLev system is effectively negligible. However, the levitated droplet of methanol increased in temperature at a rate of 4.13 x $10^{-2}°Cs^{-1}$, meaning that it takes approximately 24 seconds for the droplet to increase the temperature by 1 degree. This appears to be linked to the molar enthalpy of vaporization of the substances, but also to the surface area of the droplet as it evaporates. A graph showing the droplet temperature over time for the studied substances is shown in figure 2.8, it shows negligible temperature change in the droplet of deionised (DI) water but significant increase in the droplet of methanol, the propanol droplets experienced moderate temperature increase.

2.2 Proteins and macromolecular crystallography

Proteins are large and complex molecules which play a critical role within living things. They are often described as the building blocks of life as they play a key part in the generation of new cells, tissue repair and many other functions within organisms. The study of protein structure can help to understand the functions of proteins, which can be used in the research and development of medicines. Medicines can bind to proteins which are causing diseases within the body and relieve the symptoms by changing its shape [44].

Proteins at a fundamental level are complex molecules comprising carbon, hydrogen, nitrogen and oxygen and often include sulphur and phosphorus [45]. These atoms are bonded to form amino acids, of which the generalised structure is shown in figure 2.9. The atoms shown in blue are commonly referred to as an amino group, that in red is called a carboxyl group and the green “R” is a place holder for a bonded group of atoms which is unique to a specific amino acid, distinguishing them from one another.

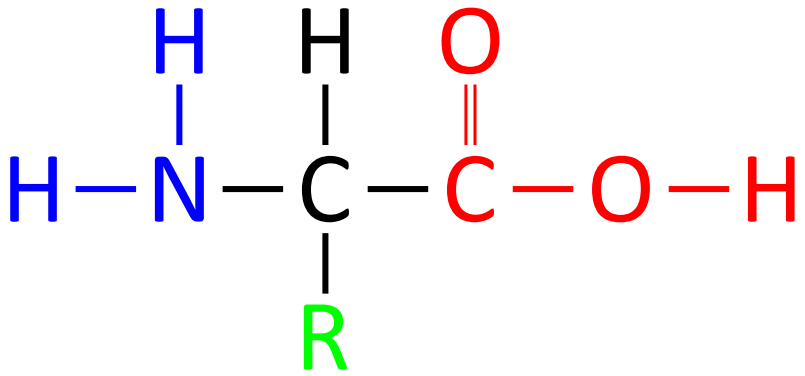

Figure 2.9: *The generic structure of an amino acid. That shown in blue is the amino group, that in red is the carboxyl group and the green "R" denotes a group which is specific to an individual amino acid.*

There are twenty protein creating amino acids, known as proteinogenic amino acids. Amino acids bond together by expelling a water molecule as the amino group bonds to the carboxyl group. These may form chains which are called peptides or proteins depending on their length [46].

Proteins differ from each other by the combination and sequence of the amino acids it is comprised of. The repeating "R" group in the protein chain could be any of those which is found in the proteinogenic amino acids. There are many thousands of unique naturally occurring protein variations that have already been discovered [45].

Protein synthesis is an elaborate process which naturally occurs within cells, as proteins are fundamental to most biological activity [47]. The protein may be described in terms of its primary, secondary, tertiary and quarternary structure.

The linear chain of amino acids is called a polypeptide which is constructed within cells, this is a primary structure of a protein and often referred to as the polypeptide backbone. Modification to the polypeptide chain may also occur following its construction by the cell and this forms a mature protein product. For example, insulin is composed of 2 polypeptide chains that are constructed within the cell that then bond together. This is still part of the primary structure [48].

There is a secondary structure of the protein and this refers to a repetitive sub-structure on the polypeptide backbone. This sub-structure occurs due to hydrogen bonding between atoms within the chain and can manifest as either an α-helix or a β-sheet. They have a regular geometry and both structures saturate all hydrogen bonds within the polypeptide backbone [49].

A tertiary structure is that which is most familiar, it is a three-dimensional structure formed by the folding of the α-helix or β-sheet secondary structure. This folding occurs due

to hydrophobic portions of the polypeptide chain being repelled by the liquid within it local environment and burying themselves inside the structure. This structure is only stable when bonds are formed around the hydrophobic groups to fix this structure [49].

A quaternary structure is also a three-dimensional structure, however it is composed of at least two polypeptide chains that work together to operate as a unit for a specific purpose. This final structure is stabilized by the same types of bonds as in the tertiary structure [50]. The most well-known quaternary structure is haemoglobin with the function of transporting oxygen around the human body, which is comprised of 4 individual polypeptide chains bound together through hydrogen bonding and the hydrophobic effect.

A representation of a primary, secondary, tertiary and quaternary structure is depicted in figure 2.10. The primary structure shows the linear polypeptide backbone comprised of varying amino acids which have bonded together. The secondary structure shows both the α-helix and the β-sheet depictions. The three – dimensional protein structure is shown in the tertiary and quaternary structure, owing to bonds formed around hydrophobic burying, however the quaternary structure is comprised of multiple polypeptide chains bonded together and working to achieve one task.

2.2.1 Protein Crystals

Protein crystallization is the process in which protein crystals are formed. Some protein crystals are naturally occurring to fulfil specific purposes for the organism in question, such as for storage within a seed, for encapsulation to protect from viruses or to plug leaks inside the phloem of a plant [51]. The benefit of proteins forming crystals is that x-ray diffraction may be used to determine the structure. This is due to protein crystals traditionally having an ordered and periodic arrangement of atoms, with a recurring pattern throughout the structure.

To prevent damaging the proteins, and thus influencing the results, great care must be taken with the methods used to encourage the formation of crystals. For many types of proteins, this can be a lengthy and arduous process, performed under highly controlled conditions to prevent denaturation of the protein structure [52]. There are three main methods in which controlled precipitation is completed [53]:

- Super saturation
- Salting out
- Organic solvent addition

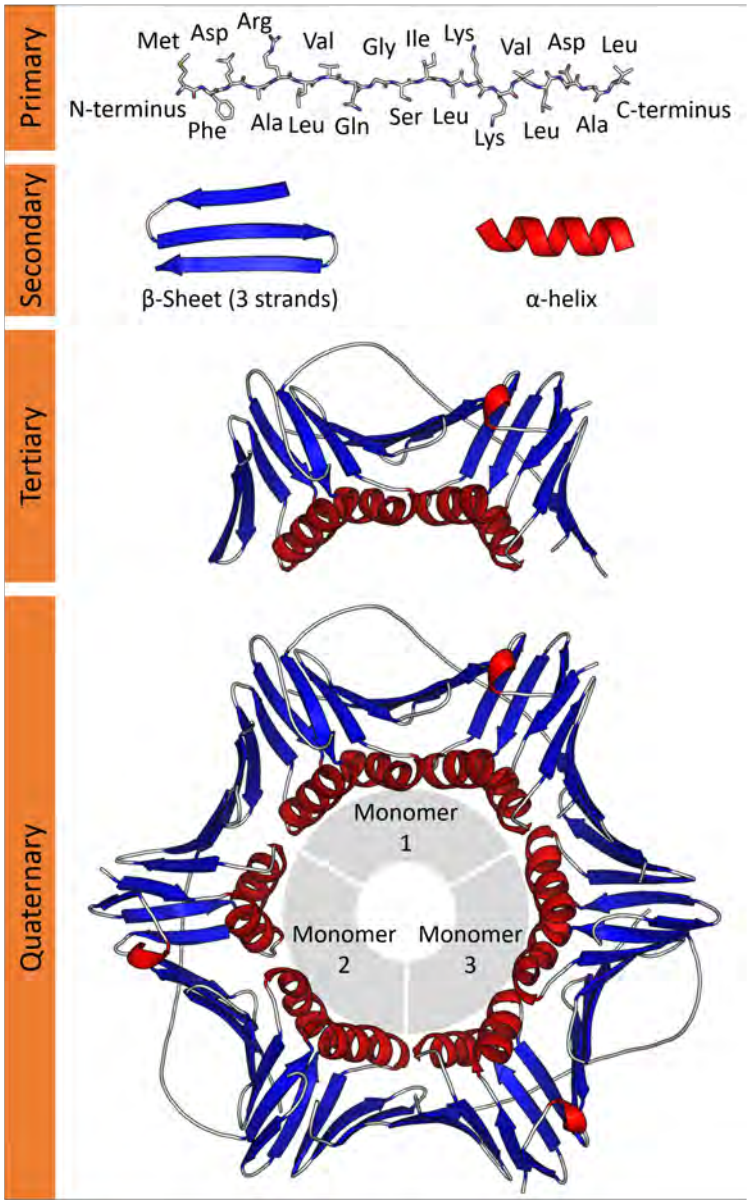

Figure 2.10: *A representation of a primary, secondary, tertiary and quaternary structure of a protein [8]. The primary structure is composed of a series of amino acids bonded together, often referred to as the polypeptide backbone of the protein. The secondary structure is either the α-helix or β-sheet, this structure is formed by hydrogen bonding occuring between atoms within the primary structure. The tertiary structure is formed through hydrophobic burying, the hydrophobic portions of the polypeptide chain is repelled by the liquid and bury themselves within the structure. The quarternary structure represents the interaction between two or more polypeptide chains and, like the tertiary structure, is stabilised through hydrogen bonding and hydrophobic burying. Reproduced under CC BY 4.0.*

Super saturation refers to the state of the solution when there is more protein molecules in the solution than there would be under normal conditions. Super saturation causes the protein precipitate to form and crystallize, in which the individual protein molecules are held together by non-covalent interactions [53].

The salting out process is a method for protein precipitation, in which protein crystals are formed. This is the addition of salts to the solution which are more reactive than the protein molecules and displace them from solution [53]. The most commonly used salt is ammonium sulfate as it is not harmful to proteins, even in high concentrations, and is also highly soluble in water [52].

The final method to form protein crystals is through the addition of organic solvents, however these often interact with the hydrophobic areas of the protein molecule and cause it to denature. Polyethylene glycol (PEG) is widely used as it is water soluble, a powerful precipitant and a weak denaturant. A simple way of causing a protein to precipitate is to add the organic solvent denaturant at a concentration just below that needed to form a precipitate, then allow the water to evaporate so that the protein molecules and solvent have increasing concentrations and form protein crystals [53].

The likelihood of protein crystal formation is highly dependent on a number of factors. These include but are not limited to:

- Protein concentration
- Solution temperature
- pH
- Ionic/Electric field strength in the solution

When the protein crystals have formed, they have a regular and repeating arrangement of the atoms and molecules they are comprised and this is called a unit cell. Within the crystals, the structure is very loosely packed with channels which are filled with the solution in which the crystals are formed, occupying approximately 40-60% of the volume of the structure [52].

2.2.2 Mother Liquor

Living systems and cells are almost exclusively based within aqueous solutions, with small ranges of temperature and pH. As a result of this, the proteins which reside within and come from living systems thrive within such solutions, and must be grown within them. This aqueous solution,

matched to the optimum temperature and pH for the protein in question, is referred to as the mother liquor [54].

Due to the large complex shapes of protein molecules, they have relatively large spaces between adjacent proteins within the crystal structure. This means that the mother liquor permeates the protein crystal structure, and other chemical compounds that may be in solution are able to diffuse freely through the crystals. The other chemical compounds could be ions, ligands, drugs or other small molecules [54].

The large spaces and consequent weak lattice forces between the protein molecules within a crystal may contribute to a generally poorer diffraction image, but it is the reason to why they have such relevance to biochemists. Thanks to the high content of mother liquor within the lattice, proteins maintain their structure as if they were still within solution. This means that we may visualise what happens in vivo by altering the mother liquors composition [54].

However, as the protein crystals tend to have such high mother liquor content within their structure, they must be kept within the mother liquor or at low temperatures which prevent the mother liquors evaporation [52].

2.2.3 X-ray diffraction

X-ray diffraction is an experimental method which uses x-rays to determine the structure of a crystal. This may be performed on simple molecules like table salt or more complex molecules like protein crystals.

Crystals are comprised of a repeating structure called a unit cell. The unit cell is the smallest unit within the crystal in which its vectors may be used to translate to an identical atom within another unit cell. The repetition of the unit cell is called the crystal lattice or Bravais lattice and each side of the unit cell is a translation vector a, b and c. The Fourier transform of this Bravais lattice is called the reciprocal lattice and it is an imaginary lattice with infinite repeating points, with translation vectors a*, b* and c* [52].

Proteins themselves are often a few nanometers in length, however the structure of a protein and the atoms of which it is comprised are hundreds of times smaller on the angstrom length scale [55]. In order to probe these structures for their atomic arrangement, a wavelength of light shorter than these length scales is necessary to achieve sufficient resolution, which is either X-rays or gamma rays on the EM spectrum. Gamma rays are not considered for this project although gamma ray diffraction is a technology used to determine the structure of crystals as the technology is not as widely used or available [56]. X-rays are generated by accelerating electrons in a vacuum tube to collide with a metal target, which causes the emission of x-rays. This

method is typically used for tabletop systems. However, synchrotrons are also used to generate x-rays [52].

A synchrotron is a cyclic particle accelerator in which a beam of particles travel around a fixed closed loop. The magnetic field that bends the path of the particle into the loop shape increases in strength during the acceleration of the particles, synchronised to the kinetic energy of the particles that is increasing. By increasing the magnetic field strength as the particles gain kinetic energy, the electrons path may be controlled as they are accelerated. This means that the path of the electrons can be large, thin and toroidal. The electrons are then maintained at a constant speed (although their acceleration changes as the electrons travel the looped path due to their directional changes). X-rays are generated as the electrons change direction around the synchrotron [57].

These x-rays are focused to a beam of varying diameter through a variety of optics. The x-rays produced are used for a variety of different applications. In the case of x-ray diffraction, they strike the crystal or target within the beam path, interacting with the electrons which surround the atoms where it is absorbed. The electron then emits a secondary x-ray which has an identical frequency and intensity to that which was absorbed [52]. This secondary x-ray may be detected when a specialised detector is in place, if a two-dimensional detector is used it results in a diffraction pattern, like that shown in figure 3.15. This diffraction pattern may be used in order to determine the electron density of the crystal structure and therefore its atomic composition and the relative positions of each atom.

The equations shown in 2.6 - 2.8 are known as the Laue conditions which lay out the requirements for a crystal to scatter x-rays, in which h, k and l are integer values, $\mathbf{S}$ is the vector describing the difference between the incident wave and the scattered wave, illustrated in figure 2.11 which is perpendicular to that which is described as the "reflecting plane" a, b and c are the vectors describing the unit cell. The full derivations can be found elsewhere [52] and will not be included in this work as they are not relevant to the construction and implementation of an acoustic levitation device for sample presentation. The Laue conditions describe that diffraction only occurs at discrete angles else the wave has an amplitude of zero. When the conditions are fulfilled the waves scatter in phase and constructively interfere, otherwise they destructively interfere.

$$\mathbf{a}\cdot\mathbf{S} = h \tag{2.6}$$

$$\mathbf{b}\cdot\mathbf{S} = k \tag{2.7}$$

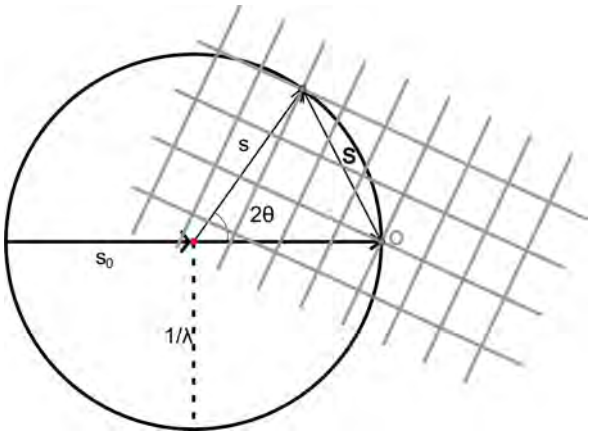

Figure 2.11: *A diagram showing the imaginary Ewald sphere and reciprocal lattice in relative position to the incident x-ray and the crystal structure. s_0 shows the direction of the incident x-ray which strikes the crystal shown in red, s shows the resultant direction of the diffracted x-ray which passes through a point on the reciprocal lattice (which is the structure shown in grey). The origin of the reciprocal lattice is labelled as O and it is positioned at the point in which the incident x-ray would intercept the Ewald sphere. The Ewald sphere has a radius of $1/\lambda$ which means that a lower wavelength of incident x-ray would form a larger Ewald sphere.*

$$\mathbf{c}\cdot\mathbf{S} = l \tag{2.8}$$

The angles with which the x-ray's diffract may be used to inform the plane spacing within the crystal lattice through the use of Bragg's law as shown in equation 2.9, where d is the spacing between planes which diffract, θ is the angle of the incident x-ray, n is an integer and λ is the wavelength of the x-ray beam. This gives rise to the theoretical maximum resolution in which the crystal can be measured when the sin function reaches its maximum value of 1, which gives a $d_{max} = \lambda/2$. However the measured angle of the diffracted wave is used to find the resolution of the dataset collected. 1.0 – 1.5Å is regarded as a high quality resolution of the crystal lattice [52].

$$2dsin\theta = n\lambda \tag{2.9}$$

In order to use the x-ray diffraction pattern to determine the electron density of the protein structure, we must remap our reciprocal lattice. This is achieved using an imaginary sphere, known as an Ewald Sphere. An Ewald sphere is an imaginary sphere with a radius of $1/\lambda$ centred on the interaction point between the incident x-ray and the crystal structure. The origin point of the reciprocal lattice can be imposed onto the Ewald sphere at the position in which the incident x-ray would intercept the sphere. The diffraction of an x-ray would travel in the direction of any point of the reciprocal lattice which intercepts the Ewald sphere. As the x-ray crystal is rotated,

the reciprocal lattice rotates allowing for additional points on the diffraction pattern owing to additional interceptions between the Ewald sphere and the reciprocal lattice. The intensity and positions of the spots on the diffraction pattern may therefore inform the composition of the reciprocal lattice and this may be fourier transformed to determine the electron density of the crystal structure. Figure 2.11 shows the concept of the Ewald sphere and the relative position of the imaginary reciprocal lattice in respect to the crystal, the Ewald sphere and the incident x-ray [52].

2.3 Diamond Light Source and Current Crystallography Sample Presentation

Diamond Light Source is the United Kingdom's national synchrotron facility located in Didcot, Oxfordshire on the Harwell Science and Innovation Campus. The design for this facility was finalised in 2001 by a group of scientists at Daresbury Laboratory, with the intention for it to be constructed in Daresbury. The name "Diamond" was conceived as an acronym meaning **DI**pole **A**nd **M**ultipole **O**utput for the **N**ation at **D**aresbury, however the location was moved to Oxfordshire. The Diamond Light Source facility produced its first user beam in 2007 and receives funding from the STFC (Science and Technology Facilities Council) and the Wellcome Trust [58].

This section provides the specifics of the facility and its synchrotron light, and the current techniques which have been used at synchrotron to present the crystal or sample to the beam.

2.3.1 Diamond's synchrotron

The synchrotron at Diamond Light Source has a storage ring which operates at an energy of 3 GeV and is 561.6m in circumference. The shape of the storage ring is a 24-sided polygon [59], bending magnets are located at each of the vertices and bend the pathway of the electrons travelling around the storage ring. As the electron path bends, synchrotron light is emitted into a beamline or "hutch" in which it passes through various optics for specific types of experiments to be performed [58]. A schematic for Diamond Light Source is shown in figure 2.12. As Diamond Light Source is a third generation light source, it also uses special arrays of magnets called undulators which cause the electrons to wiggle and emit synchrotron radiation much brighter than that produced from the electrons travelling through the bending magnets, this radiation is emitted into specific beamlines at Diamond Light Source. The naming convention of the beamlines at Diamond describes the type of synchrotron radiation which is featured, each hutch

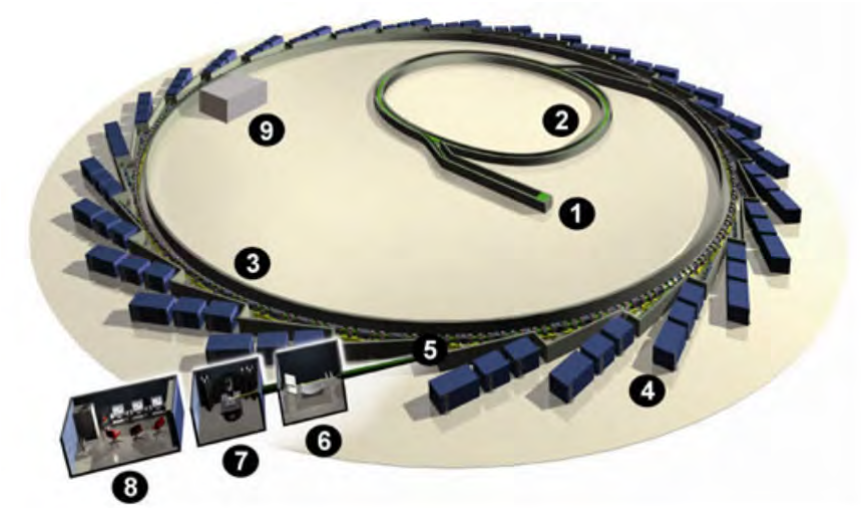

Figure 2.12: *A schematic of the beamline at Diamond Light Source [9] reproduced under CC BY 4.0. The electron gun and Linac is shown at position 1, where the electrons are injected. Position 2 depicts the booster synchrotron, where the electrons are initially accelerated. 3 is the storage ring, the large ring in which the electrons travel around at a fixed speed, the path being circular as the electrons travel through bending magnets. 5 is the "front end" which channels the synchrotron light to a beamline which is shown in 4 and made up of the optics hutch, experimental hutch and control room shown in 6, 7 and 8 respectively. Position 9 shows a radiofrequency cavity, in which the electrons are supplied with additional energy to compensate for the energy loss it experiences around the ring.*

has a name either beginning with a B or an I, to signify whether the x-ray beam is produced by the use of a bending magnet or through the use of an insertion device respectively [60].

The 32 beamlines currently in operation at Diamond Light Source feature a large range of disciplines and research focuses. Of particular interest to this work are the beamlines which undertake macromolecular crystallography to study and understand the structure of proteins or any sample in which being a liquid or within solution is its optimum environment, such as I03, I04, VMXi or I24 [61].

I24 is a microfocus macromolecular crystallography beamline, dedicated to the study of structural biology and it has been made use of within this work as the research focus aligned with the topic of the thesis.

2.3.2 Sample presentation of protein crystals

The current method used typically within modern crystallography to present the sample to the beamline is a robotic-arm sample delivery method and consists of:

- a dewer which contain pucks
- pucks which are comprised of bases, spines or cryogenic loops which hold the desired sample

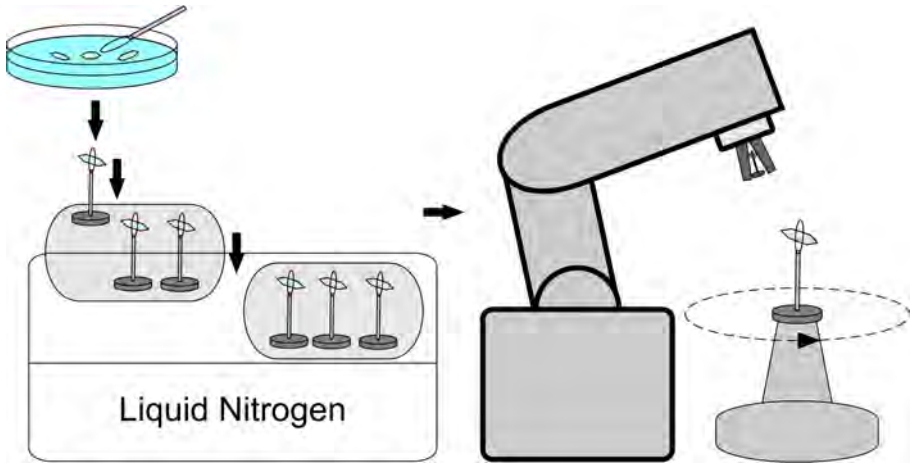

Figure 2.13: *A diagram showing the steps for sample presentation using the Stanford Auto Mounting system (SAM). From left to right, crystals are collected onto loops using a trained hand, they are mounted onto spines which are loaded onto pucks for storage and transit. The robotic arm collects the sample and fixes it to the goniometer for sample presentation.*

- a robotic arm used to transport the pucks from the dewer into position
- a goniometer in which the samples are secured.

This method first emerged at Stanford using the Stanford Auto Mounting (SAM) system [62]. There are many variations of this system used globally such as MARVIN at DESY, RoboDiff at the European Synchrotron Radiation Facility (ESRF) [63] and BART at Diamond Light Source [64].

There are many preparation steps required to ultimately present the crystal to the beamline for experimentation. Firstly, the desired crystal must be selected and hand mounted onto the chosen loop, which requires a skilled and well-trained hand. Next the mounting loops are mounted onto a spine, a standardised unit which often includes a QR code on its underside for sample recognition. This spine is now loaded into a puck to safely hold the puck for transit as well as providing a known position for the robotic arm to retrieve the sample. The pucks are arranged within a liquid nitrogen dewar which is placed within reach of the robotic arm at the beamline, which moves the sample onto the goniometer for the experiments taking place [65; 66]. A diagram showing these steps is shown in figure 2.13.

The goniometer may be moved in the x, y and z plane and rotated laterally in order to move the selected crystal into the path of the beam. As the beam width is tunable, the beam does not necessarily encompass the entire crystal and therefore the range of motion that the goniometer has allows for the selection of a specific target site on the crystal [67].

The mounted samples often have a thin layer of their mother liquor coating the sample. The mother liquor's surface tension keeps the crystal mounted onto the loop and it should match the size of the crystal approximately or be slightly larger. However, if the mother liquor's surface tension is insufficient to keep the crystal mounted to the loop, a loop smaller than the crystal may be chosen [52].

Cryocooling is also performed on the protein mounted loops while experiments are occuring, in which the a stream of nitrogen gas is directed at the crystal with temperatures between 100 - 120 K. This is performed to minimise the evaporation of the mother liquor and also done to reduce the radiation damage the x-rays inflict upon the crystal, this damage may be so extreme as to mean that there is no measurable diffraction pattern after exposure to the x-ray diffraction experiments performed at room temperature. This cooling must occur quickly, avoiding the formation of ice which damages the protein structure due to expansion. Cryoprotectants may be added to the mother liquor to ensure that the water does not freeze, of which PEG, glycerol or ethyleneglycol is traditionally selected [52].

At room temperature, radiation damage occurs much more quickly as the x-rays cause radicals to form within the sample, which leads to reactions with the protein and ultimately this destroys its crystalline order. Cryogenic temperatures reduce the damage that the protein experiences because it limits the diffusion of the solution throughout the sample and therefore limits the movement of radicals through the structure [52].

However, the cryogenic cooling of the crystal structure inhibits the movement of side chains within the protein and it restricts access to the binding sites for any added samples such as ligands. Room temperature crystallography is key to understanding the behaviour of proteins at as close to physiological conditions. It helps to provide a better understanding of protein-ligand bonding, protein structure and is used to inform the discovery of medicines [68].

2.3.3 XFEL Hub

A free-electron laser (FEL) is a type of synchrotron light source which emits short pulses of synchrotron radiation. Within this system, an electron beam and and the beam of photons travel through an undulator in line with each other, these beams interact and generate amplified and coherent radiations [69].

An XFEL facility is a facility which features a free-electron laser of which the photons are within the range of x-rays on the electromagnetic spectrum. It allows for femtosecond crystallography, where a single pulse is bright enough to generate a resolvable diffraction pattern, however it also destroys the crystals [70]. One of these facilities, called the European X-Ray

Free-Electron Laser Facility (European XFEL) is in operation in Germany. It is an international project with twelve different countries participating, and UK is one of the partners [71].

The XFEL Hub housed within Diamond Light Source has been developed in order to fully prepare the XFEL users or operators for use on the European XFEL. The focus of the hub is to develop equipment and software for the European XFEL and to train and support users through sample preparation and data processing [72].

The current method used to present crystals to XFEL is use of a liquid jet which contains the protein crystals. This is requires a high production of the crystals and mother liquor, and is extremely wasteful as not every crystal which is jetted is struck by the x-ray laser [73]. Alternatively, a drop on tape method which deposits droplets containing protein crystals onto a kapton tape conveyor belt has been used at XFEL [74]. This method requires for the timing between the droplet deposition and the XFEL beam to be synced, and it does still introduce additional material into the beam pathway.

Chapter 3

TinyLev Sample Presentation

As discussed previously, acoustic levitation only became easily accessible upon the publication of work completed by Marzo et al. [3]. This allowed off the shelf components to be mounted upon a 3D printed structure to successfully levitate both solid and liquid materials. This chapter discusses the use of this system to present protein crystals within their mother liquor to the synchrotron beamline in I24 at Diamond Light Source.

3.1 System Construction and Verification

The TinyLev acoustic levitation system is a widely used system to demonstrate the levitation of polystyrene, liquid droplets and even insects. This is due to A. Marzo authoring an instructable which informed the construction of this system to be used in a large variety of settings such as schools, laboratories and even used for online videos which has further promoted the system itself [10].

The system was constructed following the step-by-step guide laid out in the instructable [10]. The STL file which shows the 3D render of the TinyLev support structure was imported into PreForm (Formlabs, MA, United States) software and this was printed using a Form 2 (Formlabs, MA, United States) 3D printer which provides a high resolution resin structure. This resin structure was cleaned of remaining liquid resin and the undesired solid resin which was used to support the structure as it was printed. Off the shelf transducers which had had their polarities established were fitted into the TinyLev structure and the legs were electrically connected with concentric rings of tinned copper wire. The opposing polarities were connected to a L298N driver which is controlled using an Arduino Nano microcontroller which sends pulses to the driver in order to operate the transducers at 40kHz. This circuit diagram is shown in figure 3.1. The code in which the Arduino Nano is programmed is provided within the instructable and it allows for the control of the phases of the transducers to move the acoustic traps up and down or to reset their positions [10].

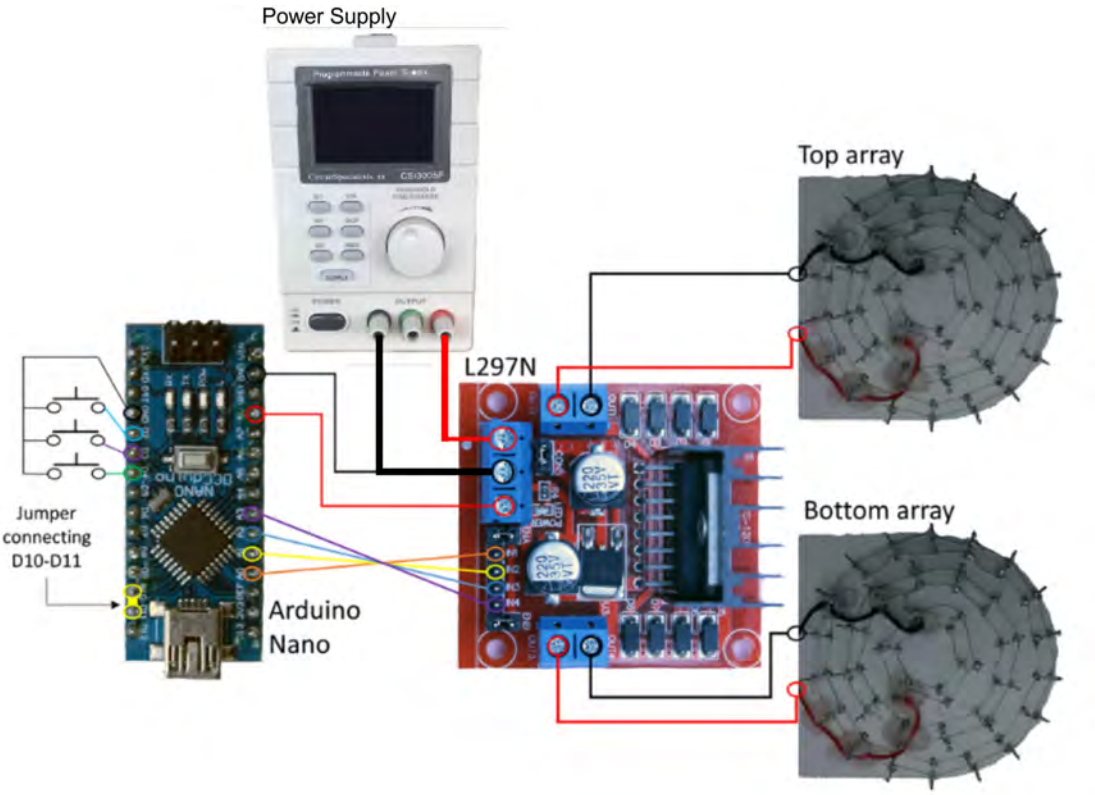

Figure 3.1: *A diagram showing the circuit configuration of the TinyLev acoustic levitator. A benchtop power supply powers the system through the 12V input on the L298N driver board. 5V is used from the board to power the the Arduino Nano. The Arduino Nano is programmed using code provided by the Acoustic Levitator Instructables. The connection of the Arduino Nano to the signal inputs on the L298N board allows for the individual control of its outputs to the transducer arrays. This figure is derived from the circuit diagram provided on the original acoustic levitator instructables [10] under CC BY-NC-SA 4.0.*

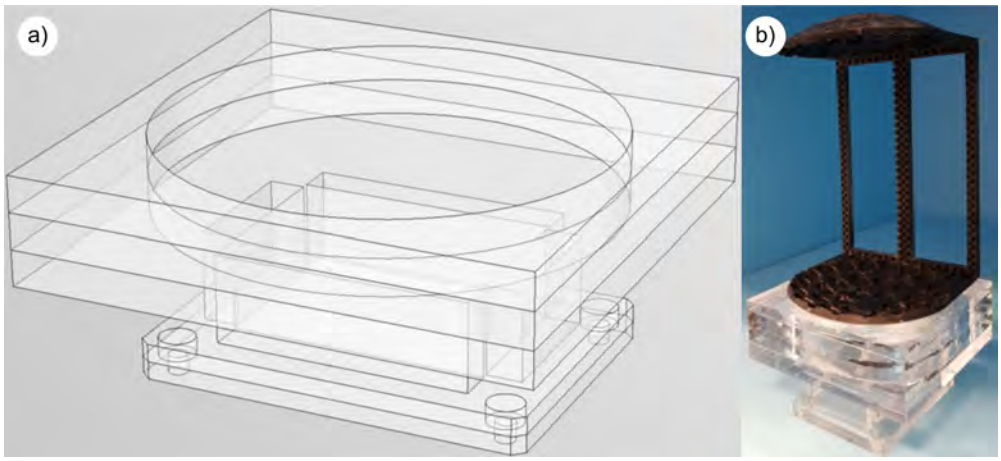

Figure 3.2: *A figure showing a) the designed adapter for between the goniometer at I24 and acoustic levitator and b) a photograph of the constructed mount, made from extruded acrylic sheets.*

In order to stand the TinyLev system upright, in the position in which the acoustic radiation forces work against gravity to suspend the droplet, an adapter is designed and cut from extruded acrylic sheets using a laser cutter. Extruded Acrylic Bonder (RS Pro, UK) was used to secure the cut sheets together by stacking the layers on top of each other. This adapter was designed to both stand the TinyLev system upright and to mount onto the vertical goniometer at the I24 x-ray beamline at Diamond Light Source. The design for this adapter as well as a photograph is shown in figure 3.2, the diameter of the hole in which the TinyLev system is sat is 85mm. This design was informed by the technical drawing for the pin base for the vertical goniometer assembly at the I24 beamline at Diamond Light Source which the adapter replaced and it is shown in appendix A. The key feature of this drawing is that it is secured to the goniometer by four M5 bolts spaced 60 mm by 41 mm apart, which was translated into the adapter design.

In order to verify the operation of the TinyLev system built, the transducers are checked one by one in order to ensure they are operating in phase with their neighbours, and if that is not the case, they are removed from the structure and replaced. These transducers are checked by powering the TinyLev system and using an additional pair of transducers which are connected to an oscilloscope to read the resultant wave. These detecting transducers are positioned directly above each emitting transducer in turn.

In addition, the acoustic field has been simulated by the original works in which the TinyLev system was published [3]. To verify the system constructed behaves identically to the system published, dry ice was held adjacent to the TinyLev whilst in operation in multiple positions and allowed to sublimate. The water vapor collected within the acoustic traps of the system, highlighting where materials may be suspended. Photographs were collected of the dry ice

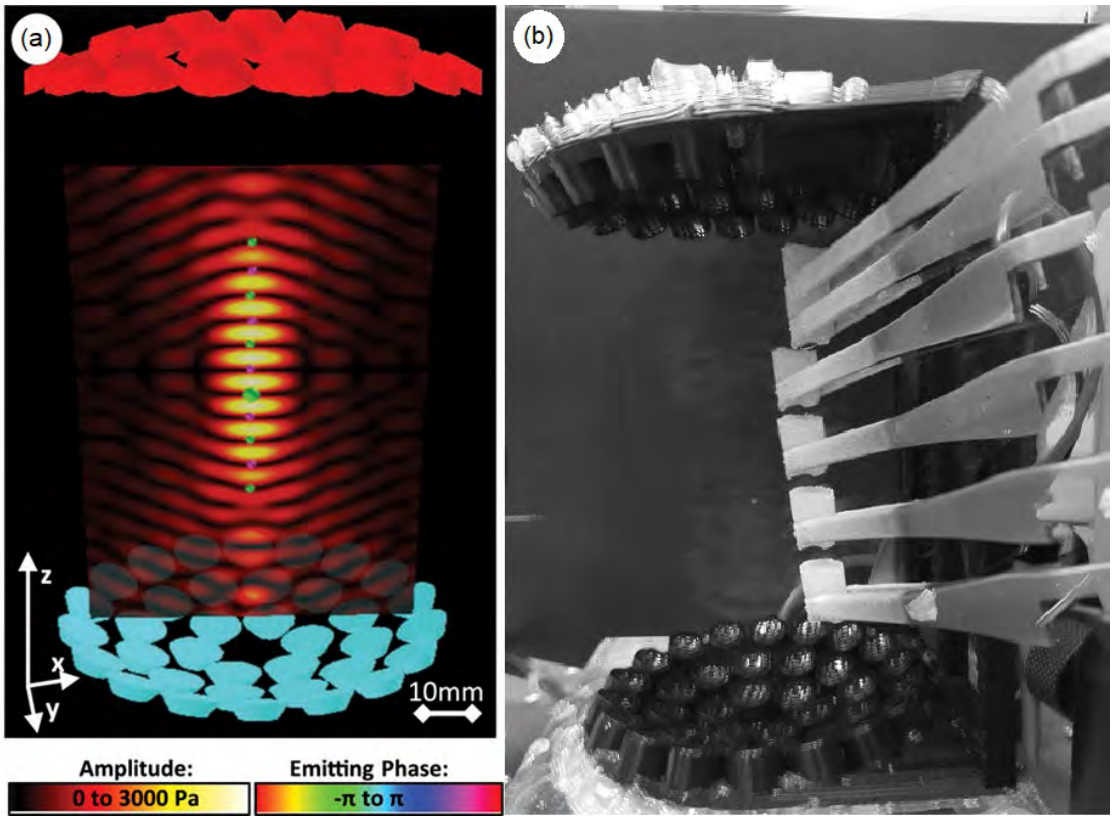

Figure 3.3: *A figure showing the simulated acoustic field of the TinyLev system from the original published works [3] in a) reproduced under CC BY 4.0. b) the acoustic field by the vapour from adjacent dry ice, captured by adding six images collected of dry ice in different positions relative to the TinyLev acoustic levitator.*

and vapor within these positions, these images were then converted to be 8-bit greyscale before combining them through the image addition feature in ImageJ software [75]. Figure 3.3 shows the simulated acoustic field on the left and the acoustic field highlighted by the dry ice on the right. This showed that the TinyLev system was constructed and behaved as the original published system as the size, shape and number of traps agreed with that which is shown in the simulation.

3.2 Droplet Properties

In this section, we discuss the properties of droplets which may be levitated within the TinyLev acoustic levitator. In the original publication of this system, Marzo et al. demonstrated that a variety of different materials and droplets of varying densities could be levitated including water, propan-2-ol and even spheres of sapphire [3]. However, preliminary experiments performed with the constructed system found that some injected droplets could not be levitated within this system because they would either destabilize and fall from the trap that it was contained within, the droplet would split into multiple adjacent traps or the droplet would not detach from the pipette tip. This section is about the factors that may cause a droplet not to be levitated.

In order to perform these experiments in a way in which the results can be recorded, the TinyLev acoustic levitator was stood upon the goniometer adapter in order for it to stand upright while data is collected. Two DCC1645C cameras (ThorLabs LTD, Ely, United Kingdom) were mounted on a 45 x 60cm optical breadboard in the positions as shown in figure 3.4, 90° from each other in order to image the droplet from these angles to determine the dimensions of the spheroid droplet. The levitated droplet was back lit by a diffused source from a pair of hammer head lamps, diffused through ground glass which is coloured with pink paper to allow edge detection when processing images collected of the levitated droplets.

Images of droplets were processed using code developed in MATLAB (Mathworks, Massachusetts, US) which is detailed in full in appendix B. This code reads in supplied images of droplets which are backlit with a red filtered light, specifically used so the selection of the green channel on the images would show information in regards to the droplet but any variation in the intensity of the light source would not be shown. A threshold is then applied to these images in order to make the droplet black and the background white. The image of the droplet is then filled to make the internal reflections also appear black. This image is then skeletonised, which outlines the droplet and deletes all other points in the image. The parameters of the ellipse are found using the $fit\_ellipse$ function [76] and these parameters are confirmed by plotting the measured ellipse using the *plotellipse* function [77] over the original images and visually ensuring

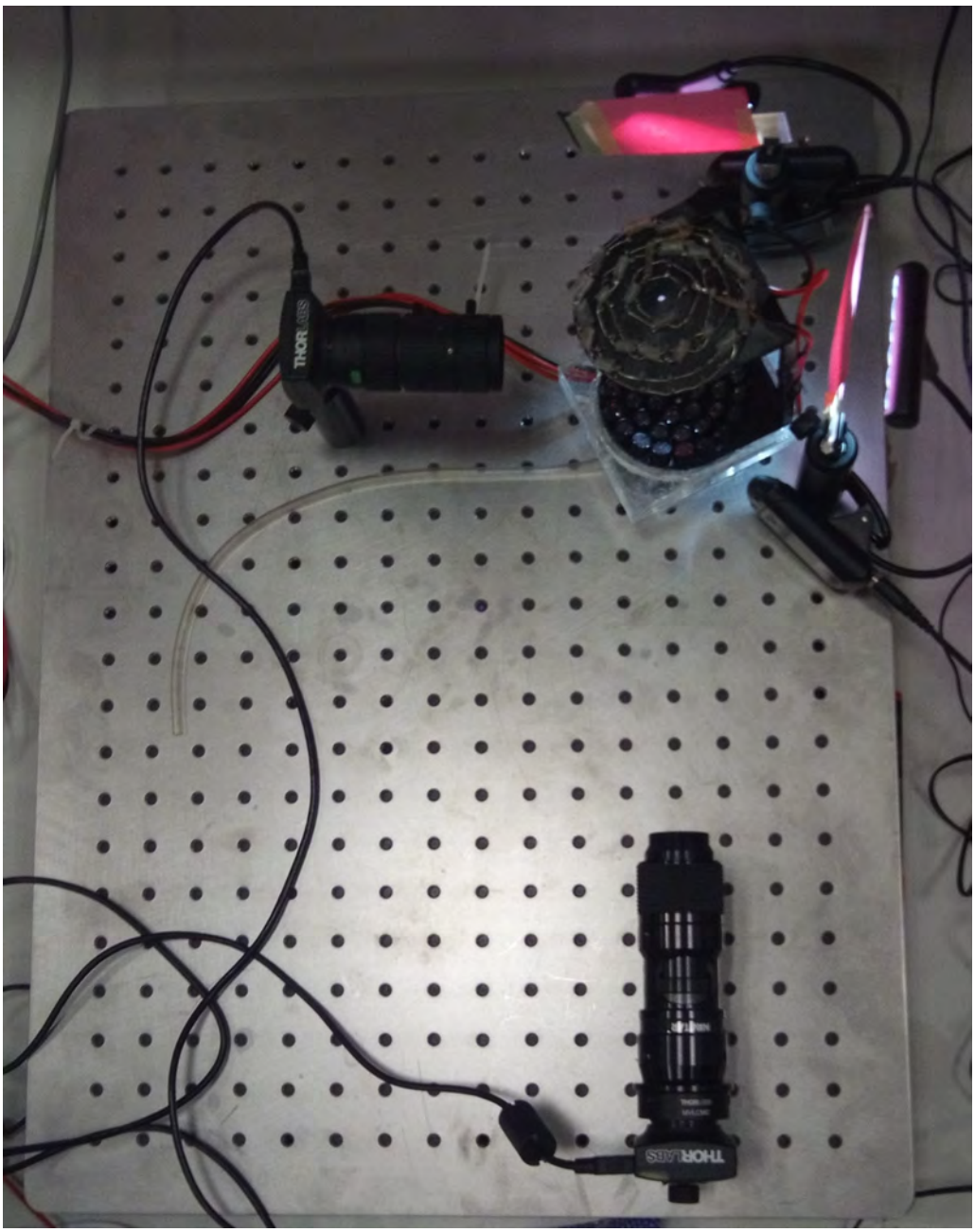

Figure 3.4: *A photograph of the camera configuration used to image droplets which have been suspended within the TinyLev acoustic levitator. The cameras are mounted upon an optical breadboard and directed toward the levitated droplet, which is backlit with two hammer head lamps diffused through ground glass coloured with pink paper.*

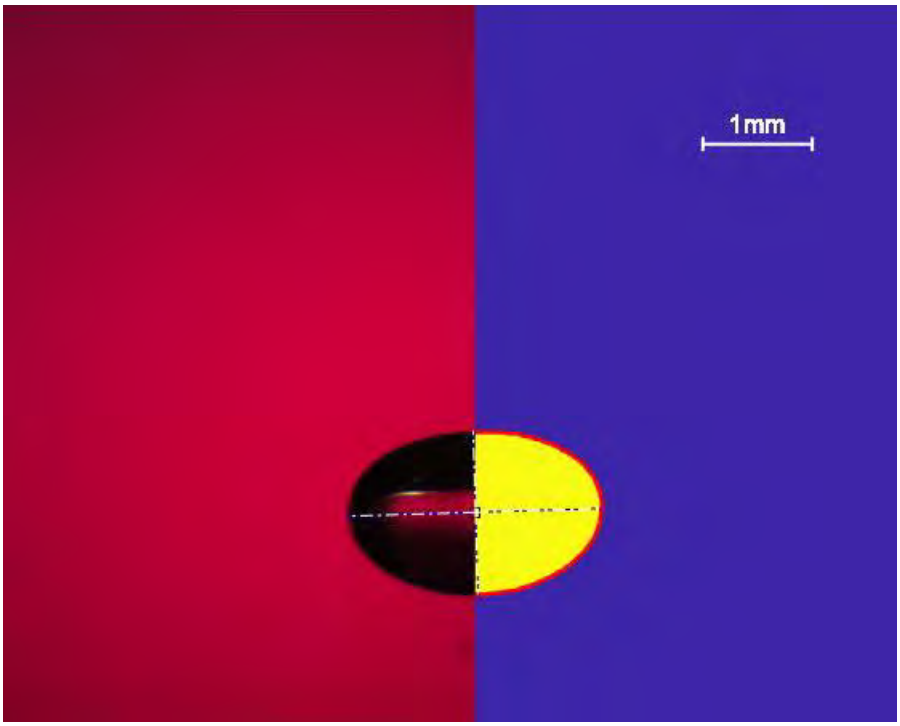

Figure 3.5: *An image comprised half of an original collected image of a levitated droplet and half of the fit output of the processing code fully detailed in appendix B. This fit outputs the dimensions of the ellipse, its rotation and its position within the frame.*

the fit. Figure 3.5 shows an image comprised of half the original droplet image and half the fit which may be visually inspected to ensure it is correct, the dimensions of the ellipse are obtained from the red outline shown on the right side of this image. This fit outputs the dimensions of the ellipse, its rotation and its position within the frame.

3.2.1 Volume

As discussed in chapter 2, the radius of a spherical particle suspended within an acoustic levitator needs to be considered in order to calculate the acoustic radiation force. From this, it may be inferred that the volume of the particle or droplet has a huge impact on its ability to be levitated. Many works suggest that the diameter of the particle must be significantly smaller than the wavelength of the sound emitted.

This section discusses the effect of droplet volume on the sphericity and stability of the droplet when it is being levitated within the TinyLev acoustic levitator. The sphericity of the droplet dictates the position which the protein crystals will be, as they tend to sediment when they are within their mother liquor suspension. And the stability of the droplet is also important as it will effect whether the droplet remains levitated as well as whether it remains within the x-ray

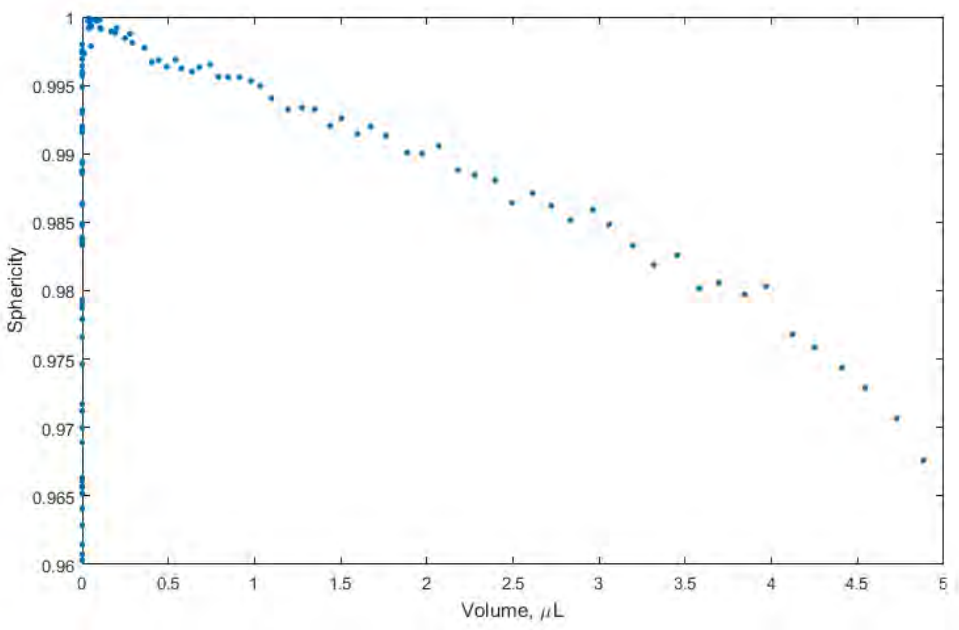

Figure 3.6: *A graph showing the effect volume has on the sphericity of water droplets when levitated within the TinyLev acoustic levitator at 11.5 V. As can be seen, lower volume droplets are more spherical than higher volume droplets for any given voltage.*

beamline at Diamond Light Source through out the duration of the experiment. Preliminary experiments revealed lateral movement of the droplets, particularly with smaller droplets which are levitated in the TinyLev system.

In the sphericity experiment, droplets of water were injected into the TinyLev system and images were collected at 60 second intervals as the droplet evaporated. This allowed the measure of sphericity at many different volumes for the various operating voltages of the levitator. In this experiment water is used as it is a volatile liquid and comprises a large proportion of the mother liquor. The collection of images at 90° angles revealed that the semi-major and semi-minor axes in both images were equal and therefore the droplets were oblate spheroids. Sphericity of oblate droplet is calculated by measuring the semi-major and semi-minor axes of the droplet which are shown in equation 3.1 as a and b respectively and used to find Ψ, which is the sphericity.

$$\Psi = \frac{2\sqrt[3]{ab^2}}{a + \frac{b^2}{\sqrt{a^2-b^2}} ln\left(\frac{a+\sqrt{a^2-b^2}}{b}\right)}, \tag{3.1}$$

The results of these experiments are presented in figure 3.6. It shows that the sphericity of the droplet increases as the volume decreases, meaning smaller droplets are more spherical. This is to be expected as the shape of the trap is non-spherical, it is a long and thin position of low acoustic pressure, so a larger droplet would deform to fit within this position.

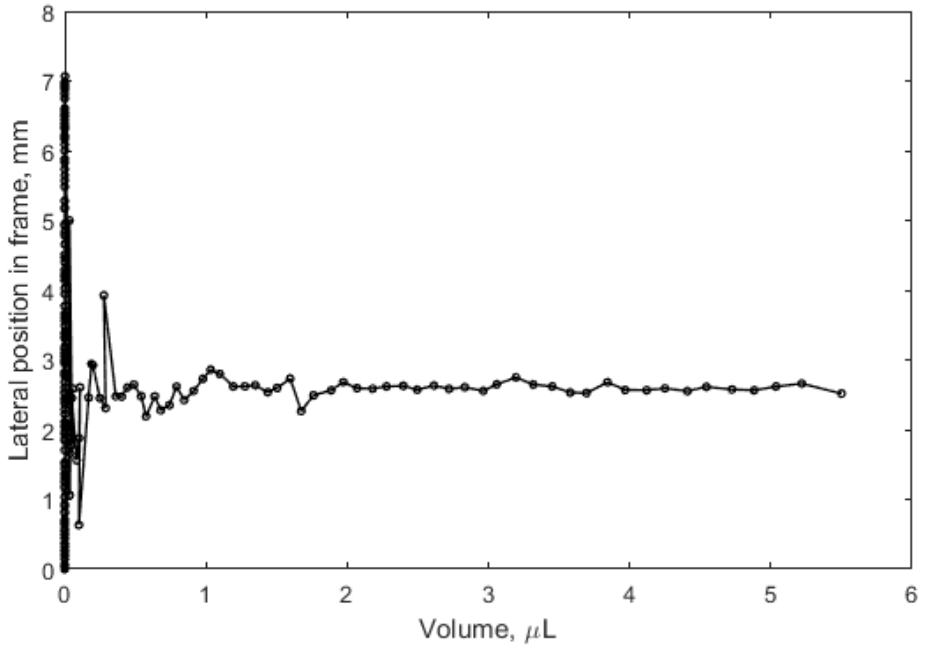

Figure 3.7: *A graph showing the lateral position within the frame of a water droplet as it evaporates. Images of this water droplet was collected every minute as its volume reduces due to evaporation. This graph indicates that the position of the water droplet is consistent between 2 - 3 μL but the smaller sub-microlitre droplets vary in position more from minute to minute.*

For the analysis of the droplets stability, the images used to determine the sphericity of the droplets were used. The lateral position of the water droplet was tracked in the images with 60 second intervals whilst it evaporated. The lateral position of the water droplet against its volume is shown in figure 3.7. This graph revealed that the droplet position fluctuated over its lifetime, but was shown to be the most stable between 2 - 3 μL. The lateral position of the droplet also varied significantly when its volume was below 1 microlitre.

3.2.2 Evaporation and Heating

The evaporation of droplets is an important factor to consider when preparing the TinyLev acoustic levitator to be used to suspend droplets in front of the x-ray beamline at Diamond Light Source. This is because if the sample evaporates significantly, the mother liquor environment may change in terms of pH and concentration, and this can cause dehydration of the protein crystals themselves which would show in the x-ray diffraction patterns.

In addition, without an automated sample delivery system, the sample must be loaded manually into the TinyLev acoustic levitation system. The hutch, which houses the x-ray beam, must then be searched for any remaining personnel and the large door shut. The person-free

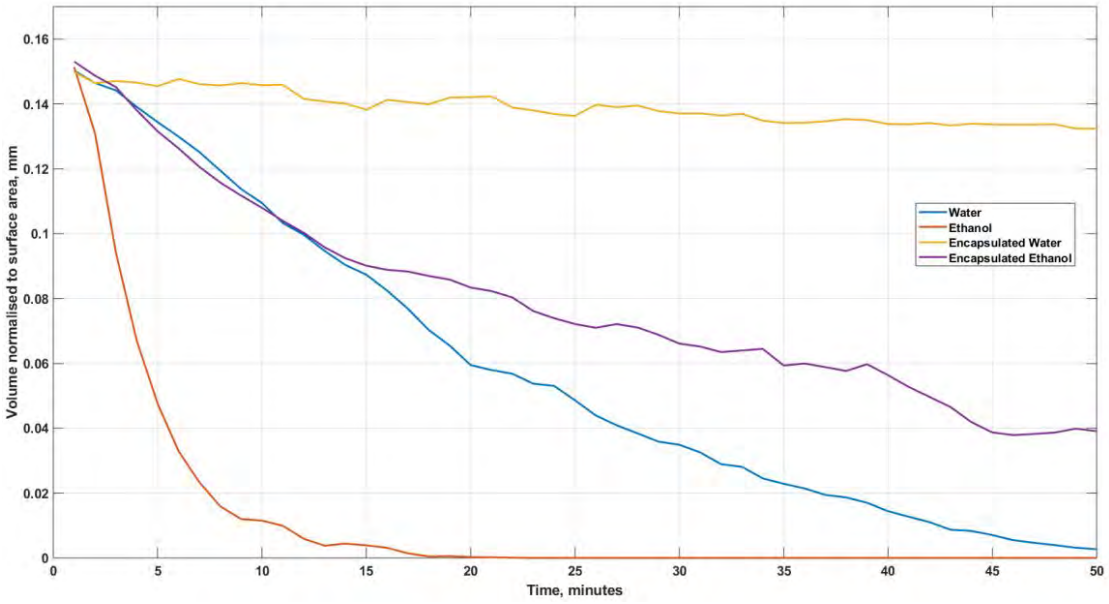

Figure 3.8: *A graph showing the volume change over time of water and ethanol with and without a silicone oil coating. There is a significant volume reduction of the ethanol and water droplets within the first 10 minutes of the experiment, this is greatly reduced by the coating of silicone oil.*

hutch is confirmed by activating a button outside the x-ray hutch and a short period of time must elapse before the beam may be turned on. The detector is moved out of the way when manually loading the sample into the acoustic levitator and it must also be moved back into place, the closest position to the sample, before the x-ray diffraction data may be collected. These processes take a few minutes so it is important that the sample does not significantly reduce in volume during this time.

In these experiments droplets of water as well as droplets of ethanol were used in order to capture images of volatile liquids and monitor the evaporation rate of the liquids within the TinyLev acoustic levitator. This data is presented in figure 3.8 and shows the decrease in droplet volume over time. From this graph we can see a significant volume reduction within the first 10 minutes of the experiment for both water and ethanol droplets, with all of the ethanol evaporating within approximately 17 minutes. As the mother liquors of the protein crystals tend to have a large proportion of water and many other volatile liquids, this data suggests that the protein crystal would dehydrate in the time between manual sample loading and data collection.

In order to determine whether the TinyLev acoustic levitator increases the evaporation rate of droplets, thermal imaging of the droplet is performed in order to find whether the droplet experiences any heating, as previous work with langevin systems suggested a temperature increase by imparting significant energy into the levitated material or substance. These experiments were

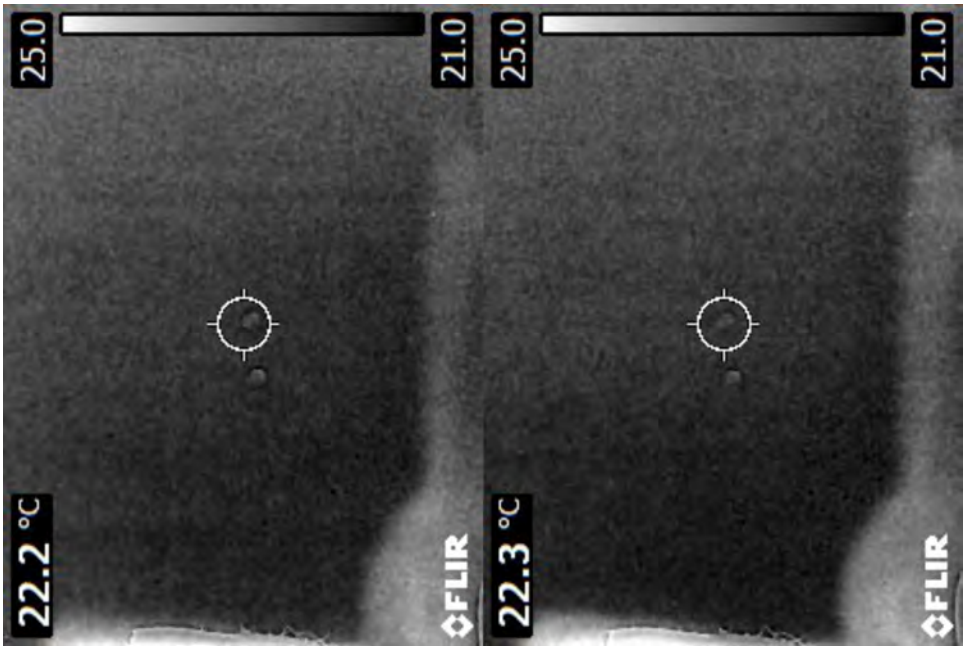

Figure 3.9: *Thermal camera images of a levitated droplet of silicone oil within the TinyLev system, the image on the left shows the temperature of the droplet when it was first deposited and the image on the right is after an hour has elapsed. It can be seen that the droplet underwent negligible temperature change, and therefore heating due to the acoustic levitator can be regarded as negligible. This is even more so since the experiments performed on the droplets at Diamond Light Source are intended to be performed during a shorter time frame within a temperature monitored hutch.*

Figure 3.10: *A time series showing an example of the droplet oscillation which causes the droplet to fall from the trap when levitated in the TinyLev acoustic levitator.*

performed on silicone oil as it is non-volatile and would remain suspended within the acoustic trap until the droplet was removed or until the system lost power. Some of these images from the thermal camera are presented in figure 3.9 and clearly show negligible temperature difference between when the droplet was first suspended to an hour later. However, to ensure that the slight variety in temperature was due to environmental factors rather than heating from the acoustic levitator, the temperature of the area behind the TinyLev acoustic was also sampled. The ratio between these temperatures was compared to ensure that it is consistent throughout the time frame of the experiment. The negligible temperature difference is likely due to the low-power transducer array which is used at a maximum voltage of 12V rather than the high-voltage langevin systems which have been used in other works.

In order to perform x-ray diffraction experiments on levitated droplets which contain protein crystals, the evaporation of the sample must be slowed in order to not cause damage to the crystal itself through dehydration. As mentioned in chapter 2, this has previously been done by cryogenically freezing the samples which are presented to the beamline, but this has been known to cause damage [78]. Ideally the samples would remain within its mother liquor and at room temperature when experiments are being performed to collect data representative of the protein crystal in situ.

3.2.3 Viscosity

Although Gor'Kov's expression does not suggest a dependence on viscosity for the levitation of a substance, preliminary experiments showed that liquids which were more viscous would not detach from the needle tip when injecting them into the acoustic levitator trap, and that liquids with significantly lower viscosity tended to become disrupted and split into multiple droplets in adjacent traps or fall out of the levitator completely. A captured series of this disruption is shown in figure 3.10.

In order to perform this experiment, droplets of silicone oil were imaged whilst suspended within the TinyLev acoustic levitator, with the voltage being changed for each image. Varying viscosities of silicone oil were used in the range of 5cst - 500 cst as these were readily available

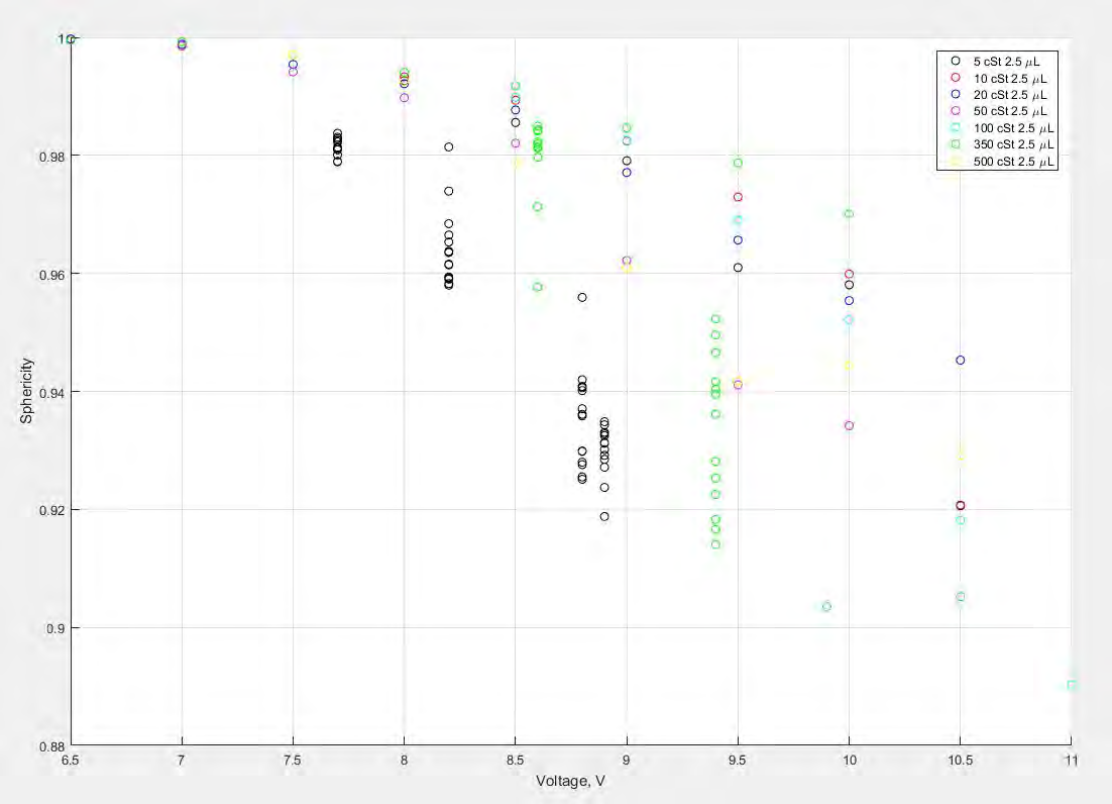

Figure 3.11: *A graph of sphericity of silicone oil droplets against operating voltage of the TinyLev acoustic levitator, varying viscosities of silicone oil was used. This graph shows a reduction in sphericity as the voltage is increased, however it suggests no relationship with the viscosity of the droplet itself.*

and gave a good range to determine whether there was any reliance on viscosity for a material to be levitated. Silicone oil was selected rather than using those materials used in preliminary experiments as silicone oil benefits from having the same density for different ranges of viscosity, as sample density does effect the acoustic radiation force on the droplet according to Gor'Kov's expression.

The data for these experiments is presented in figure 3.11. This data shows a trend in which sphericity decreases as the voltage is increased, likely due to the acoustic traps being stronger and exerting more force from the top and bottom of the droplet. However, this graph suggests that there is no relationship between the sphericity of the droplet and its viscosity.

Due to the viscosity of the silicone oil, some samples would not detach from the pipette when deposition was attempted, particularly at low operating voltages for the high viscosity samples. In addition, the low viscosity samples seemed to be disrupted and either split into multiple droplets in adjacent traps or fall from the TinyLev acoustic levitator when the system was operating at its highest voltages. 350cst silicone oil was the sample which was found to remain suspended in

the acoustic levitator for the largest range of operating voltages as it readily detached from the pipette tip and remained as a single droplet for the span of operating voltages of the TinyLev acoustic levitator.

3.3 Silicone Oil Encapsulation

Many of the desired samples of protein crystals within their mother liquor have insufficient surface tension to maintain a droplet when levitated within the TinyLev system. In order to overcome this, the droplets were coated with silicone oil as it provided stability to the droplet shape and allowed for the levitation of protein crystals within their mother liquor for x-ray diffraction experiments

In order to impart this silicone oil coating to the droplets, 10uL pipette tips were coated with Rain-X (Illinois Tool Works, USA) which is a commercial chemical hydrophobising agent. 2.5uL of 350cSt silicone oil (Sigma Aldrich, UK) was collected and then dispensed using these pipette tips, a thin layer remaining within the tip after doing so. The silicone oil with a viscosity of 350cSt was selected as the experiments performed in section 3.2.3 revealed that this particular variety of silicone oil remained stable for the largest range of TinyLev operating voltages. The sample was then collected using this same pipette and tip and was then deposited within the central trap of the acoustic levitator.

Gravimetric analysis allowed for the approximation of silicone oil which remained in the tip after its expulsion. This was performed by measuring the mass of the pipette tip before the collection of the silicone oil and after its expulsion. This left approximately 0.35uL of silicone oil coating the internal surface of the pipette tip. This method was also deployed to determine the volume of silicone oil which was imparted onto the coating of the sample. For this the sample was simply distilled water as many of the samples of interest have a high percentage of water. The mass of the pipette tip was recorded after the silicone oil expulsion but before the sample collection as well as after the deposition of the sample.

It has been well observed that the power supplied to an acoustic levitation system has a significant effect on the shape and stability of droplets which are suspended within an acoustic levitator. This relationship is demonstrated in figure 3.12, where droplet sphericity and spatial stability is presented as a function of the applied voltage through the TinyLev system which is suspending an approximately 2.5 μL silicone oil coated water droplet. Sphericity, Ψ, is calculated as shown in equation 3.1, where a and b are the semi-major and semi-minor axes of the droplet respectively and spatial stability is represented as the standard deviation of the distance that

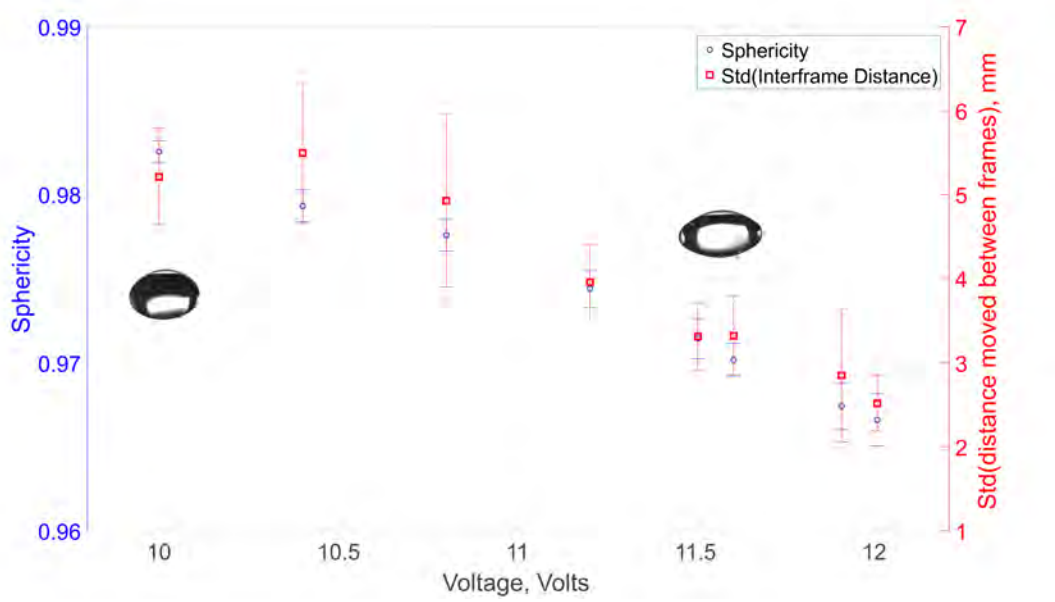

Figure 3.12: *Plot of the droplet sphericity and spatial stability as a function of applied voltage on a silicone oil coated water droplet. Voltages above 11.5V provided the greatest stability, however it caused a significant drop in sphericity. The TinyLev was therefore supplied with 11.5V for all Diamond Light Source experiments.*

the centre of the droplet moves between each image collected. A more spherical droplet is desired, as it allows for a good prediction of the protein crystals location during x-ray diffraction experiments, as the crystals tend to sediment toward the bottom of the droplet. However, a stable droplet is more important as this means the droplet is likely to stay within the x-ray beam at Diamond Light Source for the duration of any experiment performed. From the results presented in figure 3.12, it was found that a TinyLev operating voltage of 11.5V allowed for a compromise between sphericity and stability of the droplet levitated, which was spherical enough to predict the position in which the proteins crystals would be in future experiments as well as stable enough that the droplet would remain within the desired position during x-ray diffraction experiments.

3.4 Experiments at I24, Diamond Light Source

Proof of concept experiments were performed at Diamond Light Source in order to ensure that the levitation of liquids is feasible within the beam line, as well as to ensure that the acoustic levitator does not cause significant damage to the protein crystal sample within the mother liquor, so that diffraction experiments may still be performed.

3.4.1 Sample Preparation

A standard sample of lysozyme crystals from chicken egg white was selected for the proof of concept experiments as it is a very well explored structure and we would easily be able to compare the resolved structure to a large database of structures in order to determine whether there is any damage caused by the acoustic levitator. This section covers the method used to form these lysozyme crystals with a size of approximately 100-800μm.

Large lysozyme crystals with a width of 100–800μm were grown using a combination of the salting out method and seeding, a method which grows larger crystals which saves protein and improves their diffraction quality. Commercial lysozyme from chicken egg white (Product Number L4919, Sigma-Aldrich, UK) was initially re-suspended to a concentration of 25mgmL^{-1} in 100mM sodium acetate buffer solution. Micro-crystals were initially grown by mixing this protein solution 1:1 with a solution containing 28% (w/v) sodium chloride, 8% (w/v) PEG 6,000 and 100mM sodium acetate buffer solution with pH 3.0 in a centrifuge tube. After 1 hour this resulted in a highly concentrated microcrystalline slurry, each of which could act as sites to grow larger crystals. The longest dimension of any crystal was under 5μm and was diluted 1 x 10^7 fold. This seed solution was then mixed with a precipitant solution (containing 10% (w/v) sodium chloride, 25% (w/v) ethylene glycol and 100mM sodium acetate buffer solution with pH 4.8) and also with a protein solution ($75 mg mL^{-1}$ of Lysozyme in 100mM sodium acetate with pH 3.0) in a ratio of 1:2:3μL (seed:precipitant:protein). The drops were then incubated overnight at 18°C and harvested the following day.

These single crystals were collected using a 10μL pipette which had been prepared to impart a silicone oil coating as described in section 3.3. This was performed underneath a microscope to ensure the successful collection of the crystal as the crystal size was of comparable size to the pipette tip hole.

3.4.2 Equipment Setup and Alignment

The TinyLev system used is well described in Section 3.1. However, in order for it to fit on the beamline an adapter had to be constructed. This adapter was designed to be secured to the vertical goniometer on the I24 beamline at Diamond Light Source as well as to the bottom of the TinyLev system, allowing it to stand upright before the x-ray beam as shown in figure 3.13. This figure has labelled the features of the beamline, the acoustic levitator and shows the goniometer in which the system is mounted.

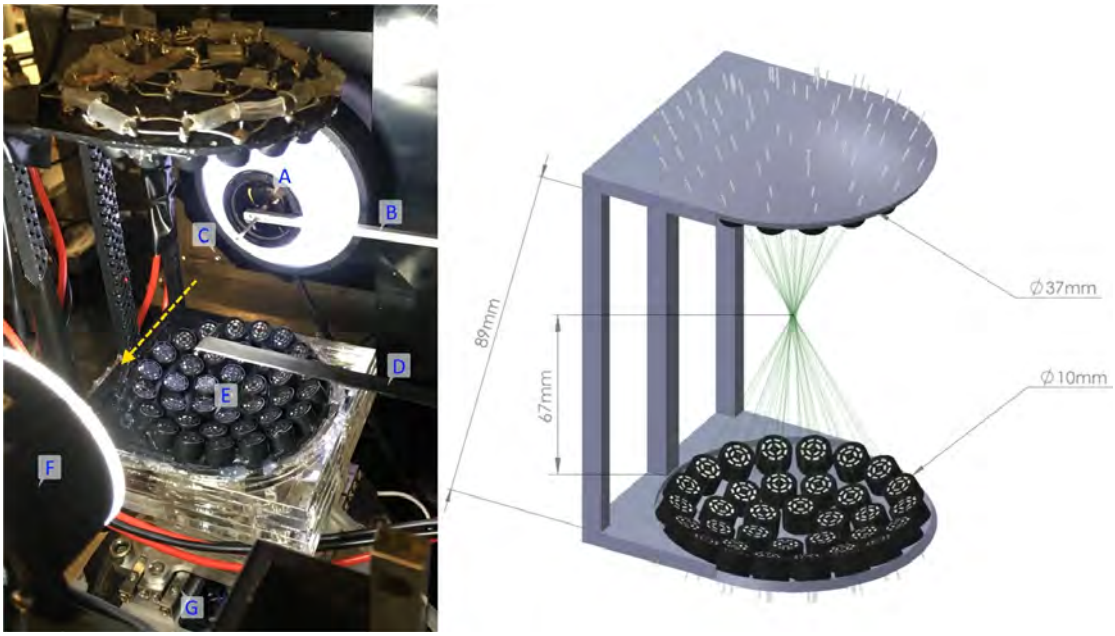

Figure 3.13: *Left: A photograph of the TinyLev system mounted on the I24 beamline at Diamond Light Source with the X-ray beam path marked with a dashed yellow arrow. (A) A high-magnification viewing system, (B) The X-ray scatter-guard, (C) A levitating droplet, (D) The beamstop located out of position, (E) The TinyLev Acoustic Levitation system, (F) a backlight used for positioniong samples which is retracted during data collection, (G) The vertical goniometer which the TinyLev system is mounted on for sample positioning. Right: The model of the TinyLev acoustic levitation system (E) annotated with key dimensions and showing the focal point of the transducer array in which a droplet sits.*

The alignment of the TinyLev is performed by suspending a 2-3mm expanded polystyrene ball within the central trap of the system and adjusting the position of the goniometer until the ball is visible on the alignment camera. Following this, the ball is removed so the fine adjustment can be made after deposition of the sample.

The silicone oil coated samples, which are prepared and collected as described in section 3.3, are deposited into the TinyLev acoustic levitator.

In the TinyLev instructable, it suggests depositing liquids using a syringe with a bent needle and the tip removed [10]. However, in order to deposit microlitre volume a 10μL pipette tip was bent approximately 4mm from the end before treating them with Rain-x and silicone oil. The droplet volumes deposited were approximately 2.5μL, they were intended to be positioned within the central trap of the TinyLev system but as the traps are positioned close to one another the droplets often fell into the traps either side of the centre. To correct the positions of these droplets, the electronic phase change capabilities of the TinyLev system were utilised to enable the fine movement of the trap to ensure its alignment to the beamline. The droplets position was confirmed using the alignment camera of the beamline, to ensure the droplet will be successfully struck by the x-ray beam.

3.4.3 Synchrotron Data Collection

The droplet containing the protein crystal within its mother liquor and coated in silicone oil is suspended before the x-ray beam at I24 within the TinyLev acoustic levitator. I24 is a tunable microfocus synchrotron beamline, meaning that the beam size may be adjusted electronically through the control of a series of mirrors and lenses. The incident area of the 0.9686Å X-Ray beam was set to 50 x 50 μm and focused using a pair of Kirkpatrick-Baez mirrors. Diffraction data was collected using a Pilatus3 6M (Dectris, Switzerland) detector running at 100Hz using all of the detector modules within the 5 x 12 matrix. Temperature and relative humidity at the position of the sample in the beamline were recorded at 21.4°C and 30% respectively, at the start of the experiment and later found to vary with a standard deviation of ±0.2°C and ±3% over a 24 hour period.

Raster scans were initially performed over the cross section of the droplets to determine the location of crystals and it was found that despite the rotational motion, the crystals sedimented towards the bottom of the droplet due to gravity as expected. This area was targeted for a data collection run on a newly mounted droplet as described in section 3.4.2 containing an estimated 4–6 crystals. 5,000 diffraction images were collected using the detector. This collection only took 50 seconds, during which time the droplet did not appear to physically change, as observed on

the high magnification camera system used for alignment. The droplet volumes were consistent over time at ambient temperature with no requirement for humidity control. The silcone oil coating did not seem to increase background X-ray scatter.

The open source Diffraction Integration for Advanced Light Sources (DIALS) [79] software package was used to analyse the diffraction data from the collected images using *dials.stills_process* to perform diffraction spot finding, space group and unit cell indexing, determination of the crystal rotation matrix, and reflection integration as proposed by Brewster [80]. An example diffraction pattern including the resolution rings can be seen in figure 3.15.

The crystal structure was solved using molecular replacement with protein data bank (PDB) entry 5KXO [81]. Molecular replacement is a trial and error process used when a related structure is available [82]. As the protein crystal studied in this experiment is lysozyme, lysozyme entries in the PDB are suitable for the molecular replacement method to be used. The automated tool phenix.autobuild [83] was used to build the model of the protein as well as Coot [84], which is a molecular- graphics application which may also validate biological macromolecules and create the electron density maps.

3.4.4 Results and Discussion

The lysozyme crystal structure (deposited under PDB entry 6QQ3 [12]) was determined from a single continuous collection run of 5,000 images on a drop containing an estimated 4–6 crystals with dimensions ranging from 100 - 800μm.

The crystallography data analysis tools described in section 3.4.3 were exploited to analyse detector frames on an individual basis as the levitating droplet does not have fixed rotation between each frame. As few as 500 images were required for a 96.7% complete data set to a resolution of 1.69Å. However, all diffraction patterns from the best data collection run were used to optimise the data set. The serial method assumes each detector frame is an individual experiment and in turn generates a crystal lattice for each instance, with different orientations. Detailed analysis of the 5,000 image structure solution revealed the presence of multiple lattices and their respective motions during the collection of the diffraction patterns. A single crystal lattice remained within the beam for 2260 frames, figure 3.16 illustrates the motion of this lattice within the droplet which is suspended by an acoustic levitator in front of the x-ray beam. It showed a rocking motion with slight rotation, but it does not limit the collection of diffraction pattern which is performed 100 times per second.

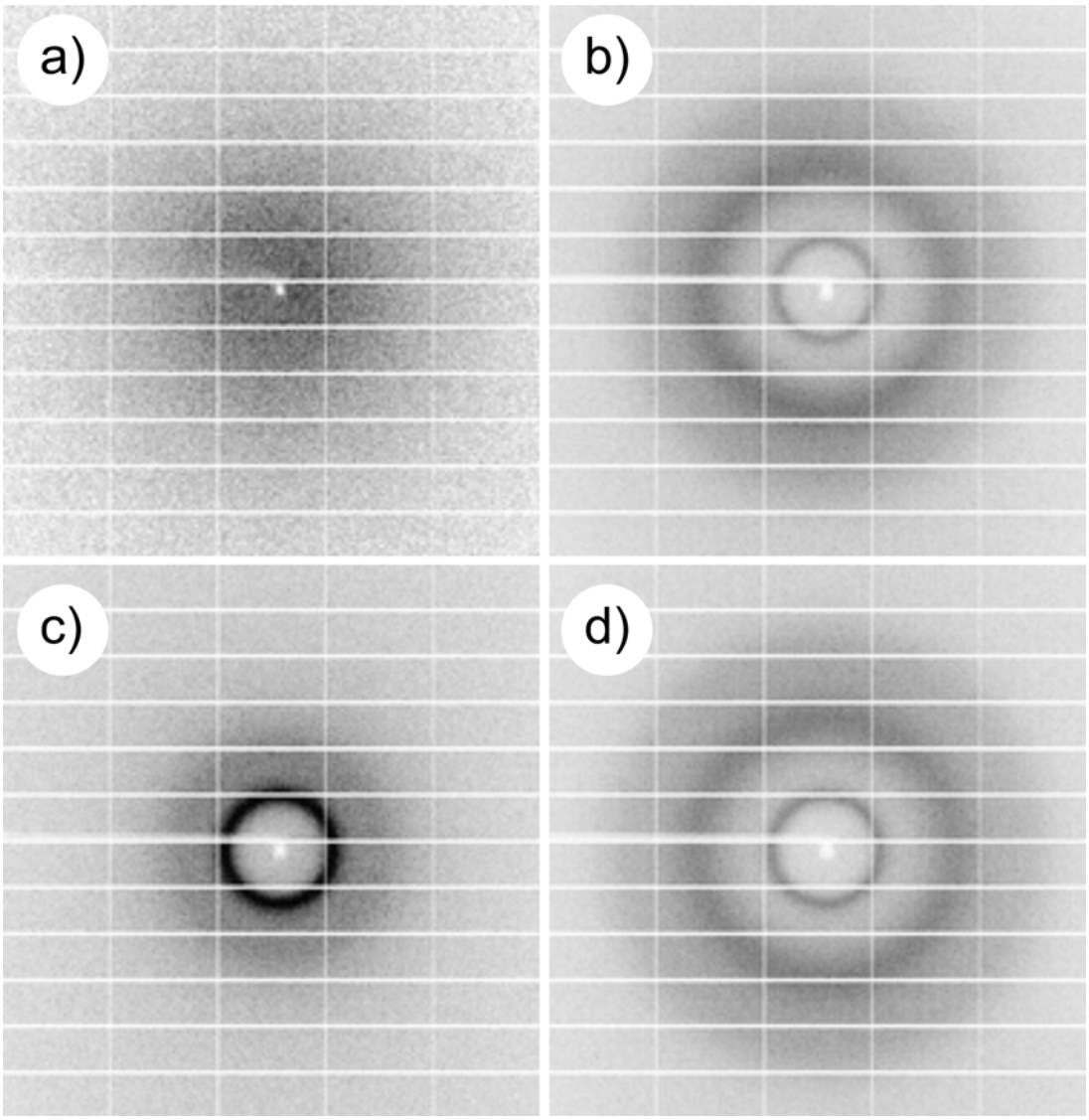

Figure 3.14: *X-ray scattering patterns collected from a) air with no droplet within the beam path, b) a levitated droplet of buffer solution, c) a droplet of 350cst silicone oil, d) a silicone oil coated droplet of water. Rings can be seen on the diffraction pattern caused by the liquids, they are rings rather than discrete spots as they represent the average distance between the electrons in the liquids.*

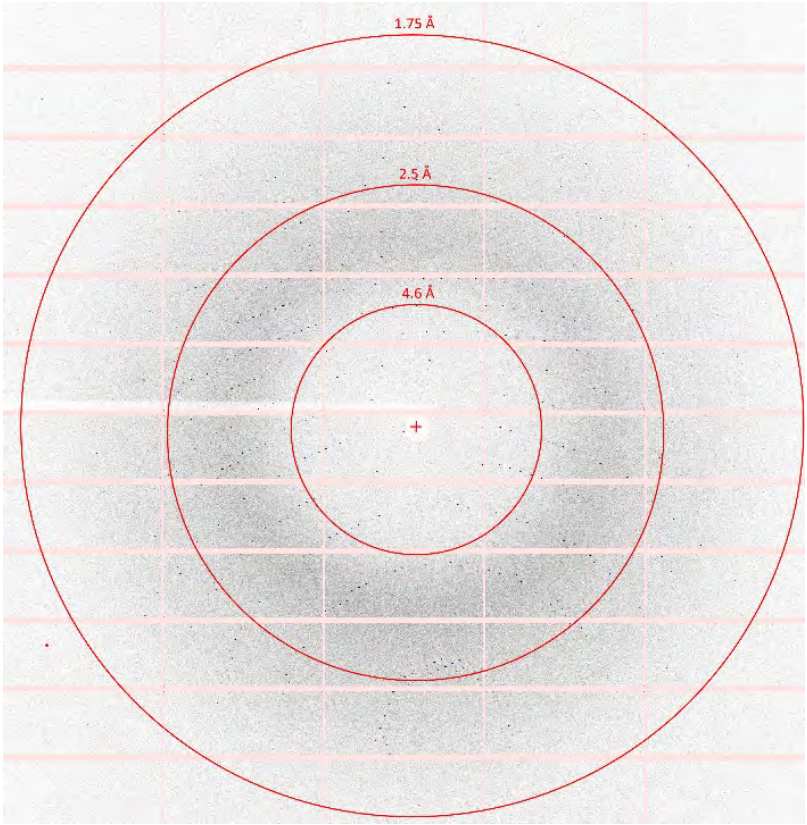

Figure 3.15: *An example image of data collected by the detector during crystallography experiments. The halo effect is created by the diffraction of x-rays through the non-crystalline mother liquor. Spots of varying position and magnitude are produced from the x-ray diffraction of the protein crystal. The resolution rings are shown on this image and show the separation between the lattice layers in a particular orientation. For example, a bright spot located on the 2.5 Å ring would represent a lattice spacing of 2.5 Å in that particular orientation. This means that this experimental set up allows for a maximum resolution of 1.71 Å.*

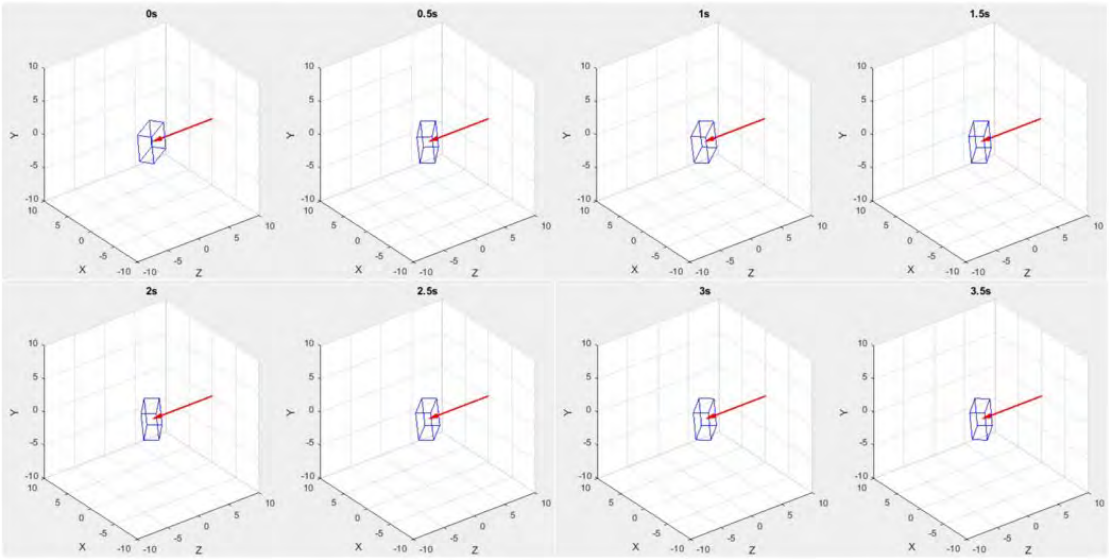

Figure 3.16: *Still image series collected from an animation which is shown in full elsewhere [11]. The collected diffraction data was used to construct the animation, to illustrate the motion of a crystal within the beamline whilst it is levitated using the TinyLev acoustic levitator. The beamline is depicted by the red arrow, and the crystal is shown in blue. These series of still images shows that the crystal exhibits a rocking motion whilst it is being levitated.*

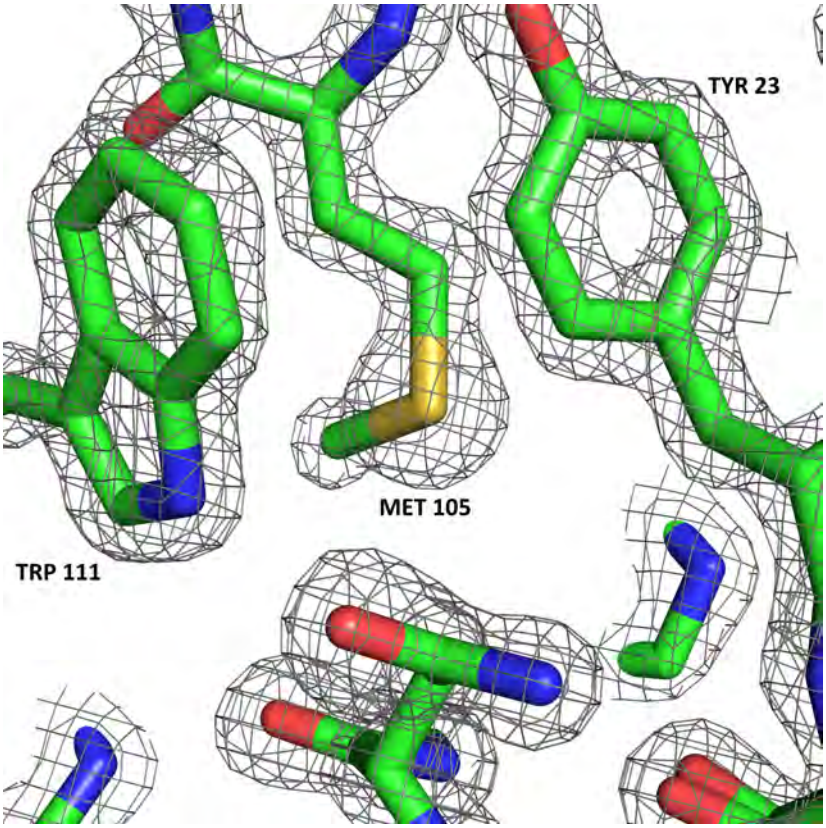

Figure 3.17: *The 3D electron density map of the lysozyme crystal in a silicone oil coated droplet of mother liquor levitated and presented to the beamline using the TinyLev acoustic levitator. PDB ID: 6QQ3 [12]. Graphics produced using PyMOL [13]*

Example electron density from the structure (available as PDB entry 6QQ3 [12]) is shown in figure 3.17. This demonstrates that an acoustic levitator is appropriate to collect high quality structural information from acoustically suspended droplets at room temperature, as the resolution of the structure is regarded as good as well as the structure being successfully identified as lysozyme.

The dose on the protein crystals was estimated from the 2260 frames collected in which a single crystal remained within the beam. The use of the RADDOSE-3D [85] program combined with the crystal size approximations calculated a diffraction weighted dose of 210 kGy for a crystal size of 100 x 100 x 200 μm and a crystal size of 200 x 400 x 800 μm is effected by a diffraction weighted dose of 150kGy.

As only 500 images were required for a 96.7% complete data set, the first and last 750 images of the 2260 image run of which the crystal remained within the beamline were compared in order to investigate whether there were any radiation induced changes. Isomorphous difference maps from these collated images did not show any features which were obviously different from each other, which suggests that there was not significant damage to the protein crystal caused by x-ray radiation or by the use of the low power TinyLev system used to confine the crystal and mother liquor over the time course of the experiment.

These results clearly show that acoustic levitation is a viable candidate for the presentation of protein crystals within their mother liquor to an x-ray beam at synchrotron. This system offers advantages over the traditional x-ray diffraction presentation methods of cryogenic samples fixed on pins which are moved in front of the beam as the suspension within this device means the sample is closer to the state it would exist within nature, with the crystal submerged in its mother liquor and at room temperature. Additionally, the contact free nature of this method will allow for sample mixing experiments to be feasible as additional substances may be added to observe the changes it causes to the sample while the experiments are being performed.

3.5 Summary

This chapter of work saw the construction of the well-established TinyLev acoustic levitator, and the confirmation of its operation using the sublimation of dry ice to highlight the traps of the device. This work also detailed the effects that volume of the suspended droplet and operating voltage of the system has on the sphericity and stability of levitated samples. Both of these properties are of interest as a more spherical droplet allows for a better approximation of a protein crystals position within the mother liquor, and a more stable droplet increases the

likelihood that the crystal would remain within the beamline throughout an x-ray diffraction experiment. Samples with surface tension which is too low cannot remain as a droplet and fall out of the acoustic levitator. Samples with very high surface tension are often unable to detach from the pipette tip. In order to levitate all droplets regardless of its surface tension, silicone oil encapsulation was imparted to the droplet which encouraged the sample to detach from the pipette and remain levitated. The TinyLev device was installed at Diamond Light Source for the proof of concept experiments using an acoustic levitator as a sample presentation method. A lysozyme protein crystal within its mother liquor was selected for these first experiments with silicone oil encapsulation also imparted. These experiments revealed that this sample presentation method is effective as the data provided the correct lysozyme crystal structure with a very good resolution, and no damage was recorded to have occurred due to the x-ray beam or the incident ultrasound from the levitator.

Although the silicone oil layer on the sample stabilised the droplet and reduced the mother liquors evaporation rate, meaning that the protein crystal within would not dehydrate, it does complicate both the automation and sample mixing processes. The imparted silicone oil would need replenishing within the pipette of an automated system, increasing the time between sample depositions. In addition, during sample mixing experiments, the added solution to the sample droplet would first have to permeate the silicone oil coating before it can mix, again increasing the length of the experiments significantly. In order to not require this silicone oil coating in future experiments, a bespoke acoustic levitator must be designed which is stronger and better confines the droplet to a single position with improved stability. The following chapter details the design considerations, construction and investigation of such a bespoke acoustic levitation device.

Chapter 4

DLS-Lev System Design

The TinyLev system was successfully used to levitate droplets within the x-ray beam at I24 at Diamond Light Source. However in order to levitate a droplet containing protein crystals and their respective mother liquor, the droplets had to be coated with silicone oil, in order to stabilise the droplets and remain suspended throughout the duration of the experiment. In addition, top loading was unsuccessful with the TinyLev system as it was not strong enough to detach droplets from the pipette or needle tip. Due to this an alternative levitation system was explored, so that sample loading would be possible from above the system, allowing sample mixing in future experiments. This chapter discusses the design and construction of such a system.

4.1 Revised Specification

Aesthetics	How the system looks is not a primary concern, as it will be designed for functionality within the constraints of the space available on the beamlines at Diamond Light Source.
Cost	There is no maximum cost for the system, however the TinyLev acoustic levitation system cost less than £100 to construct and so a good system would be similarly priced. The system should be able to be assembled in a relatively short period of time so that it can be constructed quickly for implementation on many of the beamlines at Diamond Light Source.
Customer	It will be designed to be operated by the beamline scientists of the various beamlines at Diamond Light Source. It should be easy to install and remove from the beamline so that traditional methods may still be utilized.
Environmental Considerations	The system should not interfere with the x-ray beamline.

Function	This system should facilate top-loading of samples and be able to levitate droplets of higher density than water. The droplets should easily detach from a pipette tip to be suspended in the acoustic levitator. The droplets in the system must remain suspended while the beamline hutch is searched and the beam engaged. The system will be transported between Nottingham Trent University and Diamond Light Source, so should not be fragile. It will be stored in cupboards or on shelves so cannot degrade over time.
Manufacturing	The resources available to create a prototype are a Form 2 (Formlabs, MA, USA) 3D printer, a laser cutter and workshop facilities.
Materials	The structure should be 3D printed and use off the shelf components.
Safety	Transducers should not be pointed towards the user, as this can cause tinnitus and various hearing problems. The electrical components of the system should be well insulated so that the system is not damaged if liquids fall onto it.
Size	There should be sufficient separation of either side of the designed acoustic levitator, to allow for the area between the interaction point of the droplet and the Pilatus3 6M detector to be free of all material or structures so to not cast a shadow onto the detector. The system should be short to allow plenty of space above for sample loading techniques. A 10mm hole should be situated at the top to allow for a pipette to deposit droplets into the centre of the system for suspension.

4.2 Simulation of System

A free software application for creating solid 3D CAD objects called OpenSCAD [86] was used in order to design and render the structure for an acoustic levitator. The acoustic levitator was designed based upon the TinyLev system published [3], a two-sided acoustic levitation system utilising off the shelf components. However, as only a single levitation position was desired, the transducers may be more focused toward the central position and the structure may be more curved to increase the lateral stability of any levitated material.

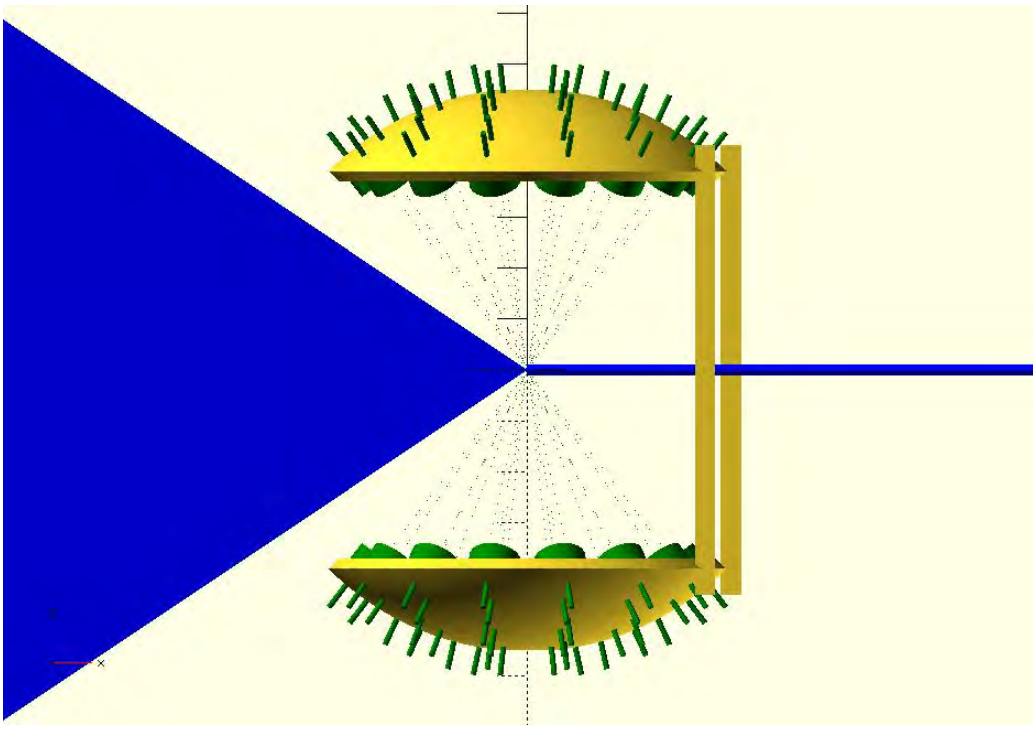

Figure 4.1: *The 3D render of the acoustic levitator designed using the code detailed in appendix C. The yellow structure is the frame itself, which is the desired object to be printed. The transducers are represented in green to ensure that the structure allows sufficient space for them to be mounted and they do not collide with one another. The blue colour represents the incident x-ray beam and a cone which covers the interaction point to the very edges of the x-ray detector at its closest position to the sample. These constructs are used to ensure that there is sufficient clearance of the acoustic levitator so as to not cast a shadow on the x-ray detector by causing diffracted x-rays to be stopped by the structure or transducers.*

In this software a script was designed in which many variables were used in order to generate and render the desired structure. The script in its entirety is featured in appendix C. The variables which are defined within this script are the thickness of the bowls, the radiuses of the transducers and their legs, the distance to the centre point of the structure, and the angle up to which the bowl extends. Also, the number of transducers and the thickness of the 3 supports between the opposing bowl structures is defined.

The script uses these variable to generate one half of the acoustic levitator and then reflect the design to the opposing side. The distance between each half of the acoustic levitator was controlled. The cone between the interaction point of the levitated droplet to the detector is overlay onto the rendered structure in order to ensure that the structure will not cast a shadow onto the detector. Transducers may be overlay onto the structure also to ensure they could be fitted once the structure has been 3D printed and that they also would not cast a shadow onto the detector.

Results published [3] suggest that the closer the opposing arrays of transducers are, the stronger the lateral and longitudinal forces acting on the droplet. In addition, distances of $n\lambda/2$ between opposing transducer arrays allow for the nodes of the incident waves to align and create positions in which the material may be levitated. These constrictions lead to the focal point to be selected at the first multiple of $\lambda/2$ which would not cast a shadow upon the x-ray detector. In this instance, the separation between opposing transducers was 11λ or 93.5mm and the full design is shown in figure 4.1.

A 10mm hole was positioned in the centre of the top and bottom array, in order to facilitate the loading of the sample.

4.3 System Construction

In order to construct the DLS-Lev acoustic levitator, the file was rendered and exported as an .stl file. This file was imported into PreForm (FormLabs, MA, USA) and support structures added in order to allow for the structure to be printed using the 3D printer (FormLabs, MA, USA). The file was set up to be printed using draft resin so that the file may be printed quickly to allow for iterations of the prototype if needed. The file was printed with a 300μm resolution as higher resolution was not necessary.

Following the printing of the structure, it was rinsed of remaining liquid resin in a bath of Propan-2-ol and the structure allowed to air dry. It was then heated to 60°C for 5 minutes whilst

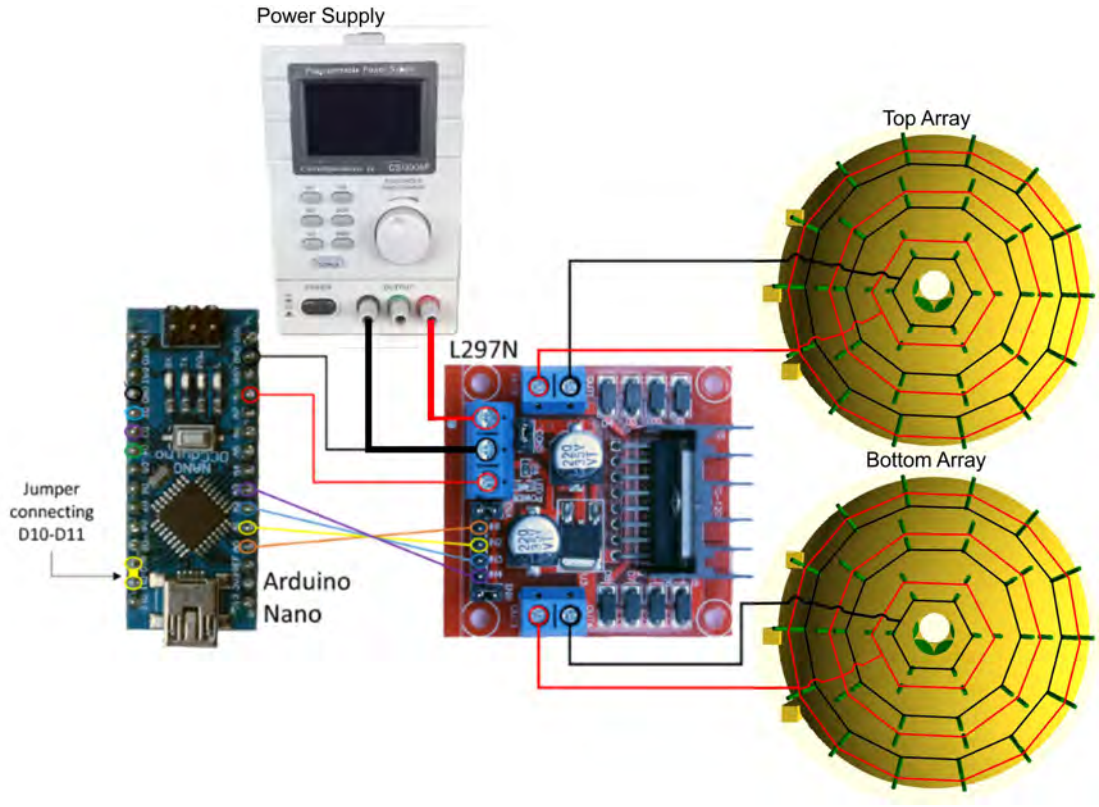

Figure 4.2: *An image showing the electronic configuration of the DLS-Lev acoustic levitation system.*

UV light was emitted from the FormCure (FormLabs, MA, USA) to increase the tensile strength of the printed structure.

The 3D printed structure is cleared of all support material and a 10mm end mill used to ensure that the indents in which the transducers are fitted are completely clear of any excess material so that they may be fit flush against the surface of the structure. The holes designed for the transducer legs are cleared of remaining material using a 0.8 mm drill bit.

Once the 3D printed structure is prepared, 60 off the shelf 10mm transducers which operate at 40 kHz are fitted into the printed structure. They are arranged within the transducer indents in concentric rings, with the positive leg through the inner ring. The legs of the same polarity are electrically connected using 0.71mm tinned copper wire soldered to each leg, also in concentric rings.

The rings connected to the positive terminals of the transducers on each side of the structure are connected to one another via a long length of red insulated stranded copper wire. The rings connected to the negative terminals of the transducers on each side are connected to one another via a long length of black insulated stranded copper wire. These 4 wires are connected to the outputs of a L298N driver which is controlled by an Arduino Nano connected to the driver

through its input. These are powered through a 12V DC power supply. This configuration is shown in figure 4.2.

The Arduino Nano is programmed with the code provided within the Aiser Marzo's instructable for an acoustic levitator. It was edited to remove the functions which allow the phase shifting of the transducers, which cause the traps to move up or down. This was done as the lateral lengths of the traps within the DLS-Lev system decrease as they tend toward the centre trap unlike the TinyLev system in which each of the traps were a similar size and length. This means that the droplet destabilises at non-central positions. This edited code is provided within appendix D with the removed sections highlighted.

4.4 Droplet Properties within DLS-Lev

Proof of concept experiments showed promise for this acoustic levitation device to be successful for its proposed purpose of depositing small droplets via an untreated pipette, depositing through a hole positioned in the top of the acoustic levitator. However, it was quickly discovered that silicone oil droplets would not be stable in the system, but water droplets were very stationary in comparison to the TinyLev acoustic levitator so in depth experimentation was further pursued as water comprises the majority of the mother liquor in which the protein crystals are grown. For this reason, a study of the sphericity of varying viscosities of silicone oil at varying voltages is not investigated for this system. However, the stability and sphericity of water at a variety of volumes and voltages is investigated.

The top loading of samples also allows the sample delivery avenue to be more easily explored which is discussed in chapter 5. As hand loading of samples is not required, the silicone oil coating of droplets is also not required as samples may be deposited and experiments performed whilst the x-ray beam is active and therefore evaporation of the sample need not be limited. In addition, sample mixing is also viable with these combinations of systems but a silicone oil coating would add a barrier that the added sample would need to diffuse through, which is not ideal. For these reasons, silicone oil coated water droplets are not considered for experimentation on this bespoke device.

4.4.1 Evaporation and Heating

The designed acoustic levitation device, the DLS-Lev, differs to the TinyLev system as it uses a more focused shape, the opposing transducers are closer to one another but it also utilises 12 fewer transducers. For this reason, it is important to study the effects that this bespoke

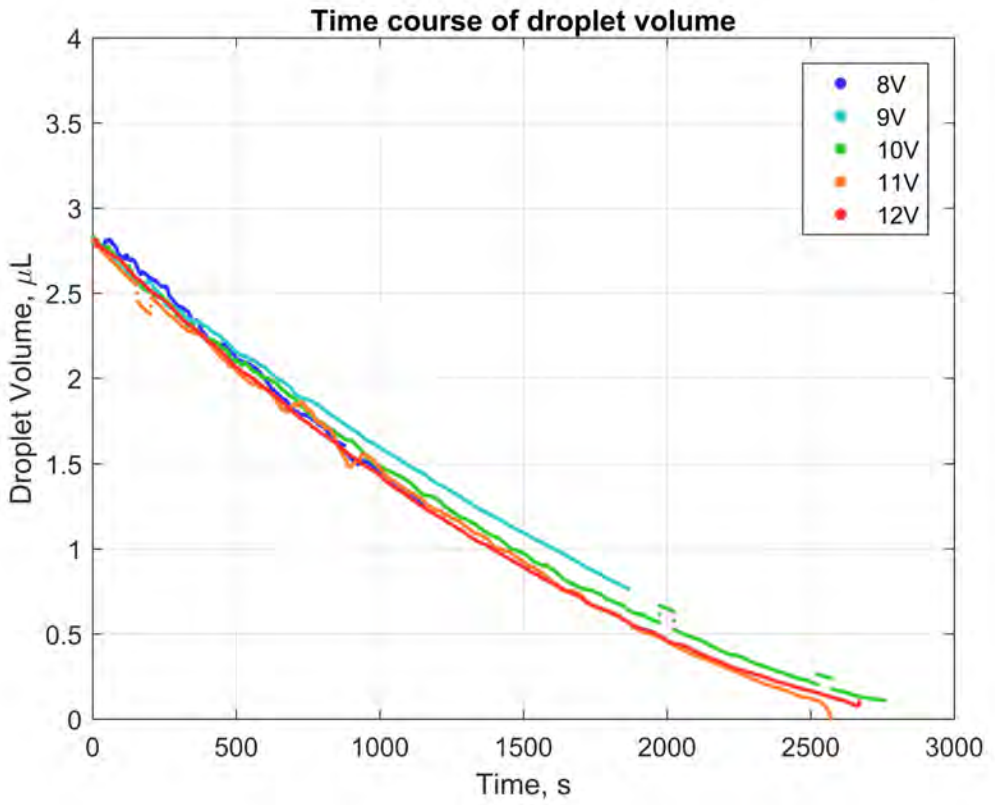

Figure 4.3: *A graph showing the volume of water droplets levitated within the bespoke DLS-Lev acoustic levitator against time. This graph presents the data collected for multiple droplets which are levitated at the varying operating voltages of the device. This shows that the different operating voltages of the DLS-Lev levitator does not increase the evaporation rate of the water droplets which are levitated. It also shows that the lifetime of a 2.75 μL water droplet within this system is over 2500 seconds or approximately 43 minutes.*

acoustic levitator has on water to ensure that it does not cause significant heating which could potentially damage any protein crystals within it, as well as to ensure that the evaporation rate of the droplets are not significantly increased which would change the concentration of the mother liquor when it is levitated.

In this experiment, droplets of water were levitated within the DLS-Lev and imaged whilst they evaporate. It utilised a DCC1645C camera (THORLABS, Ely, United Kingdom) which captured the images every second using THORCAM software (THORLABS, Ely, United Kingdom). This data is processed using the code developed in MATLAB (Mathworks, Massachusetts, US) which is detailed in appendix B and described in section 3.2.

This experiment was performed for the different operating voltages of the acoustic levitator and the data is presented in figure 4.3. This graph shows that the lifetime of a 2.75 μL water droplet within this system is approximately 2700 seconds at all operating voltages of the system, except for at 8V and 9V where the droplet had prematurely been ejected rather than the droplet evaporating. This graph also shows that there is negligible difference between the evaporation rates of the levitated water droplets at different operating voltages. This means that the evaporation rate of the water droplet need not be considered when choosing the operating voltage of the system for experiments performed at Diamond Light Source.

4.4.2 Stability

The stability of droplets is an important factor to measure for the DLS-Lev levitation device, because this dictates the ability for a droplet to remain within the beamline for the duration of any x-ray diffraction experiments. However, the factors that dictate the stability of a suspended droplet are the operating voltage of the acoustic levitator, the volume of the droplet, the material and environmental factors. Silicone oil droplets were found to be particularly unstable whilst they are levitated from preliminary observations, whilst water droplet (of which majority of the mother liquor is comprised) was observed to be extremely stable, and therefore it is the substance which will be studied in this experiment.

Water droplets are volatile and therefore their volume reduces over time, which is a factor which effects the stability of the droplet levitated. However this is also the case for droplets of mother liquor. For this reason, 50 second extracts of the image series collected are used, as this is the time required to collect 5000 diffraction patterns which allowed for detailed analysis of the protein crystal structure, as presented in section 3.4. The standard deviation of the position against the mean volume of the droplet of each 50 second series is presented in figure 4.4, for the various operating voltages of the acoustic levitator. The standard deviation of the position

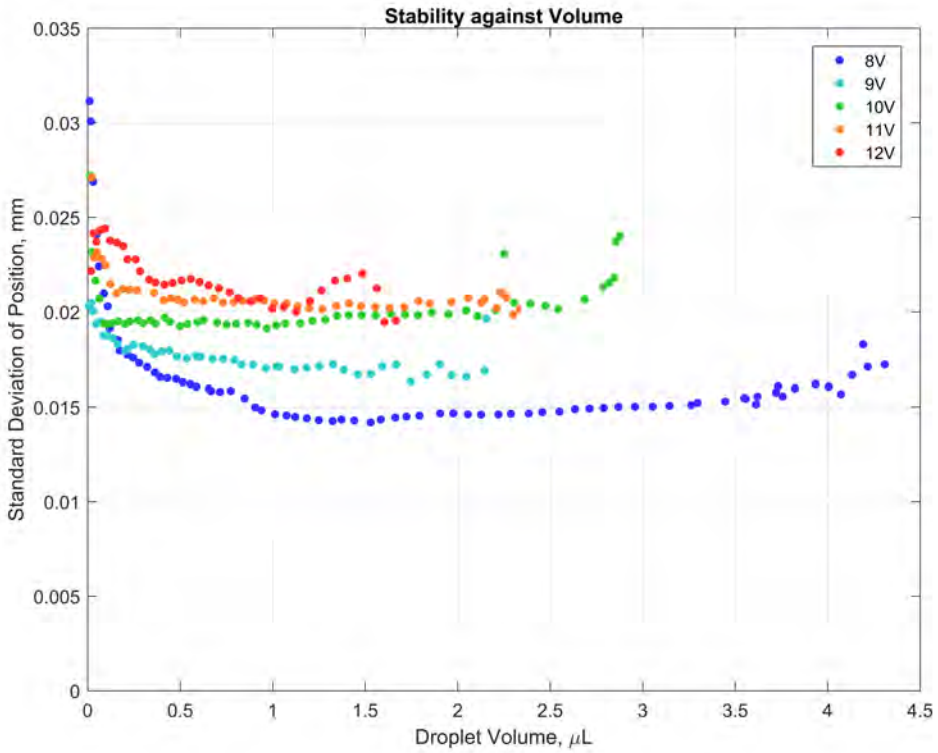

Figure 4.4: *A graph showing the stability of water droplets during 50 second periods, against their mean volume for the various operating voltages of the DLS-Lev. The stability of the water droplets has been presented as the standard deviation of the droplets position during the 50 second time frame, meaning statistically, droplets are likely to not be more than 35 μm from the mean position of the droplet at all operating voltages of the system. Droplets within the TinyLev acoustic levitator presented with a standard deviation of approximately 2.5 mm at an operating voltage of 12V at its most stable measurement as discussed in section 3.3. Contrary to expectation, a higher operating voltage of the DLS-Lev acoustic levitator does not correspond to a lower movement of the droplet between frames, but instead a lower operating voltage leads to a more stable droplet. This is likely due to increased acoustic forces present at higher operating voltages, non-uniformly applied to the droplets surface due to small variations in the topology of the levitator of the sound output of the individual transducers mounted on its surface.*

is representative of the stability of the droplet as it shows the distance from the mean position the droplet is likely to have travelled.

Contrary to expectation, the acoustic levitator operating at 12V did not correspond with the lowest standard deviation of position and therefore the greatest stability. It was instead the lower voltages which correspond to a more stable droplet within this acoustic levitator, this is likely due to an increased acoustic pressure at higher operating voltages which is non-uniformly applied to the droplet due to slight flaws within the structures topology. However, the DLS-Lev acoustic levitator did present with a significantly more stable droplet for all operating voltages when compared to the TinyLev system of which the standard deviation of the droplets position was between 2 - 6 mm (as discussed in section 3.3) in comparison to the value of below 35 μm for the DLS-Lev.

4.5 Summary

This chapter has described and investigated a bespoke acoustic levitation device named the DLS-Lev, specifically designed to be compatible with the I24 beamline at Diamond Light Source. The DLS-Lev system was first designed and rendered before it was constructed. It resembled the TinyLev system, but differed in number of transducers and their arrangement. The advantages of this system is that samples may be loaded into position through the top of the device and the droplets are incredibly stable, their movement is not detectable with the human eye as there is less than $35\mu m$ lateral displacement. As droplets may be top-loaded, the DLS-Lev is a viable candidate to trial sample mixing within the x-ray beam at Diamond Light Source, with the addition of a sample delivery system which may be operated during an x-ray diffraction experiment. The following work details the investigation of sample delivery systems, their design and implementation to dispense droplets to mix whilst suspended by the acoustic levitator.

Chapter 5

Sample Delivery and Real-Time Sample Mixing Experiments

The DLS-Lev has been shown to be a viable candidate for the top-loading of protein crystals within their mother liquor, while installed at I24. In order to use this system for sample mixing or as a permanent fixture at Diamond Light Source, a method of sample delivery must be developed so that liquids may be mixed within the levitator without having to enter the x-ray hutch during an experiment. This chapter explores the development of such a sample delivery system, and discusses the sample mixing experiments performed at Diamond Light Source using protein crystals and an enzyme which interacts with it for time-resolved experimentation.

Many more experiments were intended for this chapter of work, however due to the COVID-19 pandemic the work performed at Diamond Light Source was diverted to the research of the virus in addition to the laboratory closure at Nottingham Trent University meaning that further experimentation could not be continued.

5.1 Methods of Sample Delivery

This section features the methods that were explored in order to deposit samples of protein crystals within the acoustic levitator. These delivery systems were trialled with both the TinyLev acoustic levitator and the DLS-Lev acoustic levitator.

5.1.1 SLIPS

Slippery liquid-infused porous surfaces (SLIPS) are highly textured or porous surfaces in which a thin layer of lubricating liquid is imbibed. This lubricating layer removes the contact between the droplet and the solid surface underneath, and therefore eliminates the pinning which droplets normally experience with solid materials, creating a highly mobile droplet on this surface [87]. Glass slides which have nanoparticles or a superhydrophobising coating on the surface are

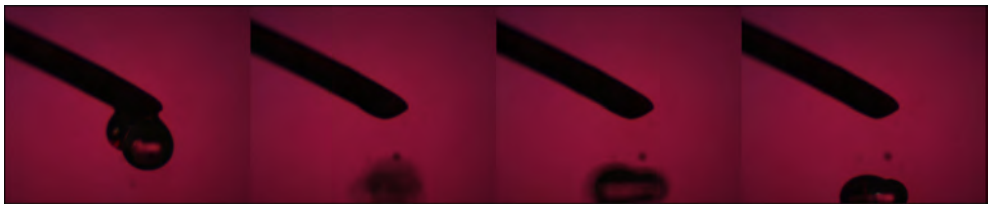

Figure 5.1: *Example image series of a droplet of water detaching from a SLIPS wire, coated in silicone oil. There is approximately 2 minutes between the first and last image in this series. These images show that SLIPS wires are viable to deposit silicone oil coated droplets into the acoustic levitator, however time is required for the droplet to reach stability.*

typically used for the creation of SLIPS material but they may also be formed on many other materials [41].

More recent developments of SLIPS on conformable mesh [88] gave the inspiration for its use with an acoustic levitation device as many mesh surfaces are acoustically transparent and allow for the levitation of polystyrene spheres and liquid substances without disrupting the acoustic field that they are placed within [89].

In order to create a SLIPS material, the solid substance must first be cleaned of any surface contaminants. This is done by sonication inside of an ultrasonic bath and rinsing the material with isopropanol and allowing to air dry. Glaco Mirror Coat Zero (SOFT99corporation, Japan) is then sprayed over the surface in a single pass and allowed to air dry, this substance is a commercially available aerosol containing silica nanoparticles suspended in a solvent which creates a superhydrophobic coating on the surface. Following the evaporation of the Glaco Mirror Coat solvent, the superhydrophobised surface is imbibed with silicone oil by dip-coating, by immersing it into a bath of silicone oil and withdrawing the surface vertically at a slow and constant speed. The surface must not be touched as that risks contamination as well as creating positions in which the droplet could be pinned, restricting the freedom of movement on the surface.

A stainless steel mesh was selected and before it was prepared to be a SLIPS, it was placed within the acoustic field of the levitator whilst a droplet was being suspended in order to ensure that it would not obstruct the acoustic field or cause significant disruption to the suspended droplet. Following its preparation it was however found that the silicone oil caused occlusion of the mesh holes and did not allow for the passage of the acoustic field and so substances and materials could no longer be levitated.

However, this preliminary experiment did show the ease in the development of these surfaces. It also demonstrated that droplets that travelled on the SLIPS picked up a silicone oil shell or coating from the SLIPS, which was a useful development in the TinyLev experiments as it

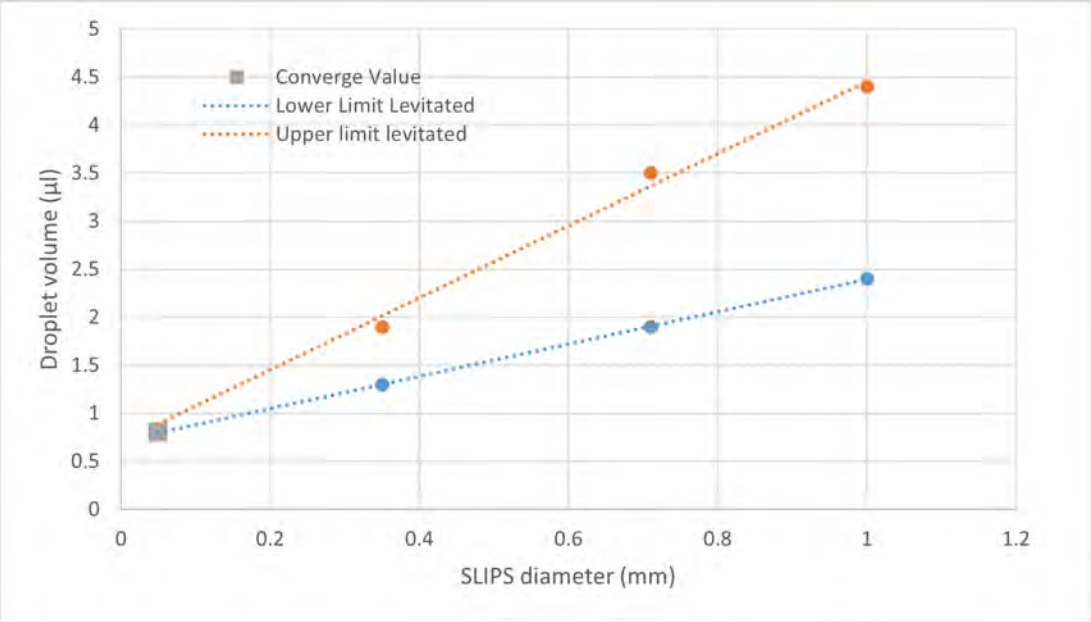

Figure 5.2: *A graph of the droplet volume with varying diameter of SLIPS wire. The range of volumes which can be levitated increases as the wire diameter is increased. For lower volumes though, a lower diameter of wire is necessary, converging to 0.8 µL on a 0.05mm wire.*

stabilized the droplets for levitation as well as reducing the rate of evaporation as discussed in section 3.3.

Conformable meshes used as SLIPS materials [88] demonstrated that the substrate used to create one of these surfaces did not need to be a flat or planar. Stainless steel wires of varying diameter were therefore investigated and prepared to become SLIPS. The first of such wires showed that the method had promise. The water droplet was deposited via a pipette on top of the wire and moved to the underside of it. Once the wire is tilted from the horizontal plane by a small amount, the droplet remains mobile and travels toward the lower side of the wire. If the tip of the lower side of the wire is within or close to a trap by a few millimetres it will be caught within but still attached to the SLIPS wire. The movement of the trap (in the case of the TinyLev by changing the phase of the transducers) or the withdrawal of the SLIPS wire will cause the detachment of the droplet for suspension within the acoustic levitator, it will laterally oscillate for a few seconds before stabilising in a singular position, and slowly over time it will lose volume, as the water evaporates, leaving the silicone oil as a droplet. An example of the detachment of the droplet from a SLIPS wire is shown in figure 5.1, there is approximately 2 minutes between the first and last image in this series.

Experiments were performed in which the voltage of the acoustic levitator was cycled as well as the volume of water droplet to be suspended. It was found that the higher the voltage, the

larger the droplet which could be suspended and the smaller the droplet could be detached from the tip, as surface tension increases as the volume of the droplet decreases. Also the larger the diameter of the SLIPS wire, the larger the range of volumes which could be detached from the tip in order to be levitated. These results are illustrated in figure 5.2, and shows that the droplet volume which may be detached and levitated converges to a volume of approximately 0.8 μL on a 0.08mm diameter SLIPS wire. The droplet size levitated from any given SLIPS wire is dependent on the diameter of the wire itself as droplets which are too large do not have sufficient surface tension in order to stay attached and travel down the underside of the wire and they simply fall from it.

The limitations of this technique however is that as the diameter decreases, the strength of the wire also decreases and therefore tends to sag under the weight of the droplet. Glass capillaries could be used rather than stainless steel wire however this introduces fragility into the surfaces which is not the case with the stainless steel, which can be reused by replenishing the silicone oil on its surface. If a glass capillary were to be used there would be potential for it to shatter and risk operator injury as well as damage to adjacent equipment when installed at the I24 beamline at Diamond Light Source.

This method would still require an additional sample delivery system in order to deposit multiple samples into the acoustic levitator as well as a withdrawal system to ensure that the wire does not remain within the beam during experiments. These surfaces are not commercially available and therefore would need to be prepared before their use in addition to the sample of interest. Therefore this sample delivery method is not practical as a permanent installation for x-ray diffraction experiments.

5.1.2 Pipette

A variable volume pipette, often referred to simply as a pipette, but not to be confused with the traditional glass variety, is typically a hand held device used to deposit an accurate volume of a liquid substance. There is a large range of volumes that may be used based upon the type of pipette selected. From previous experiments performed using a syringe and hypodermic needle, paired with knowledge of the size of the traps within an acoustic levitator operating at 40kHz, the droplet volume which could be levitated would be less than 5μL.

The surface of the tip of a typical pipette is such that it does not interfere with the emitted sound from the transducers within an acoustic levitator. So, its presence within the space occupied by the acoustic levitator would have little effect on the continued suspension of the deposited droplet.

There are a variety of methods that may be used to automate a pipette in order to dispense consistent volumes. If a manual pipette is selected, this would require a mechanism to physically depress the plunger of the pipette. This would need to be calibrated for each individual volume which it would be used to collect as the distance that the plunger is depressed varies based upon the volume collected. This is not the ideal method as it would be vulnerable to misalignment due to the installation of the droplet delivery system at Diamond Light Source. So although it would be the lower cost method, it would have have more potential for failure.

Electronic dispensing systems have been designed and manufactured to be sold on the market, however such systems cost thousands of pounds which is outside the budget of a prototype system before wide scale deployment. In addition, many of these dispensing systems are for existing processes and as such often are only offered for enclosed systems that would warrant contact free droplet dispensing due to safety concerns about the chemical reaction being performed, the caustic or carcinogenic properties of the substances or the potential bio-hazard that the substance might possess which warrants contact-free handling of the material.

As an enclosed dispensing system would introduce crystalline material, typically glass, into the path of the x-ray beamline as well as the path of the diffracted x-rays, such systems can not be considered for this prototype as the data collected would include that from the material placed within the beam path and as such would not be a true representation of the intended container free presentation method for synchrotron experiments.

The most ideal method of pipetting would be to modify an electronically controlled pipette, so that it may be operated remotely. The electronic pipette chosen is a 0.2-10μl Picus variable electronic pipettor (Biohit, Finland) and this pipette features a button which collects or dispenses a desired volume of a substance, it also allows for multi-dispense which is the collection of a large volume of the desired substance for it to be dispensed in multiple smaller droplets. This would be ideal for saving additional time between repeated experiments.

Inside of the pipette, a pair of circuit boards are used to control the operation of the pipette, there is a small button featured on one of the circuit boards which is activated by pressing the button on top of the pipette, this causes the pipette to actuate, collecting or dispensing a substance. This pipette may be modified to be remotely actuated by connecting a relay to the terminals of the button on the circuit board in order to bypass the need to press the button on the pipette so that it may be operated from a distance.

5.2 System Construction

In order to construct the automated pipette system which was found to be the most viable solution for sample delivery, the electronically controlled pipette must be deployed as well as a method to move the pipette from a position in which it may collect a sample to a position in which it could be deposited into the acoustic levitator. This must be able to be controlled from outside of the x-ray hutch at Diamond Light Source and powered either through portable sockets or through a wall plug.

5.2.1 Delivery system

The automated electronic pipette must be moved between the position in which it collects the sample and deposits it in the acoustic levitator, this must be controlled electronically from outside the I24 hutch at Diamond Light Source. To reduce the number of moving parts within the system, a singular central linear actuator and a servo are used to move the pipette between the samples and the acoustic levitator.

Figure 5.3 shows a 3-dimensional rendering of the initial prototype of the sample delivery system, made in SolidWorks (Dassault Systèmes SOLIDWORKS Corporation, MA, United States). The frame is constructed using 20mm V-Slot aluminium extrusion (Ooznest, United Kingdom) and is designed to be mounted on the breadboard located above the beamline within the I24 hutch as the goniometer has a weight limit of approximately 3kg. It measures 60cm by 104cm by 25cm in the length, height and depth dimensions respectively.

An Arduino Mega 2560 micro-controller is programmed to control the extension of the linear actuator and the rotation of the servo which both determine the position of the pipette. Four retroreflective photoelectric sensors (Omron, Japan) are used to set the bounds of the pipettes position and limit its movement so it does not cause damage to the surrounding equipment. These sensors are mounted on manual rails so that their position may be moved during installation at Diamond Light Source.

A console featuring six buttons was constructed to input the users intention to move the pipette and to collect or dispense the sample within the acoustic levitator. This console is shown in figure 5.4 and includes LEDs that light up to provide warnings to the user about the position of the pipette. It is powered using a 12V DC supply and inside the console, various electronics which outputs the desired power to the linear actuator, servo, LEDs and photoelectric sensors.

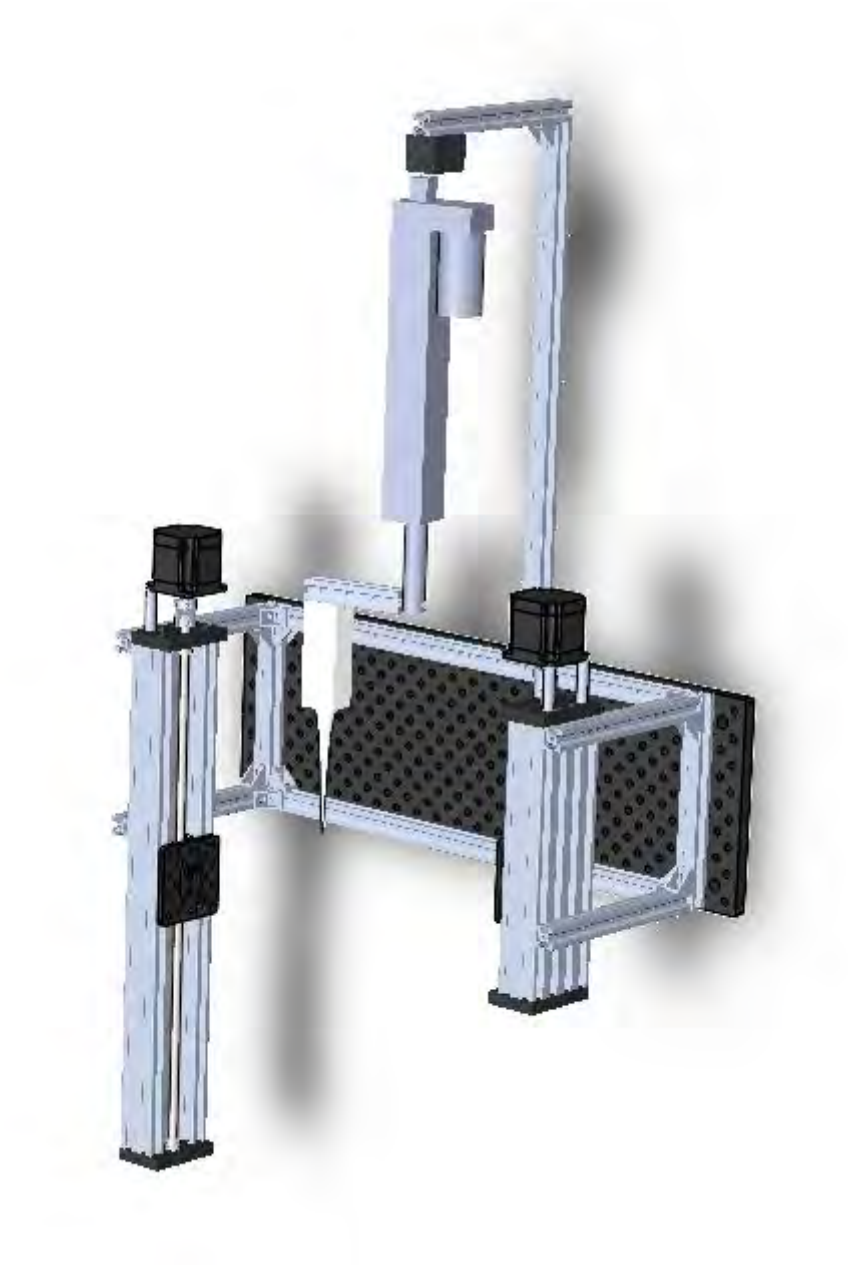

Figure 5.3: *A design of the prototype sample delivery system, the frame is constructed to support the linear actuator and allow for the freedom of movement to collect the sample from the right hand side of the setup and deposit the droplet to where the acoustic levitator will be used to suspend it.*

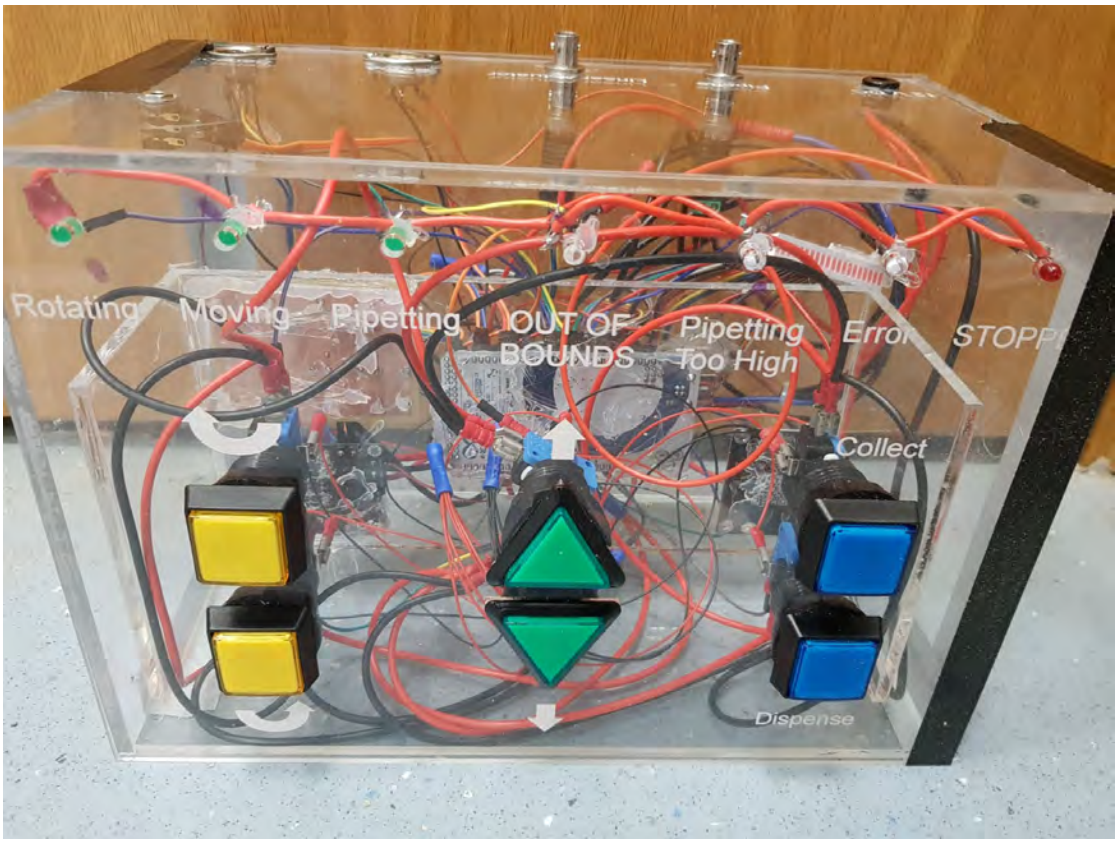

Figure 5.4: *A photograph of the control console, it contains an Arduino Mega 2560 microcontroller pre-programmed with code which allows the user to input commands through the buttons located on its top-side. These buttons input the desire to move the linear actuator up and down, rotate the servo left and right and collect and deposit a droplet. The retroreflective photoelectric sensors input their state to the control console in order to limit the commands recorded to only that in which are valid as described by the code.*

The fully commented code in which the Arduino Mega 2560 is programmed with is shown in appendix D, and it reads the input signals from the photoelectric sensors and the button panel and outputs signals for the operation of the LEDs, linear actuator, servo and pipette.

Due to the position on the pipette in relation to the servo in combination with its weight, it causes an imbalance of the servo and causes it to tip. The pipette is then not in the intended upright position to collect the sample and deposit it into the acoustic levitator. In order to counteract this tipping, 800g of weight is fixed onto the opposing side of the servo to act as a counter balance.

Additional support is added to the frame to increase the strength of the structure and ensure that each of the components remain in their intended position throughout transport and installation. The operation of the droplet delivery system is tested in the laboratory setting before its installation at Diamond Light Source.

5.3 Experiments at I24, Diamond Light Source

This section covers the installation and experiments performed with the DLS-Lev acoustic levitator and the sample delivery system at the I24 hutch at Diamond Light Source. X-ray diffraction data was collected on lysozyme protein crystals within their mother liquor levitated within the DLS-Lev acoustic levitator prior to being mixed with $(GlcNAc)_4$ ligand suspension in which further x-ray diffraction data was collected. This data collection allows for a comparison between the TinyLev and DLS-Lev acoustic levitators as well as showing the feasibility of sample mixing within this system.

5.3.1 Installation

During a routine beam shut down at Diamond Light Source, the installation of the sample delivery system and the DLS-Lev acoustic levitator took place. A cardboard stencil of the delivery system was created by tracing the outline of the structure. This stencil was used to determine whether the surrounding equipment would obstruct the delivery system and to ensure its installation would not cause any damage to the beamline equipment by colliding with any of the alignment cameras or the other structures present.

The delivery system was affixed to the breadboard using four 2 inch M6 bolts through holes cut within the top of the delivery systems frame. Figure 5.5 shows the installed droplet delivery system affixed to the breadboard above the beamline at I24 at Diamond Light Source, important features of the system are labelled such as the pipette, servo and linear actuator. The DLS-Lev

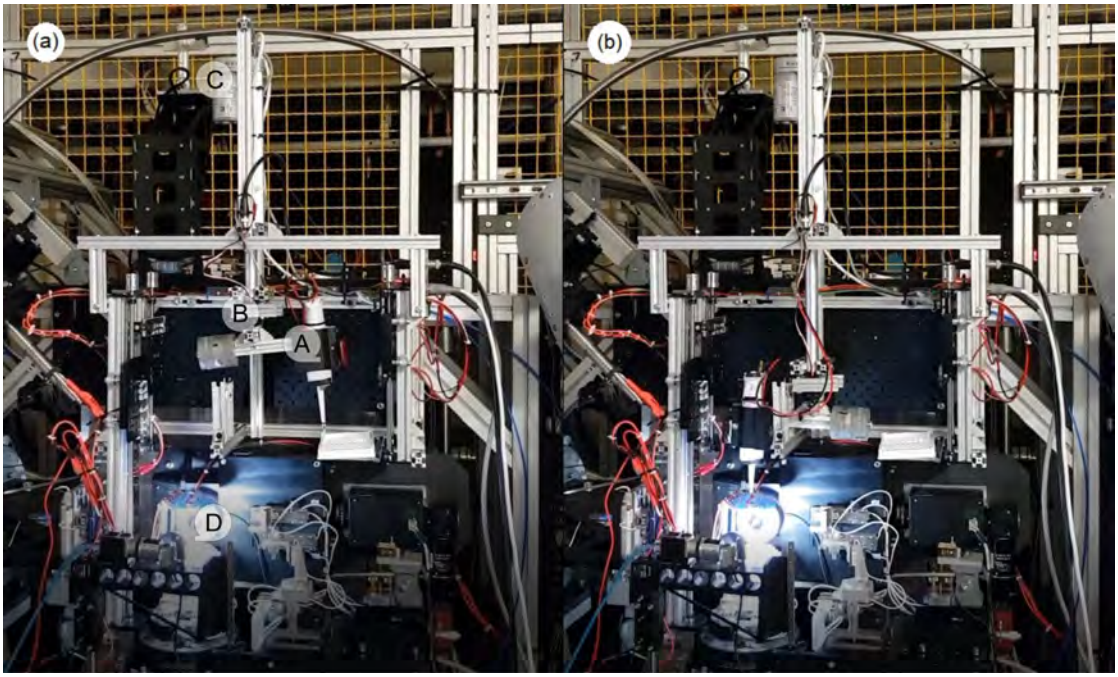

Figure 5.5: *A pair of photographs of the prototype sample delivery system installed at I24 above the position in which a sample, levitated in DLS-Lev, will be struck by the x-ray beam during the experiments. (a) shows the position in which the sample is collected, (b) shows the position in which the sample is deposited. The labels on photograph (a) show the features of the experimental setup. A indicates the pipette, B is the position of the servo, C is the position of the linear actuator and D labels the DLS-Lev acoustic levitator.*

acoustic levitation device was mounted upon the goniometer adapter, as described in previous experiments in section 3.4. This adapter was secured to the sample positioning stage using four bolts, and this allowed for the rotation of the device as well as changes to its elevation. A droplet of water was loaded into the central trap of the acoustic levitator in order to adjust the goniometer so that the droplet sits in a position in which it would be struck by the x-ray beam. When this position is found, the positions of the retroreflective sensors are adjusted so that the lower left sensor is active when the pipette is in the deposition position. Before experiments were performed upon droplets of protein crystals within their mother liquor, the system was tested within the hutch environment after it was installed to determine the successful sample delivery into the DLS-Lev acoustic levitator.

This sample delivery prototype was evaluated to determine whether it would be effective for large scale roll out on the relevant beamlines at Diamond Light Source. The success rate of deposition into the acoustic levitator was not high due to the wobble caused from the rotation of the servo. It would often cause movement of the pipette, which would in turn miss the 10mm hole located at the top of the acoustic levitator. The wires connecting the console to the sample delivery system were not long enough for the control of the operation outside of the hutch at I24.

As the control console for the sample delivery system would not be able to reach outside the the hutch for experiments and because it was unreliable at depositing droplets into the acoustic levitation device, an on the fly solution was established to allow for sample mixing experiments to still be performed. This included disconnecting the pipette actuation from the the control console and trailing 2 insulated wires from the the pipette to the outside of the hutch where they could be manually short-circuited to dispense the sample at its position.

5.3.2 Sample Preparation

The substances used to show that the DLS-Lev acoustic levitator is suited to the presentation of protein crystals to the I24 beamline at Diamond Light Source are lysozyme crystals and $(GlcNAc)_4$ ligand. Lysozyme was selected as historically it was the first enzyme structure to be solved and therefore is a very well known structure [90], in addition to also being selected for TinyLev experiments in section 3.4, so it allows for a close comparison between the sample presentation methods of the TinyLev and DLS-Lev devices. The $(GlcNAc)_4$ ligand was selected as it is a known compound to be catalysed by lysozyme [91].

Lysozyme crystals with a width of 100 μm were grown using a similar method used to grow homogeneous rectangular crystals [92]. High purity lysozyme from chicken egg white (Product Number L4919, Sigma-Aldrich, UK) was initially re-suspended to a concentration of 50mgmL^{-}1

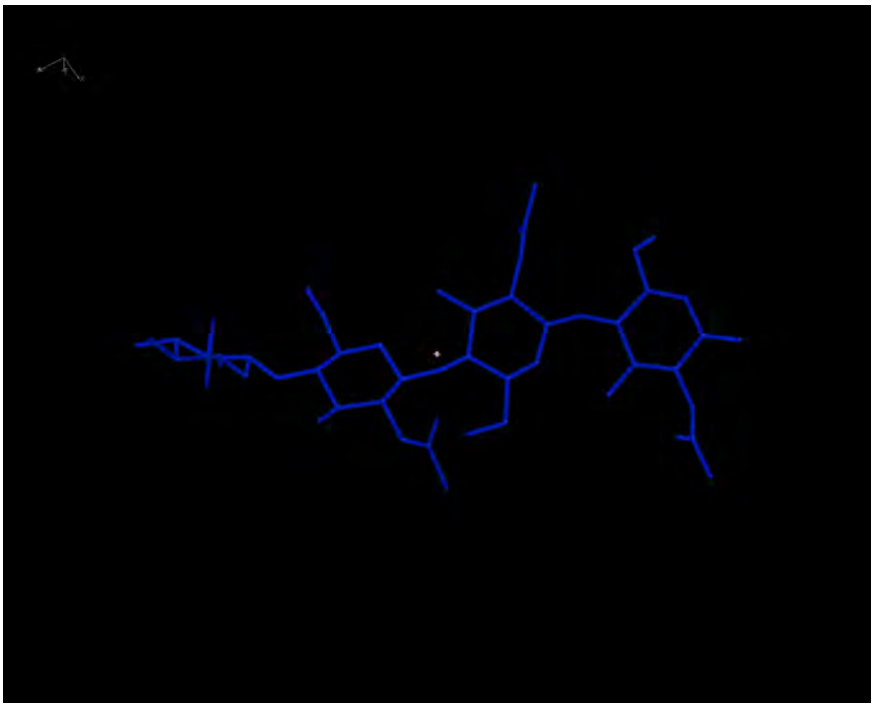

Figure 5.6: *The structure of the $(GlcNAc)_4$ ligand, which is a molecule comprised of four sugars.*

in distilled water. This suspension was mixed with an equal measure of precipitant solution containing 0.1M Hepes (a buffering agent) with a pH of 7.5, 0.2M Ammonium Sulphate and 20% PEG3350 at room temperature. This mixture was mixed for 10 seconds before being left for an hour for the lysozyme crystals to grow.

The lysozyme crystals with a 40 μm width were also grown similarly to other work [92]. However, these crystals were grown by re-suspending high purity lysozyme from chicken egg white (Product Number L4919, Sigma-Aldrich, UK) within 100mM sodium acetate buffer solution at a concentration of $50 \text{mgmL}^{-}1$ at 30 °C. This suspension was mixed 1:1 with a solution of 20% w/v NaCl, 6% PEG 6000 in 1M sodium acetate buffer solution, adjusted to pH 3.0. For 10 seconds this mixture was vortexed and then left without agitation for an hour for the crystals to grow.

A ligand called $(GlcNAc)_4$ or tetraacetylchitotetraose (Product Number OT04211, Biosynth Carbosynth, UK) was prepared by dissolving the powder within distilled water to a concentration of 75mM. This ligand is a tetrasaccharide, a carbohydrate which gives four molecules upon its hydrolysis. The structure of this ligand is shown in figure 5.6.

The mixing of the lysozyme crystal and $(GlcNAc)_4$ ligand should show the binding of $(GlcNAc)_4$ to specific sites of the protein if successful. Following this binding, the $(GlcNAc)_4$ molecule is hydrolysed, leading to four water molecules and four GLcNAc residues being released from the protein binding sites [93].

5.3.3 X-ray Diffraction Experiments

A 3.5μL sample containing multiple 100μm lysozyme crystals within its mother liquor was suspended within the installed DLS-Lev acoustic levitation device operating at 10V. The voltage allowed for the easiest detachment of the sample from the pipette tip whilst minimising the voltage to maximise the stability of the suspended droplet. This sample was loaded using a manual pipette, allowing for the automated pipette, primed with the $(GlcNAc)_4$ ligand suspension, to be prepared for the sample mixing experiments discussed later in section 5.3.4.

A search of the hutch was performed, in which it was checked that the area was cleared of personnel and this was confirmed by pressing a button outside the hutch once the door was secured shut. The Pilatus3 6M (Dectris, Switzerland) detector was moved to its closest position to the x-ray beam.

X-ray diffraction experiments were performed on the crystals floating within the suspended droplet of its mother liquor. As discussed previously, I24 is a tunable microfocus synchrotron beamline which allows for the electronic adjustment of the beam size through the remote control of various mirrors and lenses. Due to the stability of the droplet at its position, the beam size was selected to be 30 x 30 μm. The diffraction data was collected using the Pilatus3 6M (Dectris, Switzerland) detector operating at 100Hz and using all of the available detector modules within the 5 x 12 matrix. The collection of 5000 diffraction images was facilitated by the use of the 0.9686 Å x-ray beam being used without a shutter, which allowed for the data set to be collected within 50 seconds, which did not show any physiological difference to the droplet upon completion.

The diffraction data was analysed and the crystal structure was solved using molecular replacement, the model of the structure was built using Coot [84]. This data confirmed that the protein crystal under investigation was lysozyme and produced the electron density overlay onto the structure as seen in figure 5.7, this data had a 1.8 Å resolution. This experiment confirms that the DLS-Lev acoustic levitator may be used as a sample presentation method for the I24 beamline at Diamond Light Source. This system also allowed for data collection from smaller crystals in comparison to the TinyLev device, as well as allowing top loading which will facilitate sample mixing.

The crystal appeared to be intact and without radiation induced changes to its structure, it also did not appear to suffer any structural damage due to its suspension within the DLS-Lev acoustic levitator.

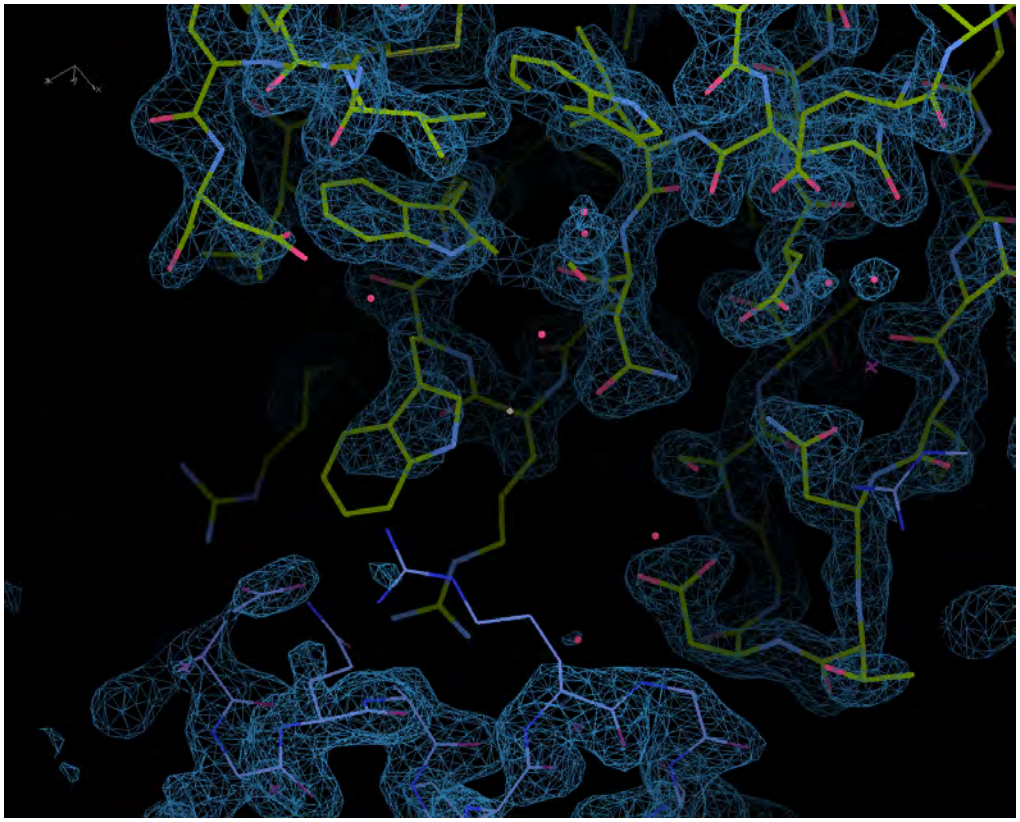

Figure 5.7: *A section of the electron density map of a 100 μm lysozyme crystal from chicken egg white suspended within its mother liquor levitated with the DLS-Lev acoustic levitator. The resolution of the electron density map is 1.8 Å. The data presented confirms the expected protein structure and therefore shows that the DLS-Lev acoustic levitator is a good method to present protein crystals to the x-ray beamline.*

5.3.4 Sample Mixing Experiments

As discussed in section 5.3.1, the unreliability of the sample delivery system and the lack of control from outside the hutch was solved by trailing two wires, which were connected to the pipette actuation, outside of the hutch to be manually short circuited and cause the pipette to dispense its sample. This pipette was pre-loaded with the ligand suspension and primed in a position a few millimetres above the interaction point between the droplet and x-ray beam.

Upon the collection of the diffraction patterns from the lysozyme crystals, as described previously in section 5.3.3, the x-ray beam was stopped but the hutch remained cleared and closed. The camera which could view the position of the sample was engaged. The goniometer and the acoustic levitator were raised vertically so the levitated droplet met the position of the automated pipette tip, at which point the pipette is actuated by quickly connecting and disconnecting the two wires from outside the hutch. This deposits the ligand suspension into the same trap as the protein crystal within its mother liquor. The acoustic levitator mounted to the goniometer is then returned to its original position for the collection of x-ray diffraction data.

The beam settings were the same as described in section 5.3.3, and were processed using Coot [84]. The difference between the 100 μm crystal structure before and after the addition of the ligand within solution was visually identified by overlaying the electron density maps onto the same crystal structure. The two electron density maps overlay onto the structure of lysozyme are shown in figure 5.8 and they both have a resolution of 1.8 Å, the regions shown in blue are the parts of the map which correspond to the structure of lysozyme. The red structures indicate parts of the electron density map which are missing in comparison to the structure used for molecular replacement, and the green structures indicate additional structures within the electron density map, these are likely due to different chemical compositions of the mother liquor for the very small sized structures. The green structures of which arrows are pointed at are structures which are too large to correspond to molecules of water and the wrong shape to correspond with molecules of PEG. It is possible that these structures correspond to the appearance of the $(GlcNAc)_4$ ligand as they seem to fit the structure.

In order to detect the presence of the ligand within the protein crystal structure, it must permeate throughout the entire structure. This process usually takes approximately 5 minutes which was later verified by an offline experiment on crystals which were held between layers of mylar sheet and soaked within the ligand suspension. The x-ray diffraction experiments on the levitated droplet were performed approximately 3 minutes after the ligand and protein crystals within solution made contact, and therefore the ligand did not have sufficient time to diffuse through the entire crystal.

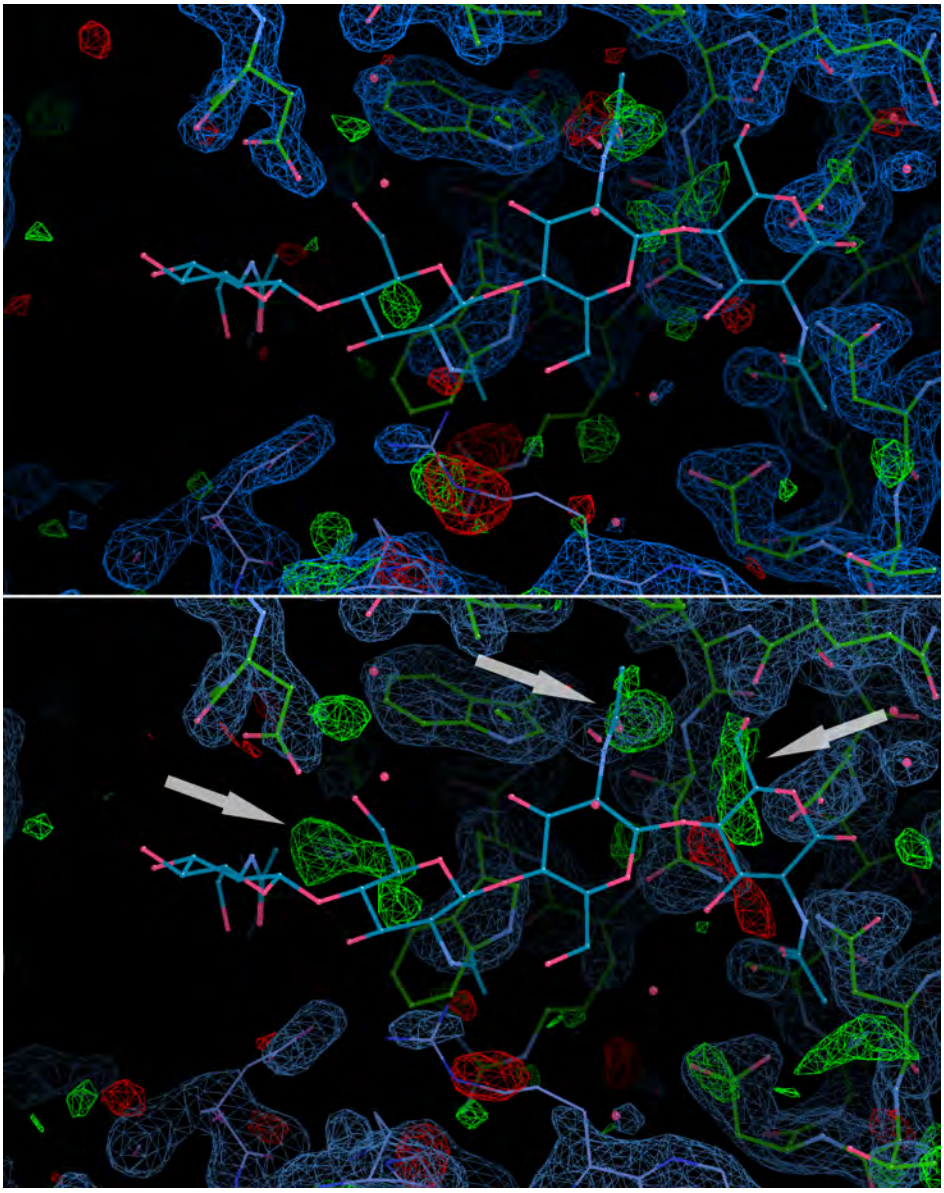

Figure 5.8: *Two images showing the electron density of the lysozyme protein crystal, the top image shows the structure before the addition of the $(GlcNAc)_4$ ligand and the bottom image shows the structure after the $(GlcNAc)_4$ ligand suspension has been added to the levitated droplet of mother liquor containing the 100 μm lysozyme crystals. There is approximately 7 minutes between the data collection used for the top and bottom images, with the mixing event occurring approximately 3 minutes before the collection of the data used for the bottom image. The areas of the structure which are highlighted with arrows correspond with positions which the ligand is expected to be found, however it seems that the suspension did not have sufficient time to diffuse throughout the entire crystal and so the entire structure is not apparent.*

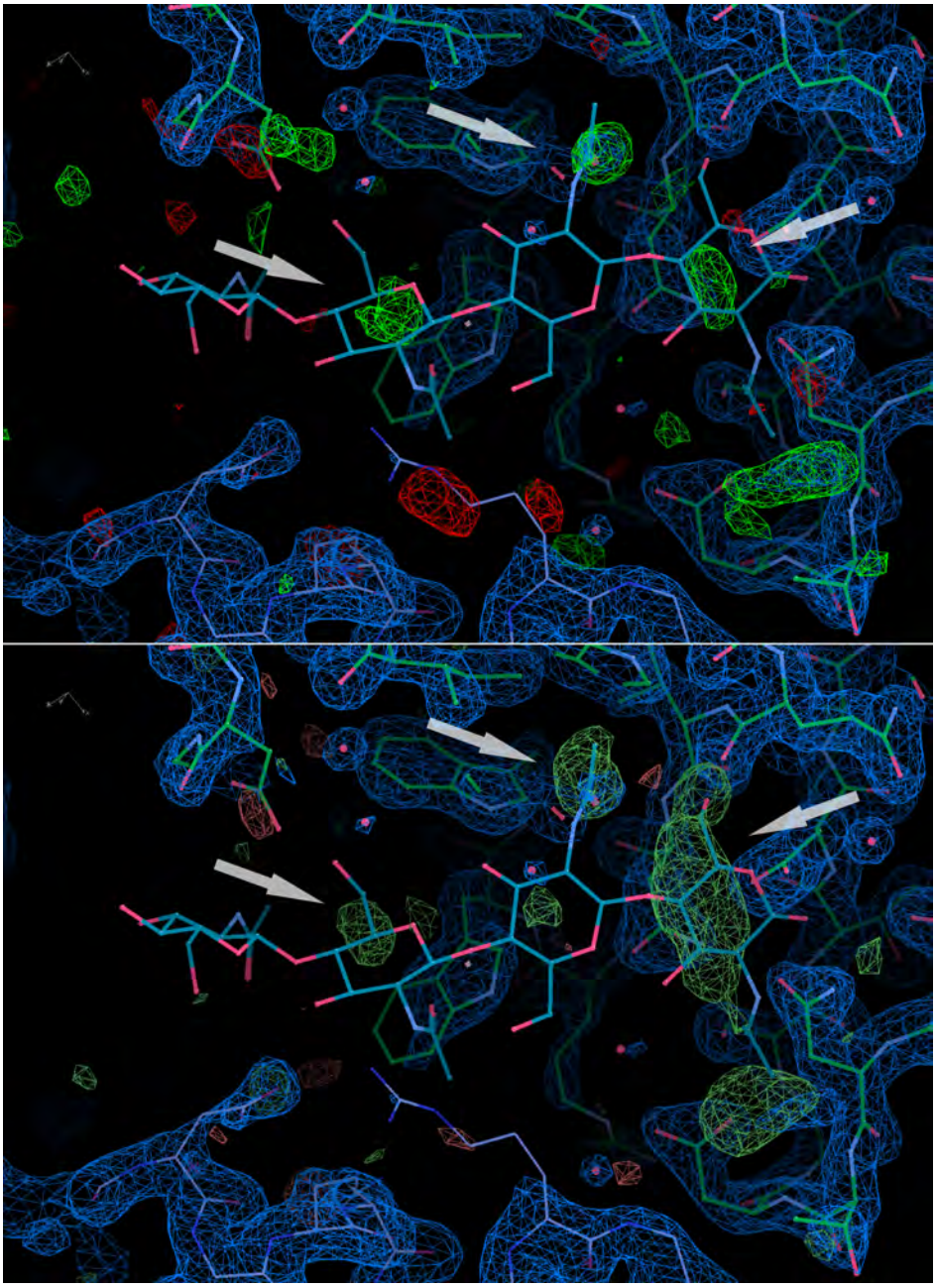

Figure 5.9: *Two images showing the electron density of the 40 μm lysozyme protein crystal after the addition of the $(GlcNAc)_4$ suspension. The top and bottom images show the electron density of this structure approximately 1 minute and 4 minutes after the mixing event respectively. Arrows point to the regions of interest which appear to grow in size and show increased agreement with the structure and expected position of the $(GlcNAc)_4$ ligand between the two electron density maps.*

Data collection on 40 μm lysozyme crystals before and after the addition of the $(GlcNAc)_4$ ligand suspension was performed using a smaller beam width of 7 x 7 μm. However, the data collected before the mixing event did not yield results, likely due to misalignment to the beam. Two datasets were collected after the mixing event and these were used to create the electron density maps shown in figure 5.9. The top image was generated from a dataset collected approximately 1 minute after the mixing event and the bottom image was generated from a dataset collected approximately 4 minutes after the mixing event. These electron density maps have a resolution 1.9 Å. The arrows on these electron density maps point to green structures which do not correspond with the structure of the lysozyme crystal. These structures do correspond with portions of the expected electron density of the $(GlcNAc)_4$ ligand, and as time progressed between the top and bottom images, they agree with the theory that the ligand suspension must diffuse through the crystal structure for longer to detect its entire structure.

In order to collect data from various points within the life cycle of this specific ligand, its binding to the protein crystal and it subsequent breakdown without the protein crystal dehydrating, an eppendorf tube containing a slurry of protein crystal may be loaded with the ligand and buffer solution and periodically collected and dispensed into the acoustic levitator. This would utilise serial crystallography methods as x-ray diffraction experiments would be performed on different crystals in each instance.

5.4 Sample Delivery System #2

As mentioned in section 5.3.1, the designed sample delivery system was unreliable at depositing droplets into the acoustic levitation device due to the wobble present during the extension of the linear actuator as well as the rotation of the servo causing the pipette to change position in relation to its support, this means the pipette tip would often strike the top of the levitator rather than travel through the 10mm hole. Therefore, a new sample delivery system was designed in order to minimise these errors, which increases support around the moving parts of the system and was more modular, in so far as it would not need to be dismantled and reconstructed for installation.

For this next sample delivery system, rather than a linear actuator and servo combination, a pair of linear actuators which run on tracks was used, to ensure that there would not be excessive movement in the horizontal plane. The Solidworks (Dassault Systèmes SOLIDWORKS Corporation, MA, United States) design of such a system is shown in figure 5.10, this design also includes the electronics connected to the system, two stepper motor drivers were used to

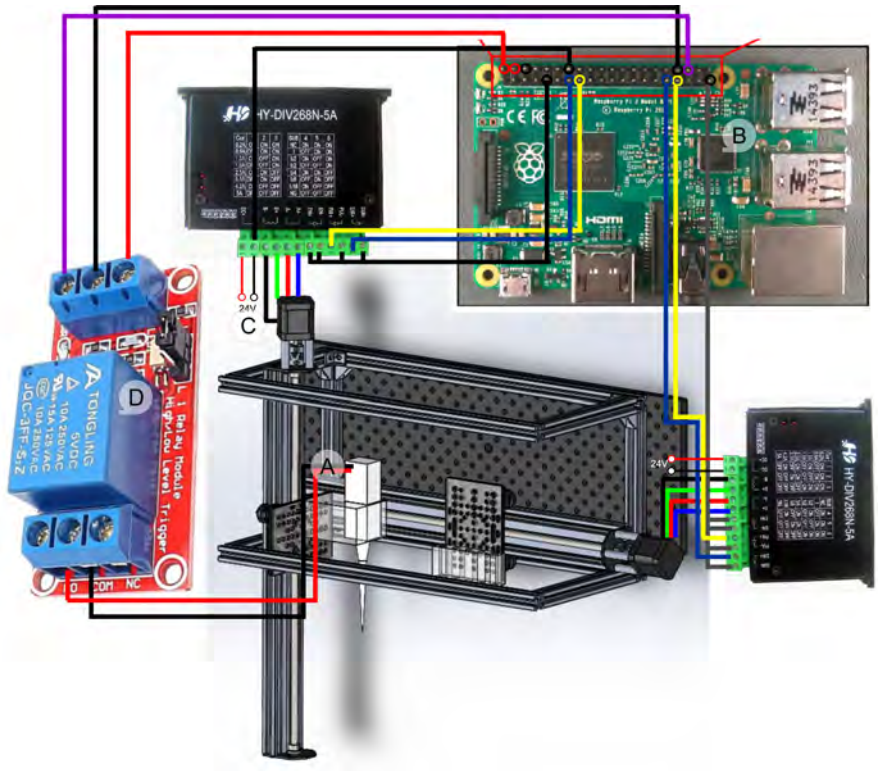

Figure 5.10: *The connection diagram of the automated dispenser constructed to dispense liquid droplets into the DLS-Lev. A indicates the position of the automated pipette, B shows the Raspberry Pi which is programmed with the code used to operate the drivers and relay shown in C and D respectively. The drivers power the rotation of the motors, which in turn cause the carriages to move.*

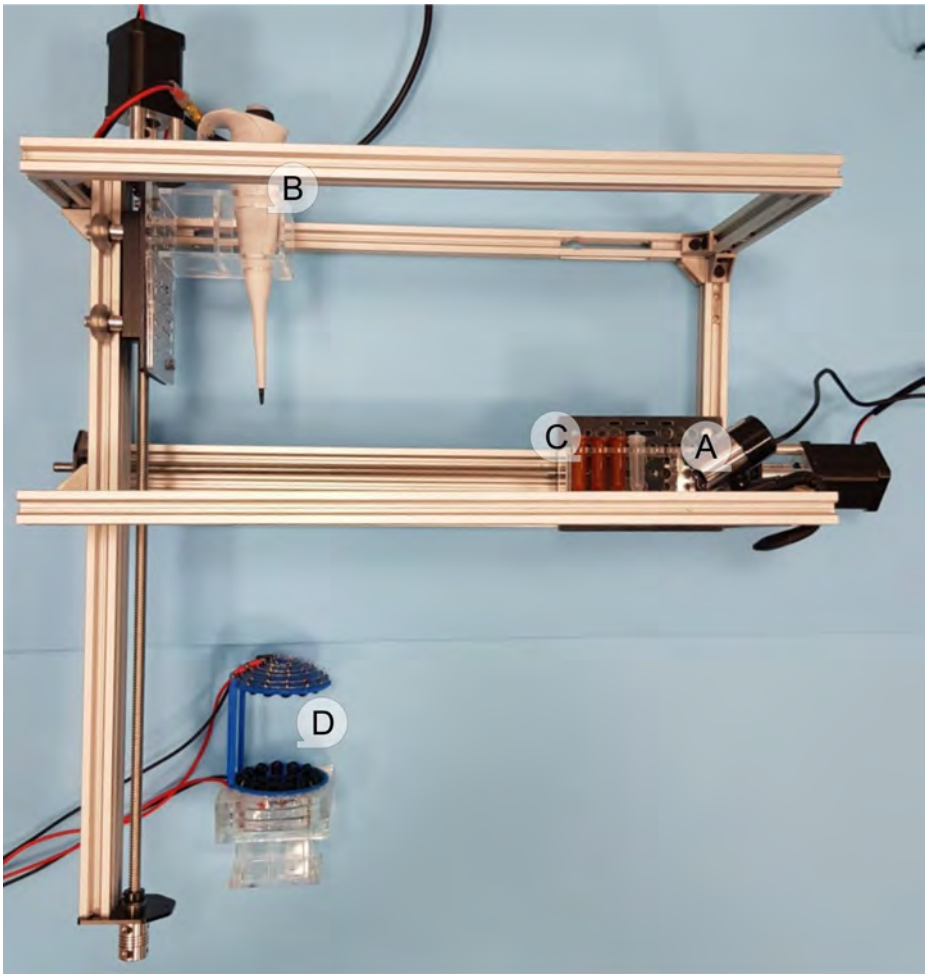

Figure 5.11: *A photograph of the constructed sample delivery system with notable features labelled. A shows the position of the webcam which is pointed toward the area in which the pipette will meet the acoustic levitator. B shows the pipette in its home position which may be moved to the bottom of the linear actuator. C shows the samples in their home position, which may be moved into the pathway of the pipette for sample collection. D shows the relative position of the acoustic levitator to the sample delivery system when it is installed at Diamond Light Source.*

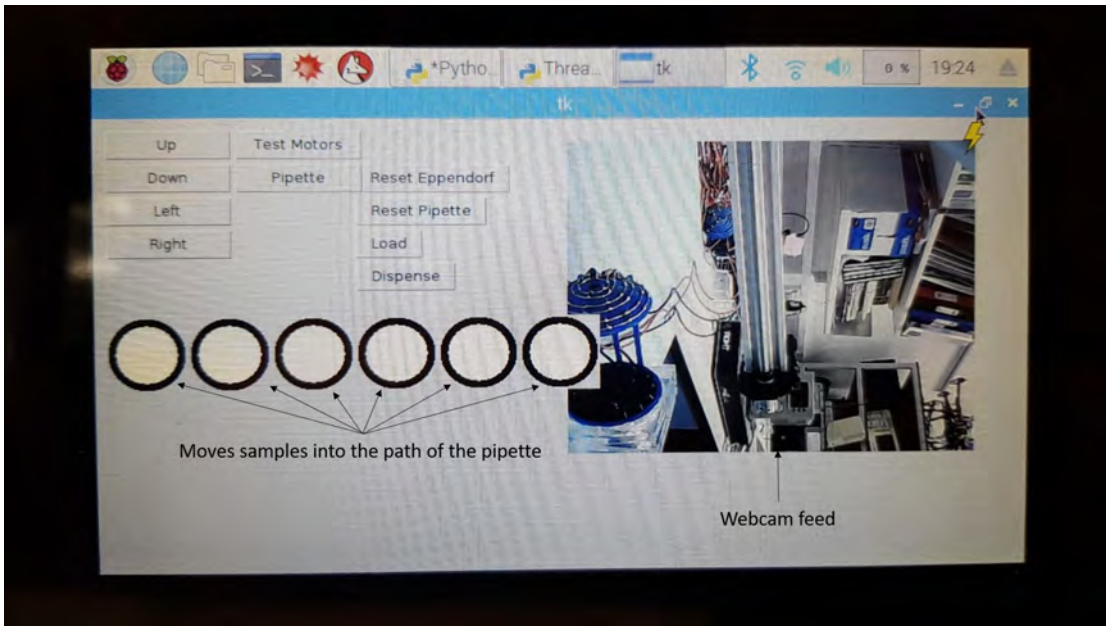

Figure 5.12: *The guided user interface (GUI) used to input the users instructions for the control of the sample delivery system, the code used to generate this GUI is shown in appendix D. The webcam is positioned in such that the interception point between the pipette tip and the acoustic levitator may be seen by the user, to ensure the pipette is not crashed into the levitator which would cause damage to the levitator and the pipette itself. The "Up" and "Down" buttons allows for the slight movement of the pipette carriage up and down respectively. The "Left" and "Right" buttons allow for the slight movement of the sample carriage. "Test Motors" moves both carriages the entire length of the track. The "Pipette" button actuates the pipette. "Reset Eppendorf" and "Reset Pipette" moves the sample carriage or the pipette carriage to their home positions. The buttons "Load" and "Dispense" moves the pipette carriage into the position in which the sample may be loaded and dispensed respectively.*

manage the movement of the stepper motors attached to either linear actuator which hold the electronic pipette and the desired samples. The drivers are controlled through the use of a Raspberry Pi 2 (Raspberry Pi (Trading) Limited, UK), programmed with code which uses a guided user interface (GUI) to convert the users instruction to movement of the delivery system. The actuation button of the pipette is electrically connected to a relay which is also controlled via the Raspberry Pi when the user inputs their desire to actuate the pipette. A webcam (which is not shown in the figure) is also connected to the Raspberry Pi and directed toward the position in which the pipette intercepts the acoustic levitator, to ensure that the pipette passes through the hole located at the top of the acoustic levitator, the live feed for this is also displayed on the GUI.

The Raspberry Pi was selected rather than an Arduino microcontroller because it is well established for the creation of GUI and is a single-board computer with its own operating system which can be remote accessed from another device through wifi, bluetooth or the use of a connected ethernet cable installed on the board [94]. These reasons make it viable for the control of the sample delivery system from several meters away through a thoroughly shielded hutch which only has a hatch allowing wires to pass through the room.

The constructed sample delivery system is shown in figure 5.11, its webcam, pipette, sample position and the DLS-Lev acoustic levitator are labelled in this photograph. This system allows for the vertical movement of the pipette carriage and the horizontal movement of the sample carriage and the actuation of the pipette. The GUI which is present on the Raspberry Pi is shown in figure 5.12 and this is also labelled, with the fully commented code which generates this provided in appendix D. The webcam feed is featured on this GUI so the user may ensure that the pipette does not damage the acoustic levitator or itself.

The sample delivery system #2 has been tested within the laboratory setting and has shown the reliable deposition of droplets into the acoustic levitator, it is modular and well supported and so transport and installation of the system does not require dismantling and reconstructing the system, which was the case with the first prototype. It has shown promise to be a useful delivery system at Diamond Light Source for use in tandem with the designed DLS-Lev acoustic levitation device. However, its installation has been delayed due to the COVID-19 pandemic.

5.5 Summary

This chapter explored the development of an automated sample delivery system to dispense droplets into the DLS-Lev device. It first discussed the SLIPS wire system which could be used

to impart the silicone oil encapsulation to a droplet of mother liquor, but this system would have needed an additional automated pipette to dispense onto it. An automated pipetting system utilising an electronic pipette, servo and a linear actuator was constructed and its operation controlled by an Arduino and a series of buttons. This system was installed at Diamond Light Source but functioned unreliably as its movement would cause the pipette to become displaced and so it did not meet the same position each time after the collection of the sample. Sample mixing was trialled within the beamline by manually loading the mother liquor droplet containing protein crystals into the suspended position within the DLS-Lev and pre-loading the ligand sample into the electronic pipette, positioning it just outside the pathway of the x-ray beam. X-ray diffraction experiments were performed on the initial droplet before the levitator was raised to meet the pipette tip and the ligand dispensed for mixing. Following this, x-ray diffraction data was collected at various points after the mixing event. The electron density maps showed that the mixed droplet had additional structures in the expected regions of the protein crystal, but insufficient time had passed for these areas to fully highlight the composition of the ligand. Further work was performed to design and construct an alternative automated pipette system. This system utilises two linear actuators that travel on carriages, one which moves the pipette vertically and the other moves eppendorfs filled with sample horizontally. This system was very stable and reliably deposited droplets into the DLS-Lev device within the laboratory setting. However, this system's installation at Diamond Light Source was delayed due to the COVID-19 pandemic closing the laboratories and restricting the types of experiments that may be performed at the beamlines.

Chapter 6

Conclusions and Future Work

6.1 Conclusions

This work has explored the use of acoustic levitation devices to suspend mother liquor droplets containing protein crystals for x-ray diffraction experiments at synchrotron. It has used established acoustic levitator systems as well as the design and construction of a unique system specifically designed for the use on the I24 beamline at Diamond Light Source. This work has also explored different methods of sample delivery in order to truly make a contactless prototype system.

The TinyLev acoustic levitation device was first explored as a preliminary system to test the proof of concept of using acoustic levitation to present samples to the beamline for x-ray diffraction experiments. Droplets were levitated within this system and imaged using two cameras and the images were analysed using code written in MATLAB. This analysis revealed that when a higher voltage is applied to the transducers within the system, the droplets experience greater lateral stability whilst being levitated but they are less spherical. The TinyLev device was investigated for its heating property to determine its suitability for its use to levitate the mother liquor, and it was determined that as the system uses low power components negligible energy was imparted into the droplet and the droplet experienced negligible temperature change during the hour time frame of the experiment. Viscosity was explored to ensure that there was no relationship between it and the shape of the levitated droplet, however it was discovered that viscosity did effect the range of voltages in which it could be levitated. Lower viscosity silicone oil droplets could be easily detached from the pipette tip however they were unstable at higher voltages and split into multiple traps. However higher viscosity silicone oil droplets could not be detached from the pipette tip at the lower TinyLev operating voltages.

Due to the success of these preliminary experiments, the TinyLev acoustic levitator was installed on the I24 beamline at Diamond Light Source. The desired sample of lysozyme crystal within its mother liquor was not stable enough to be levitated without a silicone oil coating and doing so lowered the evaporation rate sufficiently that the droplet and crystal remained hydrated

throughout loading the sample, moving the detector into place and performing the hutch search. The results from this experiment confirmed that it was a valid method to present the samples to the beamline as the structure and atomic composition of the protein crystal showed that it was lysozyme of which the structure had a resolution of 1.71 Å, and because of the contactless nature of the method, it will be ideal with the addition of an appropriate sample delivery method.

As acoustic levitation was found to be an ideal sample presentation method, a bespoke acoustic levitation device was designed, inspired by the TinyLev and named the DLS-Lev. It was designed so that all transducers point toward the centre of the system which left only a single viable position to levitate droplets, and the two sides of the structure are separated sufficiently so as to not cast a shadow on the x-ray detector. The two-sides of the levitator were much closer than that in the TinyLev acoustic levitator and so it allowed for higher density substances to be levitated and the mother liquors did not require a silicone oil coating in order to be detached from the pipette tip, levitate and remain stable. This system also allowed for top loading of the sample with a near perfect rate of levitation. There was negligible difference in the evaporation rates of water droplets at different operating voltages whilst levitated within the DLS-Lev. In contrast to the TinyLev device, the stability of the droplets suspended within the DLS-Lev acoustic levitator increased as the operating voltage of the system decreased, likely due to higher acoustic pressure surrounding the droplet at higher voltages. However, the standard deviation of the droplets position was 35 μm in the DLS-Lev, whereas the standard deviation of the position of the droplets within the TinyLev system was more than 2 mm. This shows that in a comparison between the two systems, the DLS-Lev exhibited a much more stable droplet.

Sample delivery was investigated for use with the acoustic levitators, to make them viable candidates for automated sample mixing during x-ray diffraction experiments. Side delivery was first explored so that it would also be viable to be used with the TinyLev system. SLIPS wires were investigated and they benefit from imparting the silicone oil coating to the droplet which slows the evaporation rate of the substance. However, this sample delivery method still requires an additional method to deposit the substance onto the SLIPS wire, it also requires the imbibed silicone oil on the SLIPS to be replenished between experiments. An automated pipette based delivery system was designed featuring a servo and linear actuator. This system collected the sample from the right side of the setup, raised the pipette, rotated it to the left and lowered the pipette through the hole located at the top of the acoustic levitator for actuation. This delivery system did not have a good hit rate as the movement of the servo and linear actuator caused the pipette to shake and move from its position relative to its holder so it was no longer lined up to go through the 10mm hole target featured at the top of the DLS-Lev acoustic levitator.

The automated pipette allowed for trials of sample mixing to be performed, even though the entire sample delivery system was not engaged. This was performed by depositing the lysozyme protein crystal within its mother liquor into the DLS-Lev, where it was suspended, and loading the $(GlcNAc)_4$ ligand suspension into the pipette. The tip of this pipette was positioned a few millimetres above the interaction point between the levitated droplet and the x-ray beam, at which point the x-ray hutch is cleared of personnel and the beam engaged. Data collection was performed on the lysozyme crystal within its mother liquor before the x-ray beam was turned off, the goniometer raised and the loaded sample within the pipette was dispensed into the same position as the droplet containing protein. Upon its successful deposition, the goniometer was lowered to its original position at which point additional data collection occurred. The electron density maps generated from the diffraction patterns collected for the 100 μm and 40 μm lysozyme crystals had a resolution of 1.8 Å and 1.9 Å respectively. This is slightly higher than the resolution of 1.71 Å for the lysozyme crystal levitated in the TinyLev system, however that crystal was much larger in comparison to those levitated in the DLS-Lev device. The diffraction patterns collected after the mixing event occurred showed structures beginning to appear in the regions of which the $(GlcNAc)_4$ ligand is expected, however these structures do not encompass the entire expected structure of the ligand. This is likely due to insufficient time elapsing between the samples mixing and the data collection, meaning the ligand has not yet diffused through the entire structure of the protein crystal.

An alternative sample delivery system was designed that used two linear actuators, one of these linear actuators moved up and down and had the pipette secured to it, the other had a sample holder secured to it and moved left and right into the pathway of the pipette. The system was controlled using a raspberry pi which could be remote accessed from another device and it had a near perfect hit rate to deposit droplets into the acoustic levitator in laboratory. This system is ready for installation on the I24 beamline once Diamond Light Source reopens for non-COVID experimentation though this sadly is beyond the end of my PhD programme.

This work was novel as it has demonstrated the use of low-power off the shelf transducer acoustic levitators for the sample presentation of protein crystals within droplets of their mother liquor to a beamline for x-ray diffraction experiments. It used an established system to prove the concept of these acoustic levitators and then designed and built a bespoke acoustic levitator specifically designed for use with the I24 beamline. In addition, this work trialled sample mixing during x-ray operation to open up an entire avenue of experiments that have not been possible with the traditional sample delivery methods. This will allow for substances to be added to the protein crystal and mother liquor and be investigated as they diffuse through the structure. This

will be able to be used to test the effect medicines have on proteins, and visualise their bonding sites and interactions.

6.2 Future Work

Acoustic levitation has been trialed on the I24 beamline at Diamond Light Source, and the preliminary experiments have shown promise. However, there are more tasks required in order to see this work to completion. This section discusses the proposed experiments and future of this project.

6.2.1 Permanent Installation at I24

Experiments which occur on the I24 beamline at this time are performed by mounting the protein crystals onto loops and cryogenically freezing them before a robotic arm is used to move the mounted samples into the pathway of the x-ray beam automatically. This method requires a skilled hand in order to mount crystals initially and they are kept at cryogenic temperatures with only a very thin layer of mother liquor around the crystal. This mounting and sample presentation method is not representative of the true environment the crystals would experience in vivo.

The latest droplet delivery system proposed and built within this work shows promise to be a permanent fixture at the I24 beamline to be used to minimize the man power required to mount the protein crystals onto loops the x-ray diffraction experiments. This will be because crystals within their mother liquor may be directly collected from the eppendorf tubes which contain the samples.

However, the droplet delivery system and acoustic levitator do occupy the entire space surrounding beamline, and if a user wished to present the protein crystals on loops rather than inside its mother liquor they would be unable to do so whilst both systems are installed. The acoustic levitator is light weight and portable, and it only requires the removal of four bolts in order to move it from its position in the x-ray beam path. The sample delivery system would similarly only require the removal of 4 bolts which secures its position to the breadboard above the beam shutter, however its re-installation would require alignment and would risk causing damage to the surrounding equipment, making it take some time to switch between the two delivery methods.

Therefore, in order to implement the acoustic levitator and droplet delivery system at I24 on a permanent basis, tracks would be used so that the delivery system may be moved up and away from the beamline and allow for the robotic arm to occupy that space. It would also allow for the system to move back into the correct position quickly once the delivery systems were to be switched again.

6.2.2 Roll-out to Relevant DLS Beamlines

There are 32 beamlines at Diamond Light Source, they feature a large range of disciplines and research focuses from equipment testing to imaging to analysis of geological samples. Of these beamlines, at least 6 have their main research focus as the exploration and experimentation into protein crystals and large and complex organic macromolecules.

Research completed at the I24 beamline has shown the relevance of presenting the protein crystal within its mother liquor for experimentation and these specific experiments showed acoustic levitation as a successful candidate to allow for liquid presentation. Acoustic levitation would therefore likely be a good addition to the remaining beamlines which have protein crystals as their main research focus.

The configuration of each beamline is unique in terms of the space in which samples can be presented and the configuration of the optics and the distance to the detectors. In order to utilise acoustic levitation for each of these beamlines, the system must be individually designed in order to optimise its use to ensure the volume of sample of interest may be levitated as well as ensure that the system itself does not interfere with the x-ray beam and cast a shadow on their detectors.

The VMXi beamline at Diamond Light Source has shown interest in acoustic levitation technology and using these systems for sample presentation and mixing, however their working space is significantly smaller than that in which the prototype was tested at I24, and it does not allow the room for the designed delivery system. The detector featured at this beamline is much closer to the sample position than that at I24 though and therefore would allow for the levitation device and sample delivery system to be scaled down considerably, so a bespoke system rendered using the acoustic levitation modelling code shown in appendix C with the variables for dome separation and number of transducers required changed shows promise for experimentation on this next beamline.

6.2.3 XFEL experiments

As discussed earlier, Diamond Light Source is trialling equipment to be installed at the XFEL institute in Germany. This configuration of equipment paired with the superior data collection times of the XFEL system allows for diffraction patterns to be collected much more rapidly with higher resolution. This would allow for better approximation of what a protein crystal looks like and how it behaves during sample mixing experiments, when a substance bonds to the protein crystal, breaks the polypeptide backbone or causes the crystal structure to denature and unfold the proteins.

In order to complete this work, the dimensions of the x-ray detector and its position would be needed in order to optimise the acoustic levitator using the design code provided in appendix C. And care would need to be taken to ensure that the sample delivery system would be well suited to this environment. As surrounding equipment could be damaged by the moving parts within the droplet delivery system.

Bibliography

[1] Ochiai Y, Hoshi T, Rekimoto J. Three-dimensional mid-air acoustic manipulation by ultrasonic phased arrays. PloS one. 2014;9(5):e97590.

[2] Marzo A, Ghobrial A, Cox L, Caleap M, Croxford A, Drinkwater B. Realization of compact tractor beams using acoustic delay-lines. Applied Physics Letters. 2017;110(1):014102.

[3] Marzo A, Barnes A, Drinkwater BW. TinyLev: A multi-emitter single-axis acoustic levitator. Review of Scientific Instruments. 2017;88(8):085105.

[4] Cox L, Croxford A, Drinkwater B, Marzo A. Acoustic lock: Position and orientation trapping of non-spherical sub-wavelength particles in mid-air using a single-axis acoustic levitator. Applied Physics Letters. 2018;113(5):054101.

[5] Watanabe A, Hasegawa K, Abe Y. Contactless fluid manipulation in air: Droplet coalescence and active mixing by acoustic levitation. Scientific reports. 2018;8(1):1–8.

[6] Andrade MA, Camargo TS, Marzo A. Automatic contactless injection, transportation, merging, and ejection of droplets with a multifocal point acoustic levitator. Review of Scientific Instruments. 2018;89(12):125105.

[7] Duranty E, McCardle H, Reichert W, Davis J. Acoustic levitation and infrared thermography: a sound approach to studying droplet evaporation. Chemical Communications. 2020;56(30):4224–4227.

[8] Shafee T. Protein Structure; 2016. Available from: `https://commons.wikimedia.org/wiki/File:Protein_structure_(full).png`.

[9] Bird's eye view of the synchrotron. Diamond Light Source;. Available from: `https://www.diamond.ac.uk/Science/Machine/Components.html`.

[10] UpnaLab. Acoustic Levitator; 2017. Available from: `https://www.instructables.com/Acoustic-Levitator/`.

[11] Morris R, Dye E, Axford D, Newton MI, Beale J, Docker P. Non-contact universal sample presentation for room temperature macromolecular crystallography using acoustic levitation. Scientific reports. 2019;9(1):1–10.

[12] Axford D, Docker P, Dye E, Morris R. The room temperature structure of lysozyme via the acoustic levitation of a droplet. 2019 Mar;Available from: `https://doi.org/10.2210/pdb6qq3/pdb`.

[13] Schrodinger L. The PyMOL molecular graphics system. Version. 2010;1(5):0.

[14] Brandt E. Levitation in physics. Science. 1989;243(4889):349–355.

[15] Santesson S, Nilsson S. Airborne chemistry: acoustic levitation in chemical analysis. Analytical and bioanalytical chemistry. 2004;378(7):1704–1709.

[16] Hikima T, Hashimoto K, Murakami H, Ueno G, Kawano Y, Hirata K, et al. 3D manipulation of protein microcrystals with optical tweezers for X-ray crystallography. In: Journal of Physics: Conference Series. vol. 425. IOP Publishing; 2013. p. 012011.

[17] Li C, Li L. The stable magnetic levitation of a cylindrical ferromagnetic object. Journal of Superconductivity and Novel Magnetism. 2014;27(12):2773–2778.

[18] Simon M, Geim A. Diamagnetic levitation: Flying frogs and floating magnets. Journal of applied physics. 2000;87(9):6200–6204.

[19] Rhim WK, Chung SK. Containerless protein crystal growth method. Journal of crystal growth. 1991;110(1-2):293–301.

[20] Ashkin A, Dziedzic J. Optical levitation by radiation pressure. Applied Physics Letters. 1971;19(8):283–285.

[21] Winborne DA, Nordine PC, Rosner DE, Marley NF. Aerodynamic levitation technique for containerless high temperature studies on liquid and solid samples. Metallurgical Transactions B. 1976;7(4):711–713.

[22] Morris RH, Dye ER, Docker P, Newton MI. Beyond the Langevin horn: Transducer arrays for the acoustic levitation of liquid drops. Physics of Fluids. 2019;31(10):101301.

[23] Kundt A. III. Acoustic experiments. The London, Edinburgh, and Dublin Philosophical Magazine and Journal of Science. 1868;35(234):41–48.

[24] Barmatz M, Collas P. Acoustic radiation potential on a sphere in plane, cylindrical, and spherical standing wave fields. The Journal of the Acoustical Society of America. 1985;77(3):928–945.

[25] Hoshi T, Takahashi M, Iwamoto T, Shinoda H. Noncontact tactile display based on radiation pressure of airborne ultrasound. IEEE Transactions on Haptics. 2010;3(3):155–165.

[26] Arshadi R, Cobbold RS. A pioneer in the development of modern ultrasound: Robert William Boyle (1883–1955). Ultrasound in medicine & biology. 2007;33(1):3–14.

[27] Weber J, Rey C, Neuefeind J, Benmore C. Acoustic levitator for structure measurements on low temperature liquid droplets. Review of scientific instruments. 2009;80(8):083904.

[28] Andrade MA, Buiochi F, Adamowski JC. Finite element analysis and optimization of a single-axis acoustic levitator. IEEE transactions on ultrasonics, ferroelectrics, and frequency control. 2010;57(2):469–479.

[29] Tsujino S, Tomizaki T. Ultrasonic acoustic levitation for fast frame rate X-ray protein crystallography at room temperature. Scientific reports. 2016;6(1):1–9.

[30] Andrade MA, Pérez N, Adamowski JC. Review of progress in acoustic levitation. Brazilian Journal of Physics. 2018;48(2):190–213.

[31] Hoshi T, Ochiai Y, Rekimoto J. Three-dimensional noncontact manipulation by opposite ultrasonic phased arrays. Japanese Journal of Applied Physics. 2014;53(7S):07KE07.

[32] Marzo A, Seah SA, Drinkwater BW, Sahoo DR, Long B, Subramanian S. Holographic acoustic elements for manipulation of levitated objects. Nature communications. 2015;6(1):1–7.

[33] Andersson C, Ahrens J. A method for simultaneous creation of an acoustic trap and a quiet zone. In: 2018 IEEE 10th Sensor Array and Multichannel Signal Processing Workshop (SAM). IEEE; 2018. p. 622–626.

[34] Marzo A, Caleap M, Drinkwater BW. Acoustic virtual vortices with tunable orbital angular momentum for trapping of mie particles. Physical review letters. 2018;120(4):044301.

[35] Fushimi T, Marzo A, Hill TL, Drinkwater BW. Trajectory optimization of levitated particles in mid-air ultrasonic standing wave levitators. In: 2018 IEEE International Ultrasonics Symposium (IUS). IEEE; 2018. p. 1–9.

[36] Marzo A, Drinkwater BW. Holographic acoustic tweezers. Proceedings of the National Academy of Sciences. 2019;116(1):84–89.

[37] Marzo A, Corkett T, Drinkwater BW. Ultraino: An open phased-array system for narrowband airborne ultrasound transmission. IEEE transactions on ultrasonics, ferroelectrics, and frequency control. 2017;65(1):102–111.

[38] Shen C, Xie W, Wei B. Parametrically excited sectorial oscillation of liquid drops floating in ultrasound. Physical Review E. 2010;81(4):046305.

[39] Lalanne B, Masbernat O, Risso F. Determination of Interfacial Concentration of a Contaminated Droplet from Shape Oscillation Damping. Physical Review Letters. 2020;124(19):194501.

[40] Erbil HY. Evaporation of pure liquid sessile and spherical suspended drops: A review. Advances in colloid and interface science. 2012;170(1-2):67–86.

[41] Guan JH, Wells GG, Xu B, McHale G, Wood D, Martin J, et al. Evaporation of sessile droplets on slippery liquid-infused porous surfaces (slips). Langmuir. 2015;31(43):11781–11789.

[42] Park J, Moon J. Control of colloidal particle deposit patterns within picoliter droplets ejected by ink-jet printing. Langmuir. 2006;22(8):3506–3513.

[43] Schiffter H, Lee G. Single-droplet evaporation kinetics and particle formation in an acoustic levitator. Part 1: Evaporation of water microdroplets assessed using boundary-layer and acoustic levitation theories. Journal of pharmaceutical sciences. 2007;96(9):2274–2283.

[44] Vuignier K, Schappler J, Veuthey JL, Carrupt PA, Martel S. Drug–protein binding: a critical review of analytical tools. Analytical and bioanalytical chemistry. 2010;398(1):53–66.

[45] Whitford D. Proteins: structure and function. John Wiley & Sons; 2013.

[46] Lloyd-Williams P, Albericio F, Giralt E. Chemical approaches to the synthesis of peptides and proteins. vol. 10. CRC Press; 1997.

[47] Lodish H, Berk A, Zipursky SL, Matsudaira P, Baltimore D, Darnell J. The three roles of RNA in protein synthesis. In: Molecular Cell Biology. 4th edition. WH Freeman; 2000. .

[48] Dodson G, Steiner D. The role of assembly in insulin's biosynthesis. Current opinion in structural biology. 1998;8(2):189–194.

[49] Nölting B. Protein folding kinetics: biophysical methods. Springer Science & Business Media; 2005.

[50] Petsko GA, Ringe D. Protein structure and function. New Science Press; 2004.

[51] Doye JP, Poon WC. Protein crystallization in vivo. Current opinion in colloid & interface science. 2006;11(1):40–46.

[52] Drenth J. Principles of protein X-ray crystallography. Springer Science & Business Media; 2007.

[53] Rhodes G. Crystallography made crystal clear: a guide for users of macromolecular models. Elsevier; 2010.

[54] McPherson A, Gavira JA. Introduction to protein crystallization. Acta Crystallographica Section F: Structural Biology Communications. 2014;70(1):2–20.

[55] Erickson HP. Size and shape of protein molecules at the nanometer level determined by sedimentation, gel filtration, and electron microscopy. Biological procedures online. 2009;11(1):32–51.

[56] Sirdeshmukh D. Gamma-ray diffraction–A powerful tool in crystal physics. Current Science. 1997;p. 631–640.

[57] Chao AW, Mess KH, et al. Handbook of accelerator physics and engineering. World scientific; 2013.

[58] Materlik G, Rayment T, Stuart DI. Diamond Light Source: status and perspectives. The Royal Society Publishing; 2015.

[59] Storage Ring. Diamond Light Source; 2020. Available from: `https://www.diamond.ac.uk/Science/Machine/Components/storagering.html`.

[60] Inside the Machine. Diamond Light Source;. Available from: `https://www.diamond.ac.uk/Home/About/FAQs/Inside-the-Machine.html`.

[61] Macromolecular Crystallography (MX). Diamond Light Source; 2021. Available from: `https://www.diamond.ac.uk/Instruments/Mx.html`.

[62] Smith CA, Cohen AE. The stanford automated mounter: Enabling high-throughput protein crystal screening at SSRL. JALA: Journal of the Association for Laboratory Automation. 2008;13(6):335–343.

[63] Nurizzo D, Bowler MW, Guichard N, McSweeney S, Theveneau P, Guijarro M, et al. Automated data collection based on RoboDiff at the ESRF beamline MASSIF-1. In: AIP Conference Proceedings. vol. 1741. AIP Publishing LLC; 2016. p. 030032.

[64] O'Hea J, Burt M, Fisher S, Jones K, McAuley K, Preece G, et al. BART: development of a sample Exchange system for MX beamlines. In: 16th Int. Conf. on Accelerator and Large Experimental Control Systems (ICALEPCS'17), Barcelona, Spain, 8-13 October 2017. JACOW, Geneva, Switzerland; 2018. p. 1919–1922.

[65] Snell G, Cork C, Nordmeyer R, Cornell E, Meigs G, Yegian D, et al. Automated sample mounting and alignment system for biological crystallography at a synchrotron source. Structure. 2004;12(4):537–545.

[66] Pflugrath J. Practical macromolecular cryocrystallography. Acta Crystallographica Section F: Structural Biology Communications. 2015;71(6):622–642.

[67] Allan D, Collins S, Evans G, Hall D, McAuley K, Owen R, et al. Status of the crystallography beamlines at Diamond Light Source. The European Physical Journal Plus. 2015;130(3):1–20.

[68] Maeki M, Ito S, Takeda R, Ueno G, Ishida A, Tani H, et al. Room-temperature crystallography using a microfluidic protein crystal array device and its application to protein–ligand complex structure analysis. Chemical Science. 2020;11(34):9072–9087.

[69] Jaeschke EJ, Khan S, Schneider JR, Hastings JB. Synchrotron light sources and free-electron lasers: accelerator physics, instrumentation and science applications. Springer; 2016.

[70] Martin-Garcia JM, Conrad CE, Coe J, Roy-Chowdhury S, Fromme P. Serial femtosecond crystallography: A revolution in structural biology. Archives of biochemistry and biophysics. 2016;602:32–47.

[71] Partner countries. European XFEL;. Available from: `https://www.xfel.eu/organization/partner_countries/index_eng.html`.

[72] Welcome to the XFEL Hub at Diamond. Diamond Light Source;. Available from: `https://www.diamond.ac.uk/Instruments/Mx/XFEL-Hub.html`.

[73] Wiedorn MO, Awel S, Morgan AJ, Ayyer K, Gevorkov Y, Fleckenstein H, et al. Rapid sample delivery for megahertz serial crystallography at X-ray FELs. IUCrJ. 2018;5(5):574–584.

[74] Fuller FD, Gul S, Chatterjee R, Burgie ES, Young ID, Lebrette H, et al. Drop-on-demand sample delivery for studying biocatalysts in action at X-ray free-electron lasers. Nature methods. 2017;14(4):443–449.

[75] Rasband W. US national institutes of health. http://imagej nih gov/ij/. 2011;.

[76] Gal O. fit_ellipse. MathWorks; 2003. Available from: https://uk.mathworks.com/matlabcentral/fileexchange/3215-fit_ellipse.

[77] Brown R. plot_ellipse. MathWorks; 2016. Available from: https://www.mathworks.com/matlabcentral/fileexchange/15125-fitellipse-m.

[78] Axford D, Owen RL, Aishima J, Foadi J, Morgan AW, Robinson JI, et al. In situ macromolecular crystallography using microbeams. Acta Crystallographica Section D: Biological Crystallography. 2012;68(5):592–600.

[79] Winter G, Waterman DG, Parkhurst JM, Brewster AS, Gildea RJ, Gerstel M, et al. DIALS: implementation and evaluation of a new integration package. Acta Crystallographica Section D. 2018;74(2):85–97.

[80] Brewster AS, Waterman DG, Parkhurst JM, Gildea RJ, Young ID, O'Riordan LJ, et al. Improving signal strength in serial crystallography with DIALS geometry refinement. Acta Crystallographica Section D: Structural Biology. 2018;74(9):877–894.

[81] Russi S, Gonzalez A, Kenner LR, Keedy DA, Fraser JS, van den Bedem H. Hen Egg White Lysozyme at 278K, Data set 1. 2016 Jul;Available from: https://doi.org/10.2210/pdb5kxo/pdb.

[82] Evans P, McCoy A. An introduction to molecular replacement. Acta Crystallographica Section D: Biological Crystallography. 2008;64(1):1–10.

[83] Terwilliger TC, Grosse-Kunstleve RW, Afonine PV, Moriarty NW, Zwart PH, Hung LW, et al. Iterative model building, structure refinement and density modification with the PHENIX AutoBuild wizard. Acta Crystallographica Section D: Biological Crystallography. 2008;64(1):61–69.

[84] Emsley P, Lohkamp B, Scott WG, Cowtan K. Features and development of Coot. Acta Crystallographica Section D: Biological Crystallography. 2010;66(4):486–501.

[85] Bury CS, Brooks-Bartlett JC, Walsh SP, Garman EF. Estimate your dose: RADDOSE-3D. Protein Science. 2018;27(1):217–228.

[86] Kintel M. OpenSCAD; 2019. Available from: https://www.openscad.org/.

[87] Smith JD, Dhiman R, Varanasi KK, Cabello ERg. Liquid-impregnated surfaces, methods of making, and devices incorporating the same. Google Patents; 2013. US Patent 8,574,704.

[88] Geraldi NR, Guan JH, Dodd LE, Maiello P, Xu BB, Wood D, et al. Double-sided slippery liquid-infused porous materials using conformable mesh. Scientific reports. 2019;9(1):1–8.

[89] Marzo A, Kockaya S, Freeman E, Williamson J. Tangible Interactions with Acoustic Levitation. In: Extended Abstracts of the 2019 CHI Conference on Human Factors in Computing Systems; 2019. p. 1–4.

[90] Blake C, Fenn R, Johnson L, Koenig D, Mair G, North A, et al. How the structure of lysozyme was actually determined. International Tables for Crystallography. 2006;p. 845–872.

[91] Ogata M, Umemoto N, Ohnuma T, Numata T, Suzuki A, Usui T, et al. A novel transition-state analogue for lysozyme, 4-O-β-tri-N-acetylchitotriosyl moranoline, provided evidence supporting the covalent glycosyl-enzyme intermediate. Journal of Biological Chemistry. 2013;288(9):6072–6082.

[92] Davy B, Axford D, Beale JH, Butryn A, Docker P, Ebrahim A, et al. Reducing sample consumption for serial crystallography using acoustic drop ejection. Journal of synchrotron radiation. 2019;26(5):1820–1825.

[93] Beyerlein KR, Dierksmeyer D, Mariani V, Kuhn M, Sarrou I, Ottaviano A, et al. Mix-and-diffuse serial synchrotron crystallography. IUCrJ. 2017;4(6):769–777.

[94] Kyaw AK, Truong HP, Joseph J. Low-Cost Computing Using Raspberry Pi 2 Model B. JCP. 2018;13(3):287–299.

Appendix A

Pin Base Technical Drawing

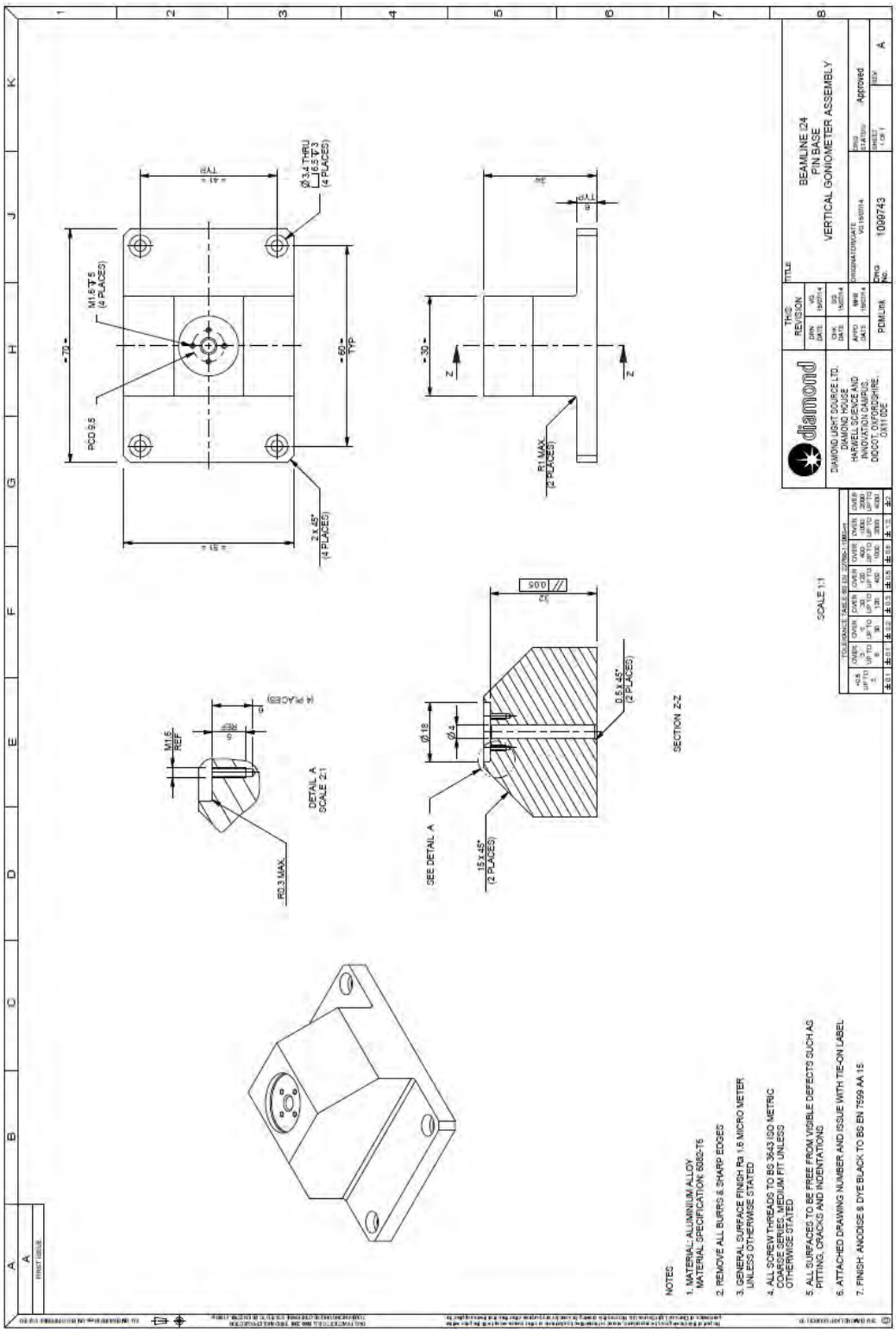

Appendix B

Image Processing code

```
%Each file should be named MATERIAL_VOLTAGE_NumberOfFrames_DELAY_RepeatNumber.tif

%Get directory contents
lof = ls('*.tif');
%for each of the files in the directory
[lolof, null] = size(lof);
elvindex=1;
for f = 1:lolof
    timindex=0;
    fname=lof(f,:);
    %Extract parameters from filenames
    dirp = strsplit(fname,'.');
    %discard the directory and split by underscore
    comps = strsplit(dirp{end-1}, '_');
    %voltage x 10
    volts(f) = str2num(comps{2});
    %Number of Frames
    Frames(f) = str2num(comps{3});
    %Time between image capture
    Delay(f) = str2num(comps{4});
    Material(f) = comps(1);

    disp(['Processing ' num2str(f) ' of ' num2str(lolof)])
    for g = 1:(Frames(f)+1-1)

        try
            ELV(elvindex) = Ellipse_Analysis_ERD_Quiet_Volatile_chanel(fname, g, 100, 3, -1);
```

```
            Tim(elvindex) = str2num(comps{4})*timindex;
            timindex=timindex+1;
            elvindex=elvindex+1;

        catch
            disp(['no more droplet, frame skipped' num2str(g)]);
        end
        close all
    end

end
save processed_dataset
```

```
%Function to process a single droplet image to find the outline and fit an
%elipse Takes two inputs and returns a structure containing the ellipse
%properties.
%
% Call as:
%
%  EL = Ellipse_Analysis_ERD_Quiet(fname, threshval);
%
% INPUTS:   fname -         full path and filename to file to process
%           fram -
%           threshval -     value of the minimum pixel intensity which will be
%                           considered droplet
% OUTPUTS:  ELV -            A structure containing the ellipse properties,
%                           see fit_ellipse for details
%
% Elizabeth Dye October 2018

function ELV = Ellipse_Analysis_ERD_Quiet_Volatile(fname, fram, threshval, chan, pola)
%Read in the image
I=imread(fname,fram);

% Select only the green channel
I = (I(:,:,chan));
I = int8(I);
if(pola==-1)
    BW = (-I)+127;
end



%Threshold the images
BW(BW<threshval)=0;
BW(BW>0)=1;
BW = logical(BW);
```

```
%Fill up the elipse
BW2 = imclose(BW, strel('disk',50));
%Skeletonise the points
BW3 = bwmorph(BW2,'remove');
%Find all points which are non-zero
[y,x] = find(BW3);
%Show the filled in image
imagesc(BW2);
%Remove outlying points
[x,y] = kill_non_circles(x,y);

%Find the ellipse
ELV = fit_ellipse(x,y);

%See if frame is empty (ELV will be 0x0)
if(size(ELV)==0)
    disp('End of useful data')
    return
end



%% Now plot it so we can see if it has worked
        a = ELV.long_axis;
        b = ELV.short_axis;
        z = [ELV.X0_in; ELV.Y0_in];
        alpha = ELV.phi;
        hold on
        plot_elipse(z, a/2, b/2, (2*pi)-alpha);
```

Appendix C

OpenSCAD code for DLS-Lev

```
$fn=40;

//Thickness of the bowl, mm
thick = 3;
//Angle up to which the bowl goes, o
da = 45;
//Focal point of the acoustic field
//(Wavelength = 8.5 mm in air for 40kHz system)
fp = 46.75;
//Radius of the pins, mm
pinsiz = 0.55;
//Radius of transducers, mm
txdiam = 5.125;
//Length of transducers, mm
txlen = 7;
//Number of transducers in each ring
//from the very centre, set to zero to skip ring
txar = [0,6,10,14];
//Size of supports, mm
supportsiz = 4;

//Calculate inner edge of bowl
rad = fp+txlen;

//Find the positions and directions of the transducers
function vectorLength(v1,v2) = sqrt(
    (v2[0]-v1[0])*(v2[0]-v1[0])+
```

```
    (v2[1]-v1[1])*(v2[1]-v1[1])+
    (v2[2]-v1[2])*(v2[2]-v1[2]));

function lookAt(v1, v2) =
    let(v = v2-v1)
    [
       0,
       acos(v[2]/vectorLength(v1,v2)),
       atan2(v[1], v[0])
    ];

module cylinderBetween(p1,p2,radius)
{
    translate(p1)
    rotate(lookAt(p1,p2))
    cylinder(vectorLength(p1,p2),radius,radius);
}

//Convert spherical coordinates to cartesian
function sph2cart(angs) =
    //Theta, Phi, r
    //echo(angs[])
    [ angs[2]*sin(angs[0])*cos(angs[1]),
      angs[2]*sin(angs[0])*sin(angs[1]),
      angs[2]*cos(angs[0])
    ];

//Make the bowl with radius, thickness and
//angle at which it stops, rotate these
//values by 360 in horizontal plane
module make_bowl(r, thickness, da)
{

 pts = [
```

```
        for (phi = [0:da]) [
        (r+thickness/2)*sin(phi)*cos(0),
        (r+thickness/2)*cos(phi)],

        for (phi = [da:-1:0]) [
        (r-thickness/2)*sin(phi)*cos(0),
        (r-thickness/2)*cos(phi)]

        ];

 rotate_extrude($fn=360){
        polygon(pts);}
   }

 //Module to draw the transducers
module makeTXs(numperring, focalpoint, pinsize, txd, txl){
    P1=[0,0,0];
    ha = atan(txd/focalpoint);
    for (npr = [0:4])
    {
        num=numperring[npr];
        elev=npr*ha*2; //*4.2
        echo(elev);
        for (i=[0:num])
        {
        P2 = sph2cart([elev,i*(360/num),focalpoint]);
        P3 = sph2cart([180-elev,i*(360/num),focalpoint]);
        // Draw focal ray lines between transducers at the top to the centre position
        cylinderBetween(P1,P2,.01);

        // Draw the transducers on top
        translate(P2)
        rotate(lookAt(P1,P2))
        {cylinder(txl,txd,txd);
```

```
            translate([txd/2,0,txl])
            cylinder(txl,pinsize,pinsize);
            translate([-txd/2,0,txl])
            cylinder(txl,pinsize,pinsize);
        }

        // Draw focal ray lines between
        //transducers at the bottom to the
        //centre position
        cylinderBetween(P1,P3,.01);

        // Draw the transducers on the bottom
        translate(P3)
        rotate(lookAt(P1,P3))
        {cylinder(txl,txd,txd);
            translate([txd/2,0,txl])
            cylinder(txl,pinsize,pinsize);
            translate([-txd/2,0,txl])
            cylinder(txl,pinsize,pinsize);
        }
        }
    }
}

//Draw the incident x-ray
//Draw a cone between x-ray interaction point
//and the edges of the detector
module addXray()
{
    color("blue")
cylinderBetween([0,0,0], [200, 0, 0], 1);
color("blue")
rotate([90, 180, 0])
    polygon(points = [[0,0], [325,-217], [325,217]],paths = [[0,1,2,0]], convexity=1);
```

```
}

//Make the top bowl, remove hole for sample deposition
difference(){
make_bowl(rad, thick, da);
makeTXs(txar, fp, pinsiz, txdiam, txlen);
cylinderBetween([0,0,-60], [0, 0, 60], 5);
}

//Make the bottom bowl, remove hole for sample deposition
difference(){
make_bowl(-rad, thick, da);
makeTXs(txar, fp, pinsiz, txdiam, txlen);
cylinderBetween([0,0,-60], [0, 0, 60], 5);
}

// Make side supports
edge = sph2cart([da, 0, rad]);
echo(edge);
translate([edge[0], 0, -rad+edge[2]/4])
cube([supportsiz, supportsiz, rad*2-edge[2]/2]);

edge2 = sph2cart([da, 30, rad]);
echo(edge);
translate([edge2[0], edge2[1], -rad+edge2[2]/4])
cube([supportsiz, supportsiz, rad*2-edge2[2]/2]);

edge3 = sph2cart([da, -30, rad]);
echo(edge);
translate([edge3[0], edge3[1], -rad+edge3[2]/4])
cube([supportsiz, supportsiz, rad*2-edge3[2]/2]);

//Draw in transducers (Comment out for printing)
color("green")
```

```
makeTXs(txar, fp, pinsiz, txdiam, txlen);

// Add the beam and the angle of acceptance
//from the sample to the detector
//(Comment out for printing)
addXray();
```

Appendix D

Control Code

```
/*
DispenseDroplet
Code created in Arduino 1.8.9 by Elizabeth Dye

This code is designed to pick up, move and dispense a droplet using a cracked
pipette(BIO511 0.2-10ul variable electronic pipettor picus), a servo and a
linear actuator.

OUTPUTS
The linear actuator should be wired to pins 1 & 2,
The Servo should be wired to pins 3 & 4,
The relay board, which controls the pipette activation, should be wired to pin 5.

INPUTS
Retroreflective sensors should be wired to pins 6, 7 & 8,
Collection button should be wired to pin 9,
Expulsion button should be wired to pin 13.

*/
// the setup function runs once when you press reset or power the board
void setup() {
// initialize digital pins as outputs.

  // Linear Actuator extension at pin 1
  pinMode(1, OUTPUT);

  // Linear Actuator retraction at pin 2
```

```
  pinMode(2, OUTPUT);

  // Rotate Servo
  pinMode(3, OUTPUT);

  // Rotate Servo (-)
  pinMode(4, OUTPUT);

  // Pipette Activated
  pinMode(5, OUTPUT);

}

// The loop function runs over and over again forever
void loop() {

// Collect the sample
if (digitalRead(9) == LOW) // Button to collect the sample is pressed
{
  if (digitalRead(8) == HIGH) // If sensor detects current position of the pipette
  {
    while (digitalRead(7) ==HIGH) // While the lower sensor does not detect pipette presence
    {
      // Extend the linear actuator
      digitalWrite(1, HIGH);
      digitalWrite(2, LOW);

    }
  }
}

// Expel a droplet from the pipette
if (digitalRead(13) == LOW)
{
```

```
  digitalWrite(5, LOW);
  delay(100);                       // sends a signal for 0.1s
  digitalWrite(5, HIGH);
  delay(2000);                      // wait for 2 seconds
}


}
```

```
################################################################
##
## Code to control the collection and dispensing of protein crystals
## within their precipitate solution, using a pair of stepper motors,
## two HY-DIV268N-5A drivers, a number of eppendorf tubes and a 0.2 -
## 10ul Picus Biohit Electronic Pipette, into a DLS-Lev Levitator on
## I24 at Diamond Light Source. Webcams have been added to ensure the
## correct operation of system.
##
## By Elizabeth R. Dye 24th Oct 2019
##
################################################################

## Import vital libraries
import time
import RPi.GPIO as GPIO
from tkinter import *
from tkinter import messagebox
import PIL
from PIL import Image, ImageTk
import pytesseract
import cv2
from threading import Thread

#set up video capture, and set sizes
cap = cv2.VideoCapture(0)
cap.set(cv2.CAP_PROP_FRAME_WIDTH, 300)
cap.set(cv2.CAP_PROP_FRAME_HEIGHT, 300)

# Define the Pi pins used to control the drivers, Enable pins are grounded

directionPin1 = 13
pulsePin1 = 15
pulseState1 = 0
```

```
directionPin2 = 31
pulsePin2 = 33
pulseState2 = 0

PipetteMotorposition = 0
EppenMotorposition = 0

Pipette = 36

#define time delay between each pulse
delay = 0.00005

#make GUI popup and insert webcam
top = Tk()
top.geometry("600x300")
top.bind('<Escape>', lambda e: top.quit())
lmain = Label(top)
lmain.place(x=400, y=20)

#call the image file for eppendorf buttons
img = PhotoImage(file="button.ppm")

def EppendorfThread(i):
    p = Thread(target=Eppendorf, args=(i))
    p.start()

def pipetteThread(i):
    t = Thread(target=pipette, args=(i))
    t.start()

def PipThread():
    d = Thread(target=Pip)
    d.start()
```

```
# Board set up, set pins to output
def setup():
    GPIO.setmode(GPIO.BOARD)

    GPIO.setup(directionPin1, GPIO.OUT)
    GPIO.setup(pulsePin1, GPIO.OUT)
    GPIO.setup(directionPin2, GPIO.OUT)
    GPIO.setup(pulsePin2, GPIO.OUT)
    GPIO.setup(Pipette, GPIO.OUT)
    return
# A function to cause the pipette activate and collect or dispense a droplet
def Pip():
    #Set up board and output pins
    setup()
    # output signal to cause collect/dispense to activate
    GPIO.output(Pipette, 1)
    # time delay of activation
    time.sleep(0.1)
    # Terminate activation
    GPIO.output(Pipette, 0)
    #time delay
    time.sleep(0.1)
    GPIO.cleanup()
    return

# A function to make the linear actuator with the pipette mounted move down
def down(steps):
    #Set up board and output pins
    setup()
    #Call global variables
    global PipetteMotorposition
    global pulseState1
    #Print variables
```

```
    print("Pipette Position = %d, down delay = %0.3fms, steps = %d"
    % (PipetteMotorposition, delay *1000, steps))
    #set direction of linear acuator movement
    GPIO.output(directionPin1, 1)
    #iterate the pulse state, to move the motor
    for i in range (steps):
        pulseState1 += 1
        GPIO.output(pulsePin1, pulseState1 % 2)
        time.sleep(delay)
    pulseState1 %=2
    time.sleep(0.5)
    PipetteMotorposition = PipetteMotorposition + steps
    GPIO.cleanup()
    return

# A function to make the linear actuator with the pipette mounted move up
def up(steps):
    #Set up board and output pins
    setup()
    #Call global variables
    global pulseState1
    global PipetteMotorposition
    #Print variables
    print ("Pipette Position = %d, up delay = %0.3fms steps = %d"
    % (PipetteMotorposition, delay *1000, steps))
    #set direction of linear acuator movement
    GPIO.output(directionPin1,0)
    #iterate the pulse state, to move the motor
    for i in range(steps):
        pulseState1 +=1
        GPIO.output(pulsePin1,pulseState1 % 2)
        time.sleep(delay)
    pulseState1 %= 2
    time.sleep(0.5)
```

```
    PipetteMotorposition = PipetteMotorposition - steps
    GPIO.cleanup()
    return

# A function to make the linear actuator with the eppendorfs mounted move left
def left(steps):
    #Set up board and output pins
    setup()
    #Call global variables
    global EppenMotorposition
    global pulseState2
    #Print variables
    print("Sample Position = %d, left delay = %0.3fms, steps = %d"
    % (EppenMotorposition, delay *1000, steps))
    #set direction of linear acuator movement
    GPIO.output(directionPin2, 1)
    #iterate the pulse state, to move the motor
    for i in range (steps):
        pulseState2 += 1
        GPIO.output(pulsePin2, pulseState2 % 2)
        time.sleep(delay)
    pulseState2 %=2
    time.sleep(0.5)
    EppenMotorposition = EppenMotorposition + steps
    GPIO.cleanup()
    return

# A function to make the linear actuator with the eppendorfs mounted move right
def right(steps):
    #Set up board and output pins
    setup()
    #Call global variables
    global EppenMotorposition
    global pulseState2
```

```
    #Print variables
    print ("Sample Position = %d, right delay = %0.3fms steps = %d"
    % (EppenMotorposition, delay *1000, steps))
    #set direction of linear acuator movement
    GPIO.output(directionPin2,0)
    #iterate the pulse state, to move the motor
    for i in range(steps):
        pulseState2 +=1
        GPIO.output(pulsePin2,pulseState2 % 2)
        time.sleep(delay)
    pulseState2 %= 2
    time.sleep(0.5)
    EppenMotorposition = EppenMotorposition - steps
    GPIO.cleanup()
    return

# A function to make the linear actuator with the pipette mounted move
def pipette(i):
    #Call global variables
    global PipetteMotorposition
    global pulseState1
    #defined positions of the pipette
    PIPETTE = 0, 21500, 77000
    PIP=PIPETTE[i]
    #calculate steps
    steps = PIP-PipetteMotorposition

    if steps>0:
        down(steps)
    elif steps<0:
        steps = abs(steps)
        up(steps)
    elif steps==0:
        print("Pipette in position")
```

```
    else:
        print("Something is wrong in dispensing")

    return


# A function to make the linear actuator with the samples mounted move
def Eppendorf(i):
    #Call global variables
    global EppenMotorposition
    global pulseState2
    #defined positions of the sample tubes
    Eppendor = 0, 189000, 199500, 211000, 221500, 232500,243000
    Tube = Eppendor[i]
    #calculate steps
    steps = Tube-EppenMotorposition

    if steps>0:
        left(steps)

    elif steps<0:
        steps = abs(steps)
        right(steps)

    elif steps==0:
        print("Already in position")
    else:
        print("Something is wrong in Eppendorf")

    return

# Function to insert a webcam stream to the GUI
def show_frame():
    _, frame = cap.read()
```

```
    frame = cv2.flip(frame, 1)
    cv2image = cv2.cvtColor(frame, cv2.COLOR_BGR2RGBA)
    img = PIL.Image.fromarray(cv2image)
    imgtk = ImageTk.PhotoImage(image=img)
    lmain.imgtk = imgtk
    lmain.configure(image=imgtk)
    lmain.after(10, show_frame)


# A test sequence to move the linear actuators their entire length.
def main():
    setup()
    down(82000)
    time.sleep(0.5)
    up(82000)
    time.sleep(0.5)
    left(260000)
    time.sleep(0.5)
    right(260000)
    GPIO.cleanup()
    return

try:
    UP = Button(top, text = "Up", command = lambda: up(500), width = 10)
    UP.place(x=10,y=10)
    DOWN = Button(top, text = "Down", command = lambda: down(500), width = 10)
    DOWN.place(x=10,y=40)
    LEFT = Button(top, text = "Left", command = lambda: left(10500), width = 10)
    LEFT.place(x=10,y=70)
    RIGHT = Button(top, text = "Right", command = lambda: right(10500), width = 10)
    RIGHT.place(x=10,y=100)
    HomeEppen = Button(top, text = "Reset Eppendorf", command= lambda: EppendorfThread(0))
    HomeEppen.place(x=220, y=40)
    A=Button(top, image=img, bd=0, command = lambda: EppendorfThread(1))
```

```
    A.place(x=10, y=180)
    B=Button(top, image=img, bd=0, command = lambda: EppendorfThread(2))
    B.place(x=80, y=180)
    C=Button(top, image=img, bd=0, command = lambda: EppendorfThread(3))
    C.place(x=150, y=180)
    D=Button(top, image=img, bd=0, command = lambda: EppendorfThread(4))
    D.place(x=220, y=180)
    E=Button(top, image=img, bd=0, command = lambda: EppendorfThread(5))
    E.place(x=290, y=180)
    F=Button(top, image=img, bd=0, command = lambda: EppendorfThread(6))
    F.place(x=360, y=180)
    ResetPip = Button(top, text = "Reset Pipette", command= lambda: pipetteThread(0))
    ResetPip.place(x=220, y=70)
    Pickup = Button(top, text = "Load", command= lambda: pipetteThread(1))
    Pickup.place(x=220, y=100)
    Dispense = Button(top, text = "Dispense", command= lambda: pipetteThread(2))
    Dispense.place(x=220, y=130)
    TEST = Button(top, text = "Test Motors", command = main, width = 10)
    TEST.place(x=120,y=10)
    PIP = Button(top, text = "Pipette", command = PipThread, width = 10)
    PIP.place(x=120,y=40)
    show_frame()



    top.mainloop()


except:
    print("Something went wrong!")
    GPIO.cleanup()
```

Appendix E

Publications

SCIENTIFIC REPORTS
nature research

OPEN

Non-Contact Universal Sample Presentation for Room Temperature Macromolecular Crystallography Using Acoustic Levitation

Received: 8 April 2019
Accepted: 24 July 2019
Published online: 27 August 2019

R. H. Morris[1], E. R. Dye[1], D. Axford[2], M. I. Newton[1], J. H. Beale[2] & P. T. Docker[2]

Macromolecular Crystallography is a powerful and valuable technique to assess protein structures. Samples are commonly cryogenically cooled to minimise radiation damage effects from the X-ray beam, but low temperatures hinder normal protein functions and this procedure can introduce structural artefacts. Previous experiments utilising acoustic levitation for beamline science have focused on Langevin horns which deliver significant power to the confined droplet and are complex to set up accurately. In this work, the low power, portable TinyLev acoustic levitation system is used in combination with an approach to dispense and contain droplets, free of physical sample support to aid protein crystallography experiments. This method facilitates efficient X-ray data acquisition in ambient conditions compatible with dynamic studies. Levitated samples remain free of interference from fixed sample mounts, receive negligible heating, do not suffer significant evaporation and since the system occupies a small volume, can be readily installed at other light sources.

Efficient micro-dimensional sample delivery is becoming increasingly important to Macromolecular Crystallography (MX) at synchrotron light sources. Improvements in X-ray optics now allow for sub-micron beam profiles, increasing the need for the development of novel methods in sample delivery and alignment. Currently, by far the most common strategy, which accounted for 97% of the published X-ray structures in 2017, relies upon a cryo-cooled sample. Cryo-cooling is principally used to reduce sample damage from the effects of the ionizing X-ray beam whilst measurements are made. However, cryogenic temperatures are not the natural state of biological molecules and the cryo-cooling process can be terminally detrimental to the crystal architecture[1]. Cryo-cooling also prohibits the observation of biological reactions in real-time and potentially locks the protein in an unrepresentative conformation[2]. In this respect, effective data acquisition methods for room temperature crystallography represent a valuable tool for structural biologists[3], albeit operating within the limits of protein crystal packing and order.

The development of X-ray Free Electron Lasers (XFELs) has led to the evolution of novel sample delivery strategies, which are now also being applied to synchrotron light sources. The brilliance of the XFEL pulse allows for a single, still diffraction image to be collected before the protein crystal is destroyed, removing the need for sample cryo-cooling. Therefore, sample delivery systems have been developed which channel large quantities of protein crystals into the XFEL beam at room temperature. These methods, including dynamic virtual nozzles[4], lipidic cubic phase (LCP) extruders[5], acoustic droplet ejectors (ADE)[6], concentric-flow electrokinetic injectors[7] and conveyor belts[8], all share a more dynamic approach to sample delivery. Since these systems operate at room temperature, samples are much closer to the typical operating temperatures of functional proteins, bringing the possibility for small molecule diffusion during the X-ray data collection. Room temperature experiments therefore allow for reaction dynamics to be probed and for structure artefacts present in cryo-cooled samples to be avoided.

[1]School of Science and Technology, Nottingham Trent University, Nottingham, NG11 8NS, UK. [2]Diamond Light Source, Harwell Science and Innovation Campus, Oxfordshire, OX11 0DE, UK. Correspondence and requests for materials should be addressed to R.H.M. (email: rob.morris@ntu.ac.uk)

In recent years synchrotron MX beamlines have adopted similar methods to those created for XFELs as some are directly transferable, such as the fixed-targets[9] and LCP extruders[10]. The success of this transfer has even inspired dedicated serial MX beamlines at PETRA[11], Germany, at MAX IV[12], Sweden, and also at ESRF, France[13], allowing for novel sample delivery and alignment methods to be explored, although some of these techniques introduce physical non-sample materials into the path of the beamline. Surface acoustic wave techniques have also been shown to be useful to present room temperature MX samples to the X-ray beam at both synchrotron and XFEL sources and have been shown to be non-destructive in respect to protein crystals[14,15].

A technique which does not introduce any crystalline non-sample material into the beamline is acoustic levitation, where the sample is presented without contact from external supports as has been previously demonstrated for MX at the Swiss Light Source[16]. This builds on other X-Ray scattering experiments with levitated samples such as at the MAX II, Sweden[17] and BESSY, Germany[18,19]. It has also been used for small-molecule X-ray diffraction experiments (for example Klimakow[20] and Nguyen[21]). Such approaches however, have not found widespread adoption owing to the fact that they typically require the construction of two frequency matched Langevin horns, a costly and challenging process. Furthermore, as the Langevin horns' frequency shifts with temperature by $\approx$4 Hz/C[22] a pre-experiment stabilisation time and a controlled temperature and humidity environment are required. Changes in temperature also impact the stability of the standing wave nodes due to the corresponding change in the speed of sound[23]. Langevin horn systems also impart significant energy into the entrapped fluids yielding high or uncontrolled temperatures during experiments.

A new generation of low cost, low power, portable and self-contained acoustic levitation devices is demonstrating renewed opportunities for the approach. The TinyLev system[24] offers contact-free manipulation with no pre-experiment conditioning.

Whilst acoustic levitators are capable of supporting almost any liquid in a suitably sized droplet, delivering such a droplet to a system can be challenging. This is particularly true when also trying to incorporate a protein crystal inside the delivered droplet. Protein crystals are typically grown in solvents with high surface tensions and therefore, the crystal solution often remains attached to the pipette tip during loading into the levitation field. Droplet stability has been shown to be improved by adding a coating of oil[25] which also brings the potential benefit of a significant reduction in sample evaporation rates (as demonstrated for octadecanol[26]).

In this study we demonstrate an application of the acoustic trap system as described by Marzo[24]. Protein crystals are suspended in single, microlitre sized droplets, coated in silicone oil and presented acoustically to the X-ray beam. Two sample forms were investigated: small numbers of 100 to 800 μm crystals and also a high density slurry of 10 to 15 μm crystals. We have found that the incorporation of silicon oil coat around the protein crystal solution dramatically increases the ease of delivering the levitating drop incorporating the sample crystal. This method has solved a significant barrier to entry for acoustically levitating MX samples and will open up new avenues of automated sample delivery. The coating will allow for the universal presentation of liquid samples regardless of their surface tension. The device both suspends the sample and also imparts a modest but sufficient motion to allow for a complete, high-quality, rotation style dataset to be recorded and processed in an efficient and routine manner. We have also determined the optimum system voltage to trap relevant sample volumes to maximise the applicability of the encapsulated droplet approach.

Results

Results of each of the experiments are presented in the following sections.

Optimisation of levitator voltage. It is well observed that, in addition to numerous system parameters, the transducer power has a significant effect on the shape and stability of droplets within acoustic levitation systems. This is due to the changes in the resulting sound pressure levels, which was previously explored using the Langevin systems[27,28]. The same was true of the TinyLev system, and the data in Fig. 1 shows the relationship between droplet sphericity (as determined using Equation 1) and spatial stability, as a function of the applied voltage for a levitated silicone oil coated water droplet. In this work, 350 cSt silicone oil was used as it offered the optimum compromise (from a range of silicone oils varying from 10 cSt to 10,000 cSt) for delivering a sufficient thickness of coating to the droplet whilst not requiring extensive time to pipette. It may be favourable in other MX experiments utilising this method to use alternative oils to ensure compatibility with the elements of the crystallisation solution or to further reduce background signals in exchange for less favourable reduction in evaporation rates.

Throughout the droplet tracking experiments, no measurable evaporation of the samples was seen, suggesting that the coating of silicone oil was sufficient to limit sample loss to the environment. An off line experiment monitoring the evaporation of water and ethanol droplets with and without silicone oil coating is presented in ESI1 confirming these findings; showing less than 5% change over the 50 minutes which an uncoated droplet took to evaporate until unconfined. The use of non-hygroscopic oils should theoretically eliminate evaporative processes entirely.

It was seen that there was a decline in the droplet sphericity as a function of applied voltage which remained above 97% until 11.5 V. The stability however, improved twofold up to 11.5 V and then fell within error estimates up to 12 V. This suggested that 11.5 V represented the best compromise between maintaining drop stability and sphericity for these samples, and was therefore used for all synchrotron experiments. This results in the presentation of an oblate cross section to the beamline of (2.30 ± 0.01) mm by (1.50 ± 0.02) mm. It is however likely, that this voltage will not be optimum for samples which have radically different densities or surface tensions such as crystallisation solutions with high concentrations of volatile components or high molecular weight poly-ethylene glycols.

Minor imperfections in the efficiency of the 72 ultrasonic transducers, slight irregularities in sample density, morphology and local air turbulance also tend to impart a slight rotation of the droplet. This rotation was

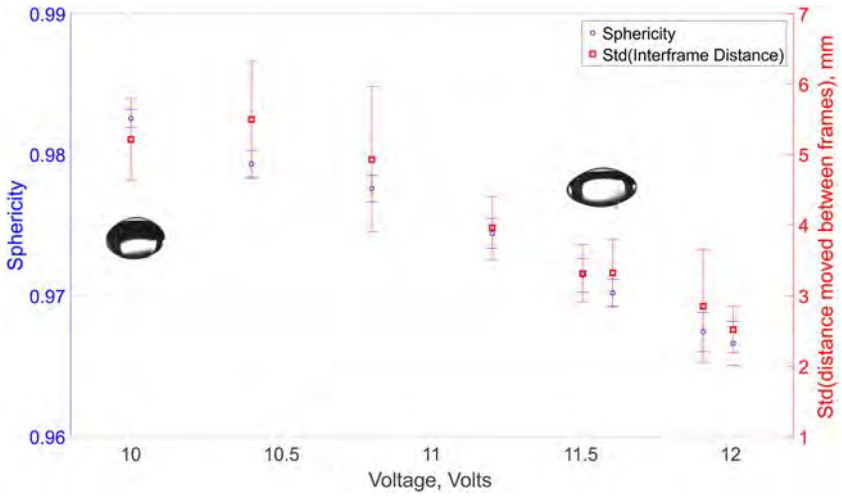

Figure 1. Plot of the droplet sphericity and stability as a function of applied voltage. Voltages above 11.5 V provide the greatest stability but with an ever increasing effect on the sphericity. This voltage was used for all synchrotron experiments.

exploited during X-ray data collection to allow the collection of a complete X-ray diffraction dataset (discussed in the following section). The suspension of such droplets against gravity using this system requires little energy and thus imparts no significant heating to the sample (confirmed by non-recorded thermal imaging), allowing for true ambient investigation of the protein structure.

Macromolecular crystallography. The lysozyme crystal structure (structure factors and coordinates have been deposited under Protein Data Bank (PDB) entry 6QQ3[29]) was determined from a single continuous collection run of 5,000 images (yielding 4,086 merged and scaled diffraction patterns) on a drop containing an estimated 4–6 crystals with dimensions ranging from 100 to 800 μm. The statistics are presented in Table 1. An example of the diffraction recorded on the detector is shown in Fig. 2(A). We have exploited serial crystallography data analysis tools to analyse detector frames on an individual basis, given the absence of a fixed axis of rotation for the levitating droplet. Although all patterns from the best single data collection run were included to optimise the data metrics of the deposited dataset, as few as 500 images were sufficient for a 96.7% complete dataset to 1.69 Å. This finding highlights the potential for the method to record structural data in an extremely rapid and efficient manner, particularly if a continuous rotation of the drop occurs. Future iterations of the system aim to eliminate this uncontrolled rotation and instead impart an induced, constant rotation by modifying the design of the transducer array, relative transducer phasing and drive electronics to further facilitate this process. ESI2 provides a movie of a droplet spinning outside of the synchrotron setup but with otherwise identical parameters to demonstrate the motion experienced.

Example electron density from the structure (available as PDB entry 6QQ3[29]) is shown in Fig. 3. This demonstrates the device's ability to produce high quality structural information from acoustically supported microlitre volumes in a completely non-contact manner at room temperature.

Processing *via* a serial method assumes each detector frame to be an individual experiment and refines an independent crystal lattice orientation for each instance. A more detailed analysis of the 5,000 image structure solution run reveals the presence of multiple lattices and their respective motions during data collection. Figure 4(C) shows a stereographic projection that plots the direction of the [001] *hkl* of each integrated lattice as indexed in P1, so as not to show symmetrically related reflections. The clusters on the plot suggest the presence of multiple crystals but could also represent crystals leaving the beam and then re-entering at a different orientation. On any one image a maximum of three lattices are detectable, occurring on 154 images and indicating an absolute minimum of 3 crystals in the drop. Assessing the number of crystals visually was not possible so the success of the transfer step from the crystallisation tray was uncertain. The largest continuous run from a single lattice is 2,260 frames (maximum separation of 3 between consecutive images). An animation has been constructed from these data to illustrate the motion of this crystal and is included in ESI3. Across the entire collection run and accounting for discontinuities, the mean oscillation step between frames is 0.64 (s.d. 0.59) or 64/s with a maximum oscillation step of around 2 or 200/s.

The 2,260 frames of single lattice data allows us to estimate a dose on this crystal using the parameters reported in Table 1, the RADDOSE-3D program[30] and estimates of the crystal sizes: a crystal of 100 × 100 × 200 μm gives a diffraction weighted dose of 210 kGy and a crystal of 200 × 400 × 800 μm gives a diffraction weighted dose of 150 kGy. This assumes the crystal remains centred on the beam as it rotates, any misset, which seems quite likely in this case, would bring additional sample volume to the beam. Exploiting the fact that near complete data could be obtained by relatively few images, further investigation of radiation induced changes to the protein structure was undertaken by comparing datasets formed from the first and last 750 images of the 2,260 image run. Isomorphous difference maps showed no significant or obvious features. However, a comparison of the two 750 image subsets did reveal a drop with an I/σI from 6.06 to 4.23 over a resolution range of 39.75–1.70 Å and from 1.14 to 0.69 in

Data collection	
Beamline	BLI24 (Diamond Light Source)
Wavelength (Å)	0.9686
Incident flux (photons per s)	3×10^{11}
Beam size (m)	50×50
Exposure time (ms)	10
Detector	Pilatus3 6 M
Sample-detector distance (mm)	325
No. frames collected	5,000
No. integrated (merged) frames	4,096 (4,086)
Scaling and merging	
Space Group	$P4_32_12$
Unit cell parameters (Å)	79.4, 79.4, 37.9
Resolution range (Å)	39.74–1.53 (1.56–1.53)
R_{split}	0.101 (0.549)
$CC_{1/2}$	0.982 (0.665)
$(I/\sigma(I))$	3.52 (0.71)
Multiplicity	101.5 (8.84)
Completeness (%)	99.5 (95.0)
Refinement	
No. reflections	18,767
No. non-H atoms (protein)	2,480
No. non-H atoms (water)	76
R/R_{free}	0.179/0.203
R.m.s.d., bond length (Å)	0.005
R.m.s.d., bond angles ()	0.767
Ramachrandran outliers (%)	0
Side chain outliers (%)	0.8
PDB code	6QQ3

Table 1. Summary statistics for diffraction data collection, processing and refinement.

the highest resolution shell (1.73–1.70 Å). This drop in $I/\sigma I$ suggests that although the obvious effects of radiation damage did not appear to manifest in the electron density, they were still present.

The potential of the device with micro-crystals was also explored with a data collection on a micro-crystal slurry of 10–15 m lysozyme crystals. Raster scanning the droplet through the beam revealed the micro-crystals sedimenting and diffraction from the bottom was powdery and not readily interpretable. However, by positioning a $20 \times 20\,\mu m$ beam just above the sedimented region, individual lattices could be recorded, indexed and integrated with a moderate hit-rate. An example of diffraction recorded on the detector is shown in Fig. 2(B) with individual diffraction spots not easily visible, in contrast to the large crystal in Fig. 2(A). In total, 1,498 useful patterns were obtained from a 10,000 image collection from a single drop; enough for a complete dataset to a resolution of approximately 2.6 Å. Figure 4(D) shows the individual lattice orientations and in contrast with the deposition dataset (Fig. 4(C)), a large number of different crystals are suggested; each contributing a smaller proportion of the total data. The limited resolution seen from the micro-crystals is a function of the significant background scatter from the liquid volume of the drop and this is illustrated in Fig. 2(C); a comparison of the scattering from the deposition data, the micro-crystal data, an oil-encapsulated droplet of buffer and air scatter. The background scatter from the drop is about 6 times larger than that of an air path, and whilst the large crystal diffraction is seen to extend beyond the edge of the detector, the much weaker diffraction from the micro-crystals disappears into the droplet-scatter at much reduced angles.

Discussion

We have presented results demonstrating the potential of acoustically levitated, oil encapsulated drops as a physical mount free method for Macromolecular Crystallography experiments. Levitation can enable efficient room temperature *in situ* X-ray data collection, in part by exploiting the fact the sample motion is not about a fixed single axis, thus potentially accelerating the acquisition of a complete set of crystal reflections.

The oil-encapsulation approach neatly side-steps the issue of droplet surface tension that can adversely affect device loading and sample stability. Additionally the non-contact nature of the technique offers advantages to traditional presentation methods utilising cryogenic sample fixed on pins[31,32] or on physical films[33]. Furthermore, oil encapsulation of droplets significantly lowers evaporation rates enabling data collection on volatile solutions and removes the complication of dehydration and variable sample volume. Similarly, the minimal energy which is imparted into the droplet in acoustic suspension ensures that there is little droplet heating, greatly reducing the risk of sample damage that can come with higher power Langevin horn systems and improving the relevance of

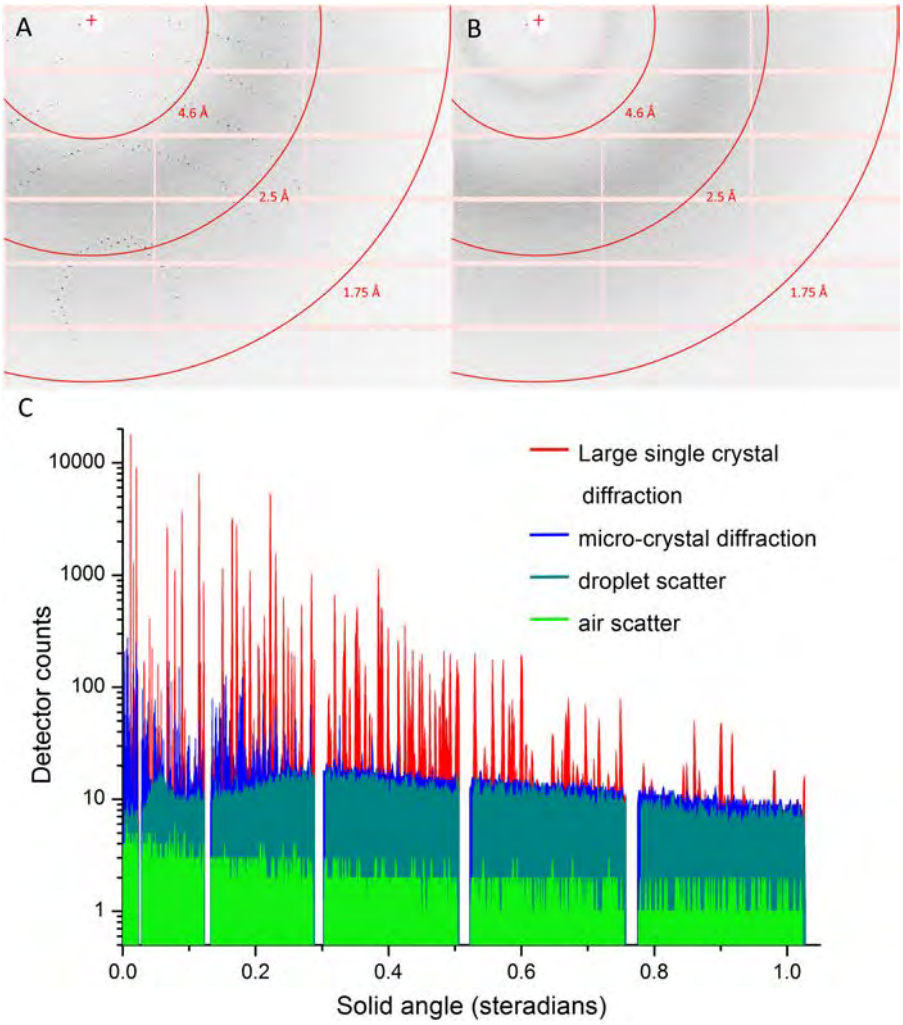

Figure 2. Composite figure illustrating sample diffraction and background scatter. (**A**) Section of detector image showing example large crystal diffraction used for structure deposition. (**B**) Section of detector image showing example micro-crystal diffraction. (**C**) X-ray scatter from levitating drop experiments as image sections taken downwards from beam-centre to edge of detector and plotted as a solid angle. The diffraction profiles represent maximum pixel values recorded over the structure deposition dataset (red) and the micro-crystal slurry dataset (blue). For comparison, 100 image averaged scatter profiles from a drop of crystal buffer with silicone oil preparation (grey) and air scatter (green) are also shown.

the resulting data. The light-weight and low-volume of the TinyLev device enabled easy location of the levitating drop to the X-ray beam since the existing beamline sample positioning stages could be used. Indeed, even raster scanning was possible to quickly assess variation in density of sample over the droplet cross-section.

Although serial methods were used for data analysis, the final dataset was more readily derived by virtue of the crystal motion. This motion allows for a larger slice of reciprocal space to be recorded than would be from a static sample with a monochromatic X-ray beam. As a result the mean oscillation width observed here of 0.64 enabled the collection of complete data with hundreds of images rather than the thousands typically required for structure determination with serial stills. With dose estimates in the hundreds of kGy range for the deposition dataset, some radiation induced changes would be expected at room temperature and a drop in $I/\sigma I$ was observed here. However, these estimates are compromised by not being able to visualise the diffracting crystal and the crystal not being aligned precisely to the beam. Currently, integrating diffraction data with an oscillation model when the crystal is rotating about a variable axis and with varying direction and speed represents a non-trivial analysis problem. Developments within the open source Diffraction Integration for Advanced Light Sources (*DIALS*)[34] software framework are being explored to improve the ease of such analysis.

The restricted resolution seen in the micro-crystal diffraction indicates that the drop volume and its contribution to background scatter is currently a limitation. We anticipate being able to reduce the droplet volume (and concomitantly the useful crystal volume) with theoretical estimates suggesting minimum droplet sizes in picolitres. This will create opportunities for studies of the more dynamic processes accessible in ambient conditions, such as *in crystallo* enzyme-substrate turnover experiments, which are greatly dependent on diffusion rates. Additionally, to enhance the applicability of the method, future work will explore automated delivery of droplets

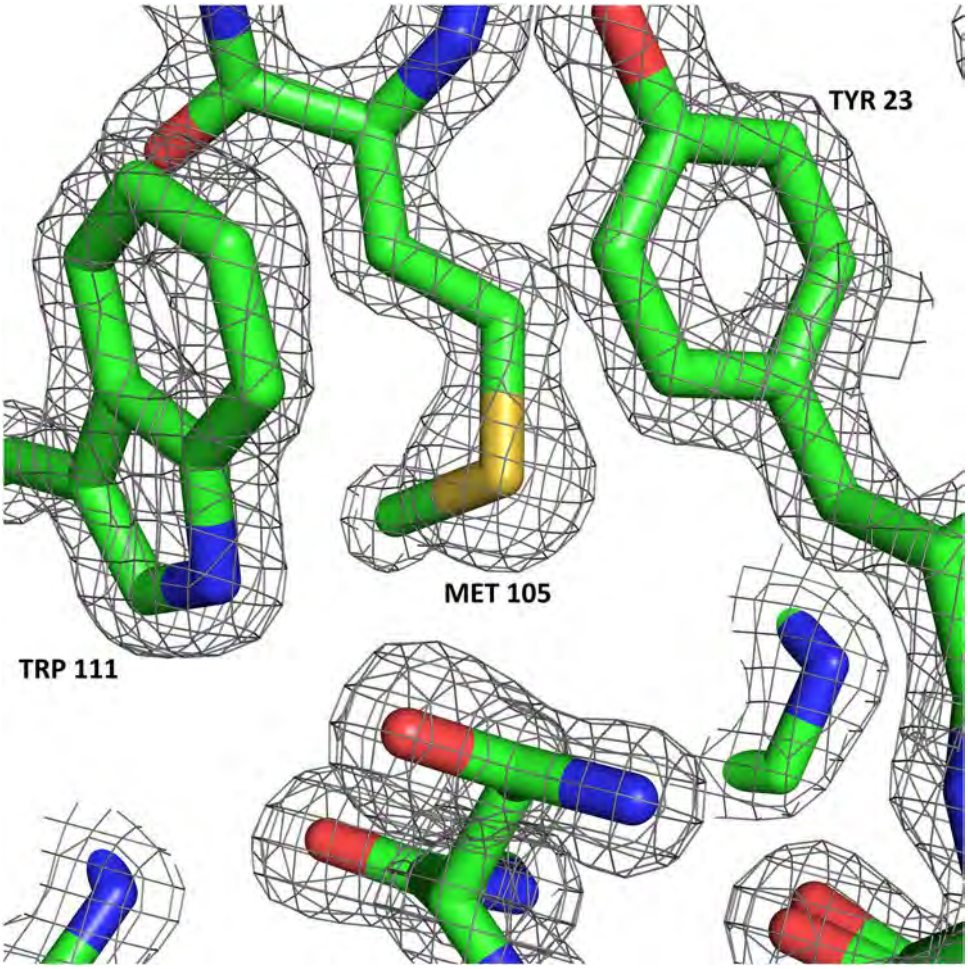

Figure 3. Example electron density (2Fo-Fc map contoured at 2.0 σ) obtained from an acoustically levitated lysozyme crystal in an oil coated droplet of mother liquor. PDB ID: 6QQ3[29]. Graphics produced using PyMOL[42].

to the acoustic nodes. Automated device loading would significantly increase throughput, potentially moving this technique towards serial injection methods but with the huge advantage of being able to hold samples at the point of X-ray interaction. A final enhancement will be a more effective control of the droplet motion to optimise diffraction data acquisition, with the aim of continuous rotation in one direction at a constant speed appropriate for the detector readout rate.

We believe the system to be suitable for deployment on other high intensity X-ray sources operating in ambient conditions, owing to its compact, fully self-contained nature, minimal power delivery and has potential to become a readily adopted sample presentation system for Macromolecular Crystallography experiments.

Equipment Setup

In this section, the sample presentation equipment is described and its effect on the fluid droplets analyzed.

Levitation system. A full description of the acoustic levitation system utilized in these experiments is described by Marzo *et al.*[24] to which the reader is directed for construction detail. For application to the beamline, an acrylic mounting system is produced allowing the device to be attached to the existing sample positioning stages (capable of positioning attached samples or devices at different angles, always in the horizontal plane, at variable vertical positions). The electronics are mounted away from the system to minimize the equipment near the X-ray beam. A photograph of the system as mounted at the beamline is shown in Fig. 5.

Droplet confinement voltage. The system has a variable input voltage which has a direct influence on the acoustic pressure imparted on trapped samples. By changing the voltage it is possible to confine fluids of different densities and size. This however, results in a change to the droplet shape tending from a spheroid to an oblate morphology.

The optimum voltage needed to acoustically trap droplets is a trade off between applying sufficient voltage to overcome gravitational effects on the droplet and reach relative spatial stability whilst maintaining as spherical a droplet shape as possible, such that the sample crystal is readily found at the lowest point. We determined the

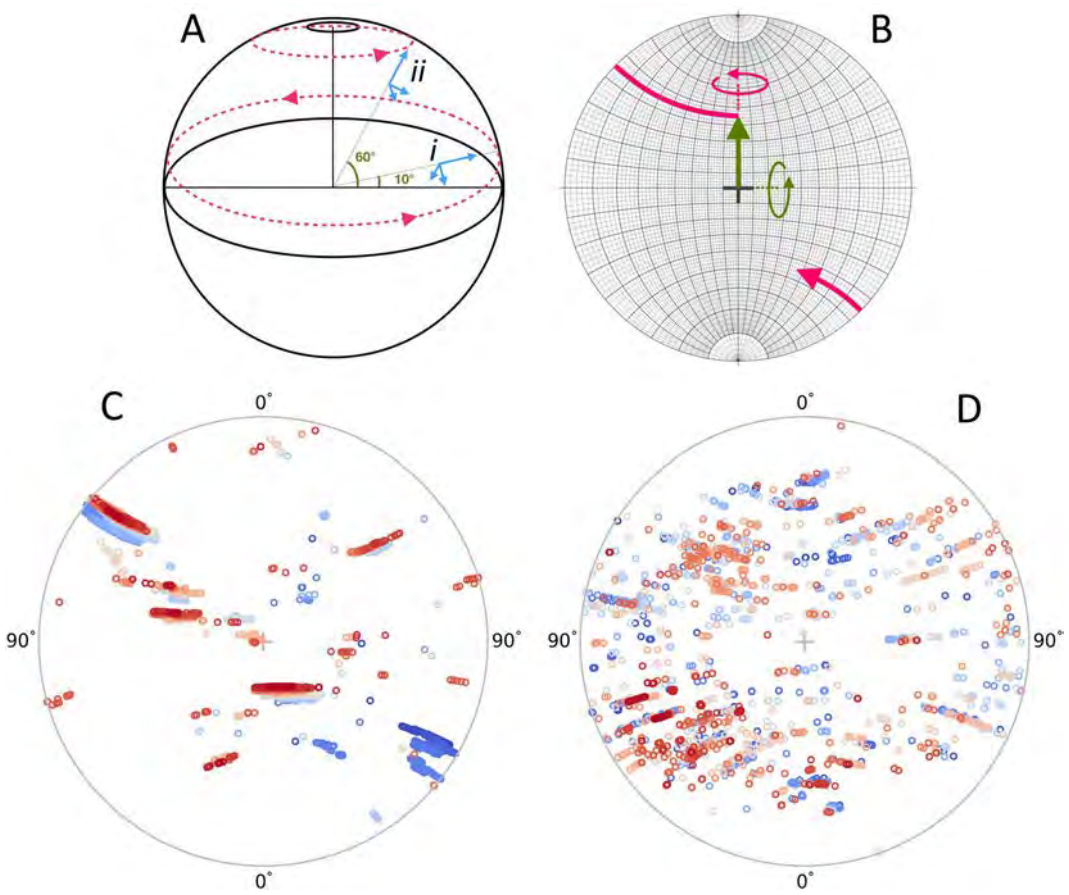

Figure 4. Stereographic projections of crystal orientations and motions. (**A**) Schematic showing two crystals *i* and *ii* inside a spherical drop angled 10° and 60° respectively to the horizontal. As the crystals rotate about a vertical axis, projections from them describe circular paths on the surface of the sphere. (**B**) A Wulff net[43] where the surface of a hemisphere of A has been projected onto the page, such that lines of longitude describe rotations about a horizontal axis (Green) and lines of latitude trace rotations about a vertical axis (pink). The [001] *hkl* reflection of the crystal is used as the reference. If the reflection is initially aligned to the beam at the origin (marked by central cross) then a rotation of 45° of this reflection about the horizontal axis will track the path of the large green arrow. From this direction the large pink arrow describes a further rotation about the vertical axis of 135° and as the reflection moves through 90\deg it appears on the lower half via its backward projection. On this plot rotations about the beam would track circles concentric to the cross. (**C**): Stereographic projection showing the direction of the [001] *hkl* (indexed in P1) from the 5,000 image collection used for the structure deposition, consisting of 4096 diffraction patterns. (**D**) Similar plot but from a 10,000 image collection run on a slurry of micro-crystals consisting of 1498 diffraction patterns. Both plots suggest rotations about the vertical axis as the patterns of points fit circles of latitude. (C) is dominated by three clusters, the largest of which (straddling both hemispheres can be assigned to 2260 patterns. (D) shows many more different tracks of points implying many more different lattices contributing to the dataset. Colours represent the recorded sequence of images: blue through pink to red. Plots (C) and (D) produced using the `dials.stereographic_projection` module[34].

optimum voltage for this experiment by capturing several series of images of the droplet confined by an acoustic field generated by different input voltages. A camera (DCC1645C, Thorlabs, USA) is focused onto the central acoustic trap and images collected as a multi-page Tiff file. These files are imported into MATLAB (Mathworks, USA) where the blue channel (as this gives the greatest droplet contrast) is thresholded and the resulting image closed (with a 50 pixel diameter disk operation) before being skeletonised for ellipse fitting using the fit ellipse function[35]. The outputs of this function are then used to calculate the sphericity according to Equation 1 and to approximate the spatial stability of the droplet by taking the standard deviation of the change in centre point between frames. ESI4 provides a movie comparing two droplet voltages and showing half original droplet image and half the output of the fit to demonstrate the suitability of this method.

There is a trade off between higher voltages which ensure stable entrapment (up to the point at which the droplets are split into smaller volumes) at the expense of maintaining sphericity and providing sufficient acoustic pressure to levitate their mass. We present a combined plot of sphericity and stability for a silicone oil coated water droplet to determine the optimum range of voltages suitable for such an experiment.

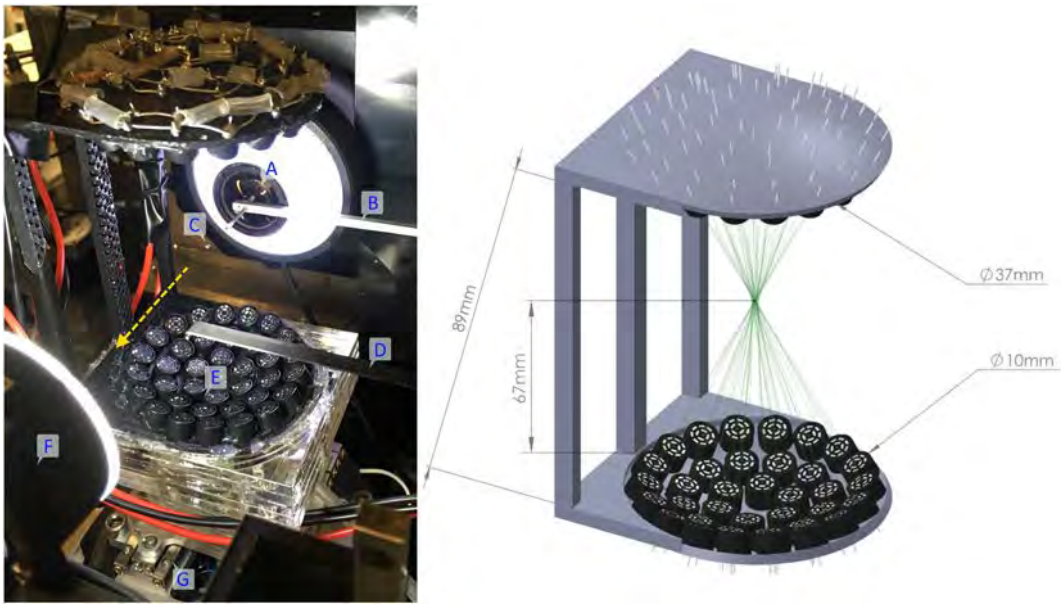

Figure 5. Left: Photograph showing the TinyLev system mounted on the I24 beamline with the X-ray beam path marked with a yellow dashed arrow. Components as labelled: (**A**) High-magnification viewing system, (**B**) X-ray scatter-guard, (**C**) levitating drop, (**D**) beamstop (out of position), (**E**) TinyLev Transducer array, (**F**) backlight (retracted during data collection), (**G**) sample positioning stage. Right: Model of the acoustic levitation system (**E**) used in this work annotated with key dimensions and showing the focal point of the transducer array.

$$\Psi = \frac{2\sqrt[3]{ab^2}}{a + \frac{b^2}{\sqrt{a^2 - b^2}} ln\left(\frac{a + \sqrt{a^2 - b^2}}{b}\right)}, \tag{1}$$

where a and b are the semi-major and semi-minor axes respectively as determined from the ellipse fitting function.

Methods

The experimental method employed to prepare a suitable crystal containing droplet and present it to the synchrotron beam is described below.

Sample preparation. Commercial lysozyme from chicken egg white (CAS Number 12650-88-3, Sigma-Aldrich, UK) was initially resuspended to a concentration of 25 mg · mL^{-1} in 100 mM Na Acetate pH 3.0. Large lysozyme crystals (100–800 μm longest dimension) were grown using seeding. Micro-crystals were initially grown by mixing the protein solution 1:1 with 28% (w/v) NaCl, 8% (w/v) PEG 6,000, 100 mM Na Acetate pH 3.0 in a centrifuge tube. After 1 hour the resultant highly concentrated microcrystalline slurry (longest dimension <5 μm) was diluted 1×10^7 fold. This seed solution was then mixed with 10% (w/v) NaCl, 25% (w/v) ethylene glycol, 100 mM Na Acetate pH 4.8 and with protein solution (75 mg · mL^{-1} in 100 mM Na Acetate pH 3.0) in a ratio of 1:2:3 μL (seed:precipitant:protein). The drops were then incubated overnight at 18 C and harvested the following day. The 10–15 μm crystalline slurry was prepared by mixing lysozyme solution (25 mg · mL^{-1} in 100 mM Na Acetate pH 3.0) with precipitant (16.8% (w/v) NaCl, 4.8% (w/v) PEG 6,000, 60 mM Na Acetate pH 3.0), 1:1 in a centrifuge tube. Crystals appeared after 1 hour and were used the following day.

In order to impart the silicone oil coating described in the levitation section to the droplet, 10 μL pipette tips were coated with a commercial chemical hydrophobising agent (Rain-X, Illinois Tool Works, USA) which was allowed to dry and prevented the adhesion of water based droplets (and thus also the extraction of the aqueous core from the silicone oil layer) to the tip. 2.5 μL of 350 cSt Silicone Oil (Sigma Aldrich, UK) was then pipetted and discarded and a thin layer retained by the tip. Gravimetric analysis suggests that this leaves approximately 0.35 μL of silicone oil coating the internal tip surface. 2.5 μL of the sitting drop or crystalline slurry was then collected using the same tip and the coated droplet transferred to the central acoustic trap which was estimated to consist of 4% silicone oil. The levitating droplet was then aligned with the beam using the beamline's sample positioning stages on to which the TinyLev device had been attached with a 3D printed adaptor mount.

Synchrotron data collection. All MX experiments conducted for this work were performed on I24 at Diamond Light Source, Harwell, UK; a tunable microfocus synchrotron beamline. The incident area of the 0.9686 Å X-Ray beam was set to 50 × 50 μm (full-width-half-maximum) focused using a pair of Kirkpatrick-Baez

mirrors, a scatterguard 5 (Left, [B]) serves to clean rather than shape the beam profile. Diffraction data were collected using a Pilatus3 6 M detector running at 100 Hz using all 5 × 12 detector modules. Full MX experiment parameters are shown in Table 1. Temperature and relative humidity at the sample position in the beamline hutch were recorded at 21.4 C and 30% respectively, at the start of the experiment and later found to vary with a standard deviation of +/−0.2 C and +/−3% over a 24 hour period.

Initially raster scans were performed over the cross section of droplets to determine the location of crystals and it was found that despite the rotational motion, crystals sedimented under gravity towards the bottom of the droplet. This area was then used as the target for a data collection run on a newly mounted droplet containing an estimated 4–6 crystals. 5,000 diffraction images were collected in 50 seconds with the detector operating in a free-running, shutterless manner. During this time no physical change was observed visually in the droplet, as observed on the integrated on-beam-axis high magnification camera system. The droplets were stable over time at ambient temperature with no requirement for humidity control. The silcone oil coating did not measurably increase background X-ray scatter, the dominant factor being the path length through the droplet.

Diffraction data processing. The images containing the diffraction data were analysed with the open source Diffraction Integration for Advanced Light Sources (*DIALS*)[34] software package using `dials.stills_process` to perform diffraction spot finding, space group and unit cell indexing, determination of the crystal rotation matrix, and reflection integration as proposed by Brewster *et al.*[36]. Individual integration files were merged and put on a common scale using the program `PRIME`[37]. Example diffraction can be seen in Fig. 2.

Structure solution. The crystal structure was solved using molecular replacement with PDB entry 5KXO[38] truncated to polyalanine. Model building was completed using `phenix.autobuild`[39] and `Coot`[40] with refinement performed with `phenix.refine`[41]. Statistics for data collection and refinement are presented in Table 1.

References

1. Axford, D. *et al. In situ*In *situ* macromolecular crystallography using microbeams. *Acta Crystallographica Section D Biological Crystallography* **68**, 592–600, http://scripts.iucr.org/cgi-bin/paper?S0907444912006749, https://doi.org/10.1107/S0907444912006749 (2012).
2. Fraser, J. S. *et al.* Accessing protein conformational ensembles using room-temperature X-ray crystallography. *Proceedings of the National Academy of Sciences of the United States of America* **108**, 16247–52, http://www.ncbi.nlm.nih.gov/pubmed/21918110, http://www.pubmedcentral.nih.gov/articlerender.fcgi?artid=PMC3182744, https://doi.org/10.1073/pnas.1111325108 (2011).
3. Orville, A. M. Entering an era of dynamic structural biology…. *BMC Biology* **16**, 55, https://doi.org/10.1186/s12915-018-0533-4 (2018).
4. Weirstall, U *et al*. Lipidic cubic phase injector facilitates membrane protein serial femtosecond crystallography. *Nature Communications*. **5,** https://doi.org/10.1038/ncomms4309 (2014).
5. Liu, W., Ishchenko, A. & Cherezov, V. Preparation of microcrystals in lipidic cubic phase for serial femtosecond crystallography. *Nature protocols* **9**, 2123–34, http://www.ncbi.nlm.nih.gov/pubmed/25122522, http://www.pubmedcentral.nih.gov/articlerender.fcgi?artid=PMC4209290, https://doi.org/10.1038/nprot.2014.141 (2014).
6. Roessler, C. G. *et al.* Acoustic Injectors for Drop-On-Demand Serial Femtosecond Crystallography. *Structure (London, England: 1993)* **24**, 631–640, http://www.ncbi.nlm.nih.gov/pubmed/26996959, http://www.pubmedcentral.nih.gov/articlerender.fcgi?artid=PMC4920001, https://doi.org/10.1016/j.str.2016.02.007 (2016).
7. Sierra, R. G. *et al.* Concentric-flow electrokinetic injector enables serial crystallography of ribosome and photosystem II. *Nature methods* **13**, 59–62, http://www.ncbi.nlm.nih.gov/pubmed/26619013, http://www.pubmedcentral.nih.gov/articlerender.fcgi?artid=PMC4890631, https://doi.org/10.1016/j.str.2016.02.007 (2016).
8. Fuller, F. D. *et al.* Drop-on-demand sample delivery for studying biocatalysts in action at X-ray free-electron lasers. *Nature Methods* **14**, 443–449, http://www.nature.com/articles/nmeth.4195, https://doi.org/10.1038/nmeth.4195 (2017).
9. Owen, R. L. *et al.* Low-dose fixed-target serial synchrotron crystallography. *Acta Crystallographica Section D* **73**, 373–378, https://doi.org/10.1107/S2059798317002996 (2017).
10. Kovácsová, G. *et al.* Viscous hydrophilic injection matrices for serial crystallography. *IUCrJ* **4**, 400–410, https://doi.org/10.1107/S2052252517005140 (2017).
11. Laboratory, E. M. B. P14.eh2 time-resolved crystallography, http://www.embl-hamburg.de/services/mx/P14_EH2/index.html. Accessed: 2019-06-14.
12. IV, M. Micromax, https://www.maxiv.lu.se/accelerators-beamlines/beamlines/micromax/. Accessed: 2019-06-14.
13. Facility, E. S. R. Id23-2 summary, https://www.esrf.eu/home/UsersAndScience/Experiments/MX/About_our_beamlines/ID23-2/overview.html. Accessed: 2019-06-14.
14. Guo, F. *et al.* Precise Manipulation and Patterning of Protein Crystals for Macromolecular Crystallography Using Surface Acoustic Waves. *Small* **11**, 2733–2737, https://doi.org/10.1002/smll.201403262 (2015).
15. Burton, C. G. *et al.* An acoustic on-chip goniometer for room temperature macromolecular crystallography. *Lab on a Chip* **17**, 4225–4230, http://xlink.rsc.org/?DOI=C7LC00812K, https://doi.org/10.1039/C7LC00812K (2017).
16. Tsujino, S. & Tomizaki, T. Ultrasonic acoustic levitation for fast frame rate x-ray protein crystallography at room temperature. *Scientific reports* **6**, 25558, https://doi.org/10.1038/srep25558 (2016).
17. Cerenius, Y., Oskarsson, Å., Santesson, S., Nilsson, S. & Kloo, L. Preliminary tests on the use of an acoustic levitator for liquid x-ray diffraction experiments. *Journal of applied crystallography* **36**, 163–164 (2003).
18. Leiterer, J., Delissen, F., Emmerling, F., Thünemann, A. & Panne, U. Structure analysis using acoustically levitated droplets. *Analytical and bioanalytical chemistry* **391**, 1221–1228 (2008).
19. Delißen, F., Leiterer, J., Bienert, R., Emmerling, F. & Thünemann, A. F. Agglomeration of proteins in acoustically levitated droplets. *Analytical and bioanalytical chemistry* **392**, 161–165 (2008).
20. Klimakow, M. *et al.* Combined synchrotron xrd/raman measurements: In situ identification of polymorphic transitions during crystallization processes. *Langmuir* **26**, 11233–11237 (2010).
21. Nguyen, T. Y., Roessler, E. A., Rademann, K. & Emmerling, F. Control of organic polymorph formation: crystallization pathways in acoustically levitated droplets. *Zeitschrift für Kristallographie-Crystalline Materials* **232**, 15–24 (2017).
22. Weber, J., Rey, C., Neuefeind, J. & Benmore, C. Acoustic levitator for structure measurements on low temperature liquid droplets. *Review of scientific instruments* **80**, 083904 (2009).
23. Xie, W. & Wei, B. Temperature dependence of single-axis acoustic levitation. *Journal of applied physics* **93**, 3016–3021 (2003).
24. Marzo, A., Barnes, A. & Drinkwater, B. W. TinyLev: A multi-emitter single-axis acoustic levitator. *Review of Scientific Instruments* **88**, 085105, https://doi.org/10.1063/1.4989995 (2017).

25. Zang, D. *et al.* Vertical vibration dynamics of acoustically levitated drop containing two immiscible liquids. *Applied Physics Letters* **109**, 101602, https://doi.org/10.1063/1.4962462 (2016).
26. Tuckermann, R., Bauerecker, S. & Cammenga, H. K. The generation of octadecanol monolayers on acoustically levitated water drops. *Colloids and Surfaces A: Physicochemical and Engineering Aspects* **309**, 198–201, http://www.sciencedirect.com/science/article/pii/S0927775707000659. A Collection of Papers Presented at the 6th Eufoam Conference, Potsdam, Germany, 2–6 July, 2006, https://doi.org/10.1016/j.colsurfa.2007.01.029 (2007).
27. Abe, Y., Yamamoto, Y., Hyuga, D., Awazu, S. & Aoki, K. Study on interfacial stability and internal flow of a droplet levitated by ultrasonic wave. *Annals of the New York Academy of Sciences* **1161**, 211–224 (2009).
28. Di, W. *et al.* Shape evolution and bubble formation of acoustically levitated drops. *Physical Review Fluids* **3**, 103606 (2018).
29. Axford, D., Docker, P., Dye, E. & Morris, R. *The room temperature structure of lysozyme via the acoustic levitation of a droplet*, https://doi.org/10.2210/pdb6qq3/pdb (2019).
30. Bury, C. S., Brooks-Bartlett, J. C., Walsh, S. P. & Garman, E. F. Estimate your dose: Raddose-3d. *Protein Science* **27**, 217–228, https://doi.org/10.1002/pro.3302 (2018).
31. Snell, G. *et al.* Automated sample mounting and alignment system for biological crystallography at a synchrotron source. *Structure* **12**, 537–545 (2004).
32. Smith, C. A. & Cohen, A. E. The stanford automated mounter: Enabling high-throughput protein crystal screening at ssrl. *JALA: Journal of the Association for Laboratory Automation* **13**, 335–343 (2008).
33. Otten, A. *et al.* Microfluidics of soft matter investigated by small-angle X-ray scattering. *Journal of Synchrotron Radiation* **12**, 745–750, http://scripts.iucr.org/cgi-bin/paper?S0909049505013580 (2005).
34. Winter, G. *et al.* DIALSDIALS: implementation and evaluation of a new integration package. *Acta Crystallographica Section D Structural Biology* **74**, 85–97, http://scripts.iucr.org/cgi-bin/paper?S2059798317017235 (2018).
35. Gal, O. fitellipse, https://www.mathworks.com/matlabcentral/fileexchange/3215-fitellipse (2003).
36. Brewster, A. S. *et al.* Improving signal strength in serial crystallography with DIALS geometry refinement. *Acta crystallographica. Section D, Structural biology* **74**, 877–894 http://www.ncbi.nlm.nih.gov/pubmed/30198898, http://www.pubmedcentral.nih.gov/articlerender.fcgi?artid=PMC6130462 (2018).
37. Uervirojnangkoorn, M. *et al.* Enabling X-ray free electron laser crystallography for challenging biological systems from a limited number of crystals. *eLife* **4**, e05421, http://www.ncbi.nlm.nih.gov/pubmed/25781634, http://www.pubmedcentral.nih.gov/articlerender.fcgi?artid=PMC4397907 (2015).
38. Russi, S. *et al.* Hen egg white lysozyme at 278k, data set **1**, https://doi.org/10.2210/pdb5kxo/pdb (2016).
39. Terwilliger, T. C. *et al.* Iterative model building, structure refinement and density modification with thePHENIX AutoBuildwizard. *Acta Crystallographica Section D Biological Crystallography* **64**, 61–69, https://doi.org/10.1107/s090744490705024x (2007).
40. Emsley, P., Lohkamp, B., Scott, W. G. & Cowtan, K. Features and development ofCoot. *Acta Crystallographica Section D Biological Crystallography* **66**, 486–501, https://doi.org/10.1107/s0907444910007493 (2010).
41. Afonine, P. V. *et al.* Towards automated crystallographic structure refinement withphenix.refine. *Acta Crystallographica Section D Biological Crystallography* **68**, 352–367, https://doi.org/10.1107/s0907444912001308 (2012).
42. Unpublished: Schrödinger, LLC. The PyMOL Molecular Graphics System, Version 1.8 (2015).
43. Whittaker, E. J. W. The stereographic projection, https://www.iucr.org/education/pamphlets/11/full-text. Accessed: 2019-06-14.

Acknowledgements

The authors would like to thank Allen Orville for encouragement and for comments on the manuscript. ERD gratefully acknowledges receipt of funding under a 50-50 PhD scholarship from Diamond Light Source and Nottingham Trent University.

Author Contributions

P.T.D. conceived the experiment and assisted with its implementation. E.R.D. constructed the levitation system, created mounting hardware and levitated samples. R.H.M. prepared the manuscript and devised the droplet delivery technique. D.A. orchestrated data collection and processed X-ray diffraction data. J.H.B. prepared the samples which were levitated and analysed. M.I.N. refined the experimental protocol. All authors reviewed the manuscript.

Additional Information

Supplementary information accompanies this paper at https://doi.org/10.1038/s41598-019-48612-4.

Competing Interests: The authors declare no competing interests.

Publisher's note: Springer Nature remains neutral with regard to jurisdictional claims in published maps and institutional affiliations.

Physics of Fluids REVIEW scitation.org/journal/phf

Beyond the Langevin horn: Transducer arrays for the acoustic levitation of liquid drops

Cite as: Phys. Fluids 31 , 1 01 301 (201 9); doi: 1 0.1 063/1 .51 1 7335
Submitted: 2 July 201 9 • Accepted: 4 September 201 9 •
Published Online: 2 October 201 9

Robert H. Morris,[1,a)] Elizabeth R. Dye,[1] Peter Docker,[2] and Michael I. Newton[1]

AFFILIATIONS

[1] School of Science and Technology, Nottingham Trent University, Nottingham NG11 8NS, United Kingdom
[2] Diamond Light Source, Harwell Science and Innovation Campus, Oxfordshire OX11 0DE, United Kingdom

[a)] rob.morris@ntu.ac.uk

ABSTRACT

The acoustic levitation of liquid drops has been a key phenomenon for more than 40 years, driven partly by the ability to mimic a microgravity environment. It has seen more than 700 research articles published in this time and has seen a recent resurgence in the past 5 years, thanks to low cost developments. As well as investigating the basic physics of levitated drops, acoustic levitation has been touted for container free delivery of samples to a variety of measurements systems, most notably in various spectroscopy techniques including Raman and Fourier transform infrared in addition to numerous X-ray techniques. For 30 years, the workhorse of the acoustic levitation apparatus was a stack comprising a piezoelectric transducer coupled to a horn shaped radiative element often referred to as the Langevin horn. Decades of effort have been dedicated to such devices, paired with a matching and opposing device or a reflector, but they have a significant dependence on temperature and require precision alignment. The last decade has seen a significant shift away from these in favor of arrays of digitally driven, inexpensive transducers, giving a new dynamic to the topic which we review herein.

INTRODUCTION

Levitation has been used for many years to manipulate materials within air and liquid environments without physical interaction with the container surface. It aims to create a microgravity environment to study the materials which are levitated. There are many forms of levitation including acoustic, magnetic, electrostatic, optical, and aerodynamic. Suspension against gravity using magnetic levitation requires either the sample to be ferromagnetic or the magnetic fields to be among the largest produced on Earth in order to levitate diamagnetic materials which has, for example, been used to levitate a frog.[1] Electrostatic levitation uses an electric field to levitate the sample, requiring a sample which can, and must, be charged in order to achieve suspension against gravity.[2] Optical levitation has only been achieved for very small and lightweight particles as it is achieved by firing a focused laser beam at the sample and utilizing the transfer of momentum from the photons to the sample surface. For this method, the refractive index of the particle must be higher than that of the medium it is suspended within, limiting this technique to a very small number of cases.[3] Finally, aerodynamic levitation is achieved using a high-pressure gas jet to suspend the material under investigation, but this causes significant agitation and may alter the sample in question.[4] In contrast, acoustic levitation is, for a wide range of cases, a superior presentation method as the variety of materials which may be levitated is far greater since there is no requirement for magnetic or chargeable samples. These systems use an emitter and reflector or multiple emitters that produce frequencies above that which can be heard by an average human, to create a series of positions in which the conditions are suitable to entrap particles or sample droplets.

Acoustic levitation was first conceived as a method to allow for microgravity experiments for space applications to be conducted on Earth, by Wang at the NASA Jet Propulsion Laboratory.[5] In this work, three orthogonal standing waves are produced using high power transducers which are capable of suspending liquid samples against gravity and imparting levitation, rotation, and oscillation. The core topics of acoustic levitation have been extensively covered in previous review articles: Work by Brandt[6] has covered the principles of the different types of levitations, whereas Andrade *et al.*[7] completed a comprehensive review of acoustic levitation.

Santesson and Nilsson[8] have also published a review to inform the use of acoustic levitators within chemistry, describing the various processes which can be aided by its use. These reviews have, however, mainly covered the use of traditional acoustic levitation systems primarily utilizing the Langevin horn. Although a key source of ultrasonic radiation, they often require more than 1000 V to power them at powers over 130 W and often cause heating to the sample which is suspended.[9,10] The modern trend toward arrays of cheaper low power off-the-shelf transducers achieves similar suspension forces to some Langevin horns but with negligible heating of the sample and typically a power supply of 12–15 V at powers less than 10 W.[11]

Acoustic levitation has been well demonstrated as a technique for the containerless suspension of samples for remote analysis. It has been used in synchrotron,[12–15] x-ray,[16–18] and Raman spectroscopy[19–21] experiments. A range of additional spectroscopy experiments have also been performed, including Fourier Transform InfraRed (FTIR) spectroscopy,[22–26] X-ray spectroscopy,[27] fluorescence spectroscopy,[28] and mass spectroscopy.[29–31]

The current state of the art for spectroscopic analysis of levitated liquid droplets using a conventional piezoelectric horn levitator is reported by Brotton *et al.*[23,25] In this work, a piezoelectric transducer oscillates at 58 kHz (using $v = f\lambda$ and the speed of sound in air at STP, yielding a wavelength in air of about 5.9 mm). In the earlier of these two papers, the largest diameter of particles that could be levitated was approximately 2.5 mm, whereas the smallest was around 15 μm. In the later paper, the size claimed was up to 3 mm which is at the half wavelength diameter limit. Their measurement system combined Raman, near-IR, UV-vis, and FTIR spectroscopies within the same measurement chamber that also allowed laser heating of the sample droplet. Owing to the small total heat capacity, the levitated particle can be heated to a high temperature and cooled over very short time scales, thus allowing for precise control of the sample temperature. Exemplary state of the art for X-ray diffraction of levitated droplets is reported by Tsujino and Tomizaki[15] at the X06SA beamline at the Swiss Light Source. Their levitation system operated at around 38 kHz (corresponding to a wavelength in air of 9 mm). Rapid spinning of the crystal orientation inside the droplet, which is typical of levitated drops, meant that additional instrumentation for sample oscillation and rotation typically used with standard crystallography was not required. Typically using a 4 μl droplet, consistent with the smallest size droplets reported by Brotton *et al.*, a dataset of 3600 diffraction images per run could be collected in a total duration of around 30 s. These parameters define the range which is needed for phased arrays to compete with the best of the Langevin horn systems for presenting liquid droplets to measurement systems.

This article reviews the acoustic levitation methods which utilize transducer arrays to levitate and manipulate objects within air and their use as a sample suspension or delivery method for measurement systems. It follows the technological development journey from levitating expanded polystyrene particles to levitating droplets through applications.

FUNDAMENTAL PHYSICS OF ACOUSTIC LEVITATION

The reader is directed to comprehensive reviews on the physics of acoustic levitation for thorough treatment of the background physics. However, in the interests of completeness and to ensure that following discussions are fully accessible, the essential analysis of the acoustic force which suspends the samples against gravity is briefly discussed here. Although the physical embodiment of an acoustic levitator may be highly complex, there are relatively few parameters needed to describe the so-called acoustic radiation force which describes the acoustic force exerted on a levitated sample. There are two primary approaches to this analysis which are discussed here. Gor'kov's expression is most often used for evaluation of small sample levitation in focal point systems, estimating the force upon a spherical particle in an arbitrary acoustic field within an ideal fluid. It considers the compressibility of the particle and that it may be set into motion due to the incident wave. In order to apply this expression, it is assumed that the radius of the spherical particle is much smaller than λ, the wavelength of the longitudinal wave which in many applications is on the order of 1–10 mm. It should be noted that for phased arrays which are the primary focus of this review article, the frequency of the transducers (which determines the wavelength) is often based on availability of mass-produced transducers used for ultrasonic range finding or level detection which is typically 38–40 kHz.

To determine the acoustic radiation force, it is first necessary to calculate the time-averaged potential U, as in the following equation:

$$U = 2\pi R^3\left[\left(\overline{p_{in}^2}/3\rho c^2\right)f_1 - \left(\rho\overline{v_{in}^2}/2\right)f_2\right], \tag{1}$$

where R is the radius of the spherical particle and $\overline{p_{in}^2}$ and $\overline{v_{in}^2}$ are the mean-square fluctuations of the pressure and velocity, respectively, at the point of the wave's interaction with the particle.

The factors f_1 and f_2 are described by the following equation:

$$f_1 = 1 - \rho c^2/p_s c_s^2, \quad f_2 = 2(\rho_s - \rho)/(2\rho_s + \rho), \tag{2}$$

where ρ is the density of the fluid, ρ_s is the density of the particle, while c and c_s are the speeds of sound within the fluid and particle, respectively.

The acoustic radiation force acting upon the particle may then be obtained from this result by finding the gradient of the potential.[32]

This approach is, however, not applicable to the levitation of large samples, and an alternative approach is needed to evaluate broad arrays such as used in haptic systems. This analysis requires determination of the acoustic radiation pressure P by assuming a plane wave as can be seen in the following equation:

$$P = \alpha E = \alpha\frac{I}{v} = \alpha\frac{p^2}{\rho v^2}, \tag{3}$$

where the ultrasound energy density is represented by E, I is the sound intensity, the speed of sound in air is given by v, p is the rms ultrasound pressure of ultrasound, and ρ is the air density. Finally, α is a constant between 1 and 2 which scales the resulting pressure to account for the reflectivity of the levitated object with a value of 1 being complete absorption and 2 being complete reflection. Using this relationship, it can be seen that by manipulating the spatial distribution of the ultrasound pressure, the acoustic radiation pressure can be controlled to provide a desired distribution for a given sample.

THE POLYSTYRENE PARTICLE YEARS

Levitation of liquid drops poses a significant challenge owing to the plethora of sample properties which dictate droplet shape. As a consequence, the levitation of expanded polystyrene particles has often heralded the introduction of a novel technique that has later been refined to accommodate liquids. Indeed, levitation was not the aim of much of the work that leads to these developments but a key development step in the production of a new generation of holographic display technologies. In *Noncontact Tactile Display Based on Radiation Pressure of Airborne Ultrasound*,[33] Hoshi *et al.* demonstrated an array of ultrasonic transducers that allowed users to feel virtual objects in air, giving tactile feedback without any mechanical contact. Their prototype consisted of an array of 324, 40 kHz ultrasound transducers where the phase and intensity of each transducer were controlled individually based on the analysis of Eq. (3) to generate an acoustic force of 16 mN over 20 mm. The same group went on to develop this into a series of acoustic levitation devices, the first of which was reported in the 2014 publication[34] in which *t*wo arrays of ultrasonic transducers were arranged opposite each other to generate a localized standing wave at arbitrary positions utilizing the so called phased-array focusing technique. This technique generates a focal point at a specific position by determining the path difference between the 0th and nth transducers and using the speed of sound within air to find an appropriate time delay as given by the following equation:

$$T_n = \frac{d_n}{c}. \tag{4}$$

By delaying the start of the square wave signal to the nth transducer by this amount, the focal point is generated.

Three advantages were identified to such airborne ultrasound focusing device (AUFD) arrays:

- The particles can be manipulated in all directions according to the movement of the localized standing wave based on the phase-delay control.
- The work space is much larger than those in previous research studies because the ultrasound wave is focused and hence delivered farther.
- The particles are kept trapped even when the acoustic axis is horizontal because the AUFDs provide a sufficient amplitude of ultrasound.

In Ref. 35, the same group utilized four arrays of transducers at 40 kHz or 25 kHz to provide three-dimensional control of expanded polystyrene particles up to 2 mm in diameter, as can been seen in Fig. 1. This work quantified the stability of the movement of the particles by changing the phases of the transducers in 1/16th wavelength (8.5 mm or 13.7 mm for 40 kHz and 25 kHz, respectively) steps, causing the particles to accelerate until they were ejected from the levitation system. The smaller 0.6 mm particles were confined for accelerations of up to 60 m s^{-2} corresponding to approximately 500 μN of force, whereas the 2 mm polystyrene particles maintained entrapment up to 30 m s^{-2} corresponding to approximately 27 mN (both calculated based on F = ma).

The concept of an ultrasonic phased array was further developed by Marzo *et al.*[36] to show that acoustic levitation can be employed to translate, rotate, and manipulate particles using a single-sided emitter array. They also introduce a "holographic acoustic elements framework" that permits the modeling and rapid generation of different traps; however, their work was still light particle rather than liquid drop based.

Developing this approach, Marzo *et al.* showed a wide range of different array structures capable of producing what they termed an acoustic tractor beam in their 2017 article.[37] These so-called tractor beams were shown to be capable of holding millimeter-sized polymer particles and even fruit-flies. Figure 2 shows the different methods used by Marzo *et al.* for generating differing phases from each transducer to produce a focal point for the acoustic field including a physical curved array, flat array with electrically differing phase, and flat array with variable tube length in addition to the

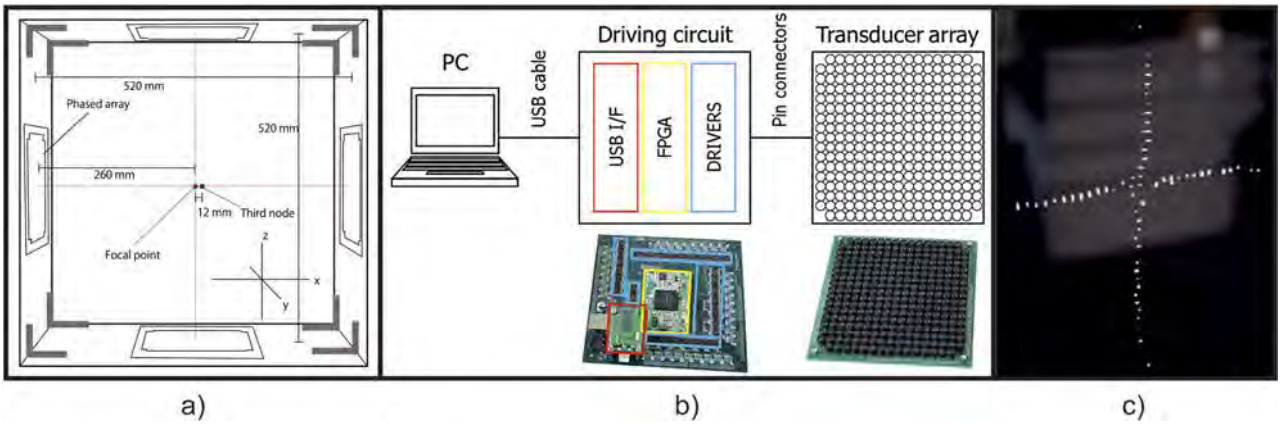

FIG. 1. Use of four arrays configured for three-dimensional control of multiple 2 mm polystyrene spheres. (a) shows relative placement of arrays. (b) shows the schematic of drive and control electronics. A demonstration of suspension of numerous polystyrene beads using the trapping system is shown in (c). Subfigures reproduced with permission from Y. Ochiai, T. Hoshi, and J. Rekimoto, "Three-dimensional mid-air acoustic manipulation by ultrasonic phased arrays," PLoS One **9**(5), e97590 (2014). Copyright 2014 Author(s), licensed under a Creative Commons Attribution 4.0 License, which permits unrestricted use, distribution, and reproduction in any medium, provided that the original author and source are credited.

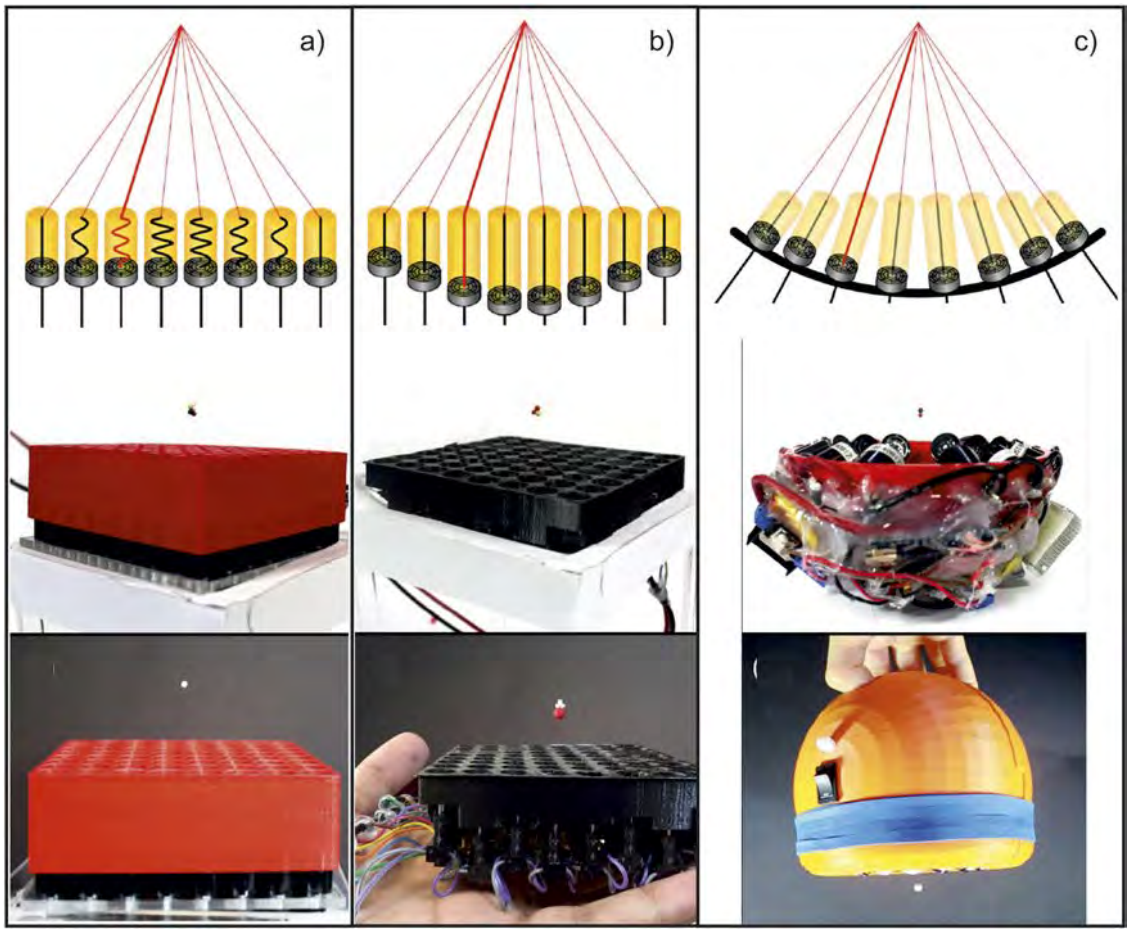

FIG. 2. Realization of various compact single sided acoustic levitation devices utilizing delay lines. Each panel shows a schematic of the approach at the top and two photographs of its use below. (a) Coiled paths to provide phase differences between transducers, (b) straight tubes of varying length to provide phase differences, and (c) the sculpted surface device where focus is achieved with transducers of similar phases. Subfigures reproduced and rearranged with permission from Marzo *et al.*, "Realization of compact tractor beams using acoustic delay-lines," Appl. Phys. Lett. **110**(1), 014102 (2017). Copyright 2017 AIP Publishing LLC.

practical realization of these methods. In this work, it was found that the curved array system was most efficient as the maximum intensity of the transducers was directed toward the target area with minimal losses.

Simulation work in Ref. 38 showcases a novel method of trap generation in order to create 2 or more simultaneous acoustic traps which levitate light spherical particles. This work builds upon that of Marzo *et al.*,[36] simulating a 16 × 16 transducer array which operates at 40 kHz. These simulations form an acoustic trap at position r_1 and a "quiet zone" at position r_2, in which the pressure is comparatively much lower. An acoustic trap at r_2 and a quiet zone at r_1 are then superposed which forms 2 acoustic traps with similar strengths and pressure gradients to suspend light particles.

Marzo *et al.* also developed virtual vortex trapping methods in Ref. 39 to explore the effects of orbital angular momentum on the stability of light polystyrene particles within an acoustic levitator which suspends particles using a vortex trapping motion. It was also found that particles larger than the wavelength of the incident sound were able to be suspended by switching the driver phases, to make the array emit two different pressure fields. The largest particle which was suspended with reasonable stability was a 16 mm expanded polystyrene ball, which had a diameter 1.88 times the wavelength of sound, which in this case is 8.6 mm.

Trajectory control of suspended particles is explored in Ref. 40. In this work, an acoustic levitator consisting of 2 opposing planar arrays with 30 transducers on either side, operating at 40 kHz, was used. Each of the transducers was powered independently and driven with a square wave which had a phase resolution of $\phi = 2\pi/128$, allowing the focal point to be moved as discussed previously. This entire setup was housed within a chamber upon a passive vibration isolation table which limited external air currents and vibrations, respectively. An expanded polystyrene particle was

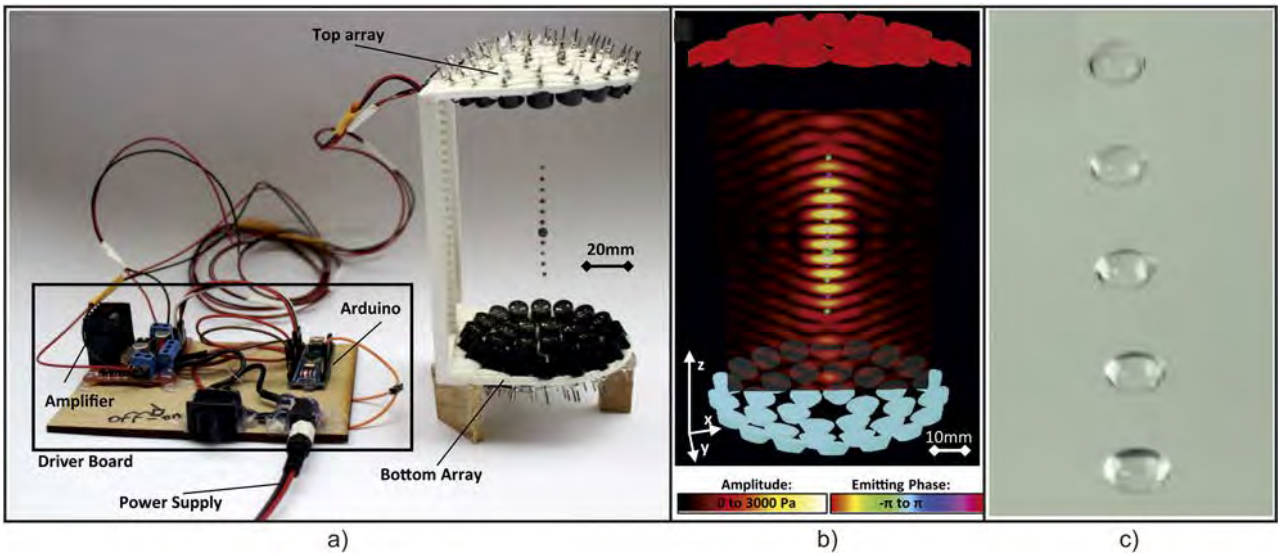

FIG. 3. The TinyLev acoustic levitation system, consisting of the driver board and 72 transducers fixed to a 3D printed twin domed structure, as shown in (a). The simulated acoustic field of such a system is shown in (b). Droplets of water suspended by the TinyLev system are shown in (c). Note their oblate morphology owing to greater vertical trapping forces than those experienced horizontally. Subfigures reproduced with permission from A. Marzo, A. Barnes, and B. W. Drinkwater, "TinyLev: A multi-emitter single-axis acoustic levitator," Rev. Sci. Instrum. **88**(8), 085105 (2017). Copyright 2017 AIP Publishing LLC.

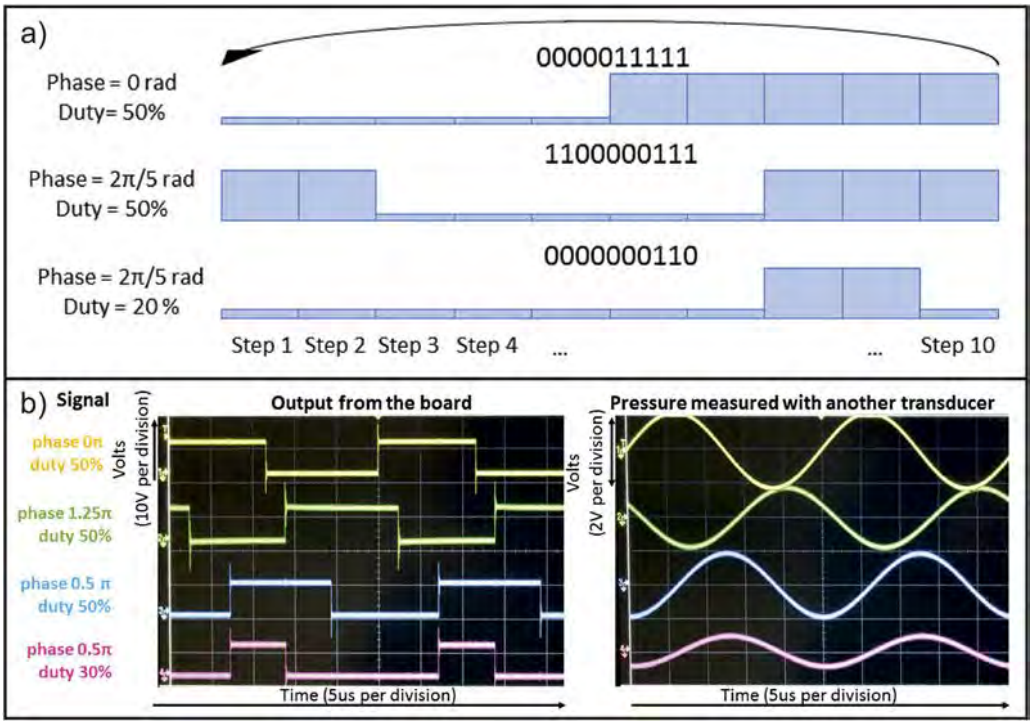

FIG. 4. Signals of the Ultraino system. Phases and duty cycles are controlled by a logic signal which is divided into 10 steps as can be seen in (a). These signals were recorded from the output of the driver board, as can be seen in the left of (b), while the responses measured from another transducer which is used as an ultrasonic microphone are shown in the right of (b). Subfigures reproduced with permission from A. Marzo, T. Corkett, and B. W. Drinkwater, "Ultraino: An open phased-array system for narrowband airborne ultrasound transmission," IEEE Trans. Ultrason., Ferroelectr., Freq. Control **65**(1), 102–111 (2017). Copyright 2017 Author(s), licensed under a Creative Commons Attribution 3.0 Unported License.

tracked through a circular pathway within the x-z plane, by changing the phases of the transducers to move the focal points. It was, however, found that the positions in which the particles reached equilibrium were not those that were desired. Corrections to this pathway were applied by comparing the equilibrium position to the target, and it was found that these corrected pathways were the desired shape assuming that the velocity of the particle was less than 1 cm/s.

Further work by Marzo *et al.*[41] has explored the capabilities of holographic acoustic tweezers to dynamically manipulate multiple particles simultaneously in midair. This is achieved using an algorithm that enables the control of the emitted field from the ultrasonic phased arrays. The two opposing planar arrays consisted of 256, 1 cm diameter transducers on each side, operating at 40 kHz. These arrays were separated by 23 cm. The algorithm is used to generate focal points at the position of the particles before controlling the transducer phases to move the foci. The minimum distance between adjacent particles was 1.3 cm as closer traps merged and inhibited independent control of the 25 total traps. Twin traps were generated in order to control the orientation of asymmetric particles. These were, however, found to be insufficient to suspend the particles; thus, rapid switching between twin traps and focal points was used to orientate and suspend particles. An example of the acoustic field of a twin trap system is shown in Fig. 5.

THE LIQUID LEVITATION ERA BEGINS

A major turning point in the application of acoustic levitation was reported in Ref. 11 building on the work in Ref. 37 but including two curved arrays facing each other. This heralded a new era of acoustic levitation allowing low cost levitation of liquid samples. While still employing the low-cost transducer array, one significant feature of this work was to use low cost Arduino microcontrollers, making it possible for anyone capable of using a soldering iron to produce a viable acoustic levitation system. The details of the design and software were made available in the form of an Instructable[42] bringing levitation to the masses. Figure 3 shows the TinyLev system and examples of levitated objects including liquid drops. This system was able to levitate objects of much higher density than expanded polystyrene balls, including pieces of ceramic, sugar, and sapphire spheres.

In Ref. 43, Marzo *et al.* present a package called Ultraino which they describe as a modular, inexpensive, and open platform that provides hardware, software, and example applications specifically aimed at controlling the transmission of narrowband airborne ultrasound. The aim of this was not only to provide a fixed design example but to allow users to define their own problem and using the supplied modeling software to predict the most appropriate array

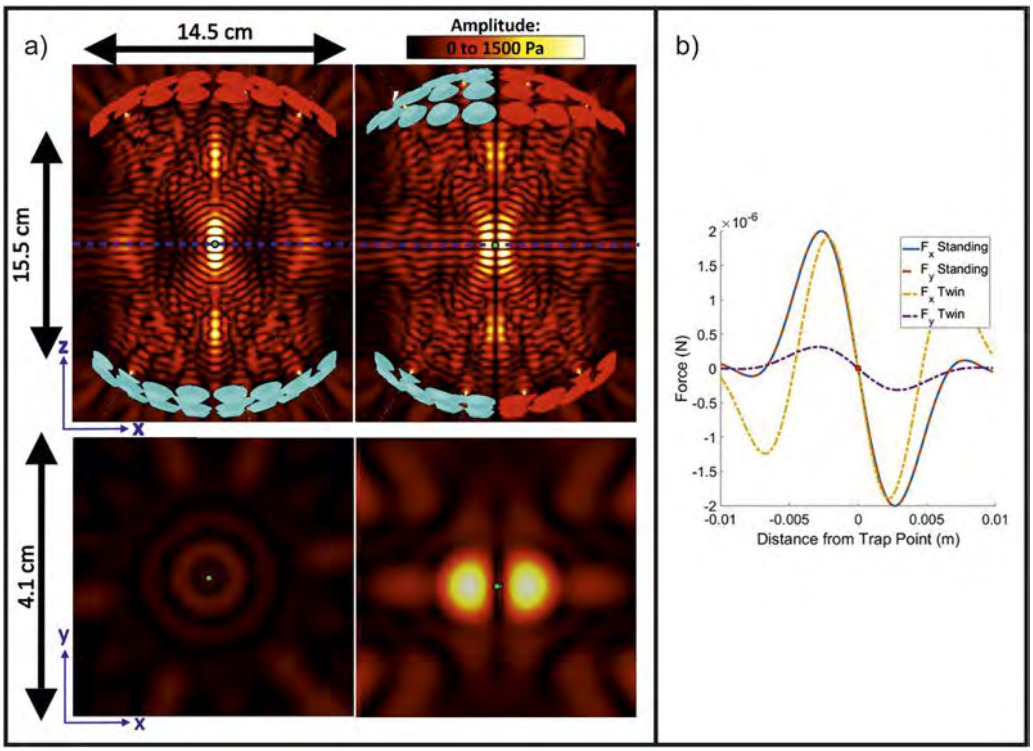

FIG. 5. The acoustic field of the so-called acoustic lock system in its multiplexed states is shown in (a) where the left images are the standing wave field and the right images show the twin trap field from the side and above in a plane which transects the central trap. The blue lines indicate the planes of the lower images. The force in the vertical and horizontal directions is shown in (b) for both of the multiplexed states. The central trap is represented as a red dot. Subplots are reproduced with permission from Cox *et al.*, "Acoustic lock: Position and orientation trapping of nonspherical sub-wavelength particles in mid-air using a single-axis acoustic levitator," Appl. Phys. Lett. **113**(5), 054101 (2018). Copyright 2018 AIP Publishing LLC.

configuration. Well-defined hardware building blocks can then be used to allow the configuration to be implemented. The realization that low-cost transducers could be driven by an amplified logic signal with variable phase and duty cycle has transformed the feasibility of phased arrays, and in Fig. 4, we show examples taken from Ref. 44. It should be noted that, even for Ultraino, liquid levitation data were only presented for a two-sided standing wave system similar to the TinyLev and not for any of the single sided configurations which lack the confinement needed for high density samples. One well known phenomenon in single axis acoustic levitation is that the samples are prone to spinning. In many cases, this is not significant, but where samples are nonspherical, such as insects, or where liquid crystal structure is to be determined, this is an important factor which must be considered.

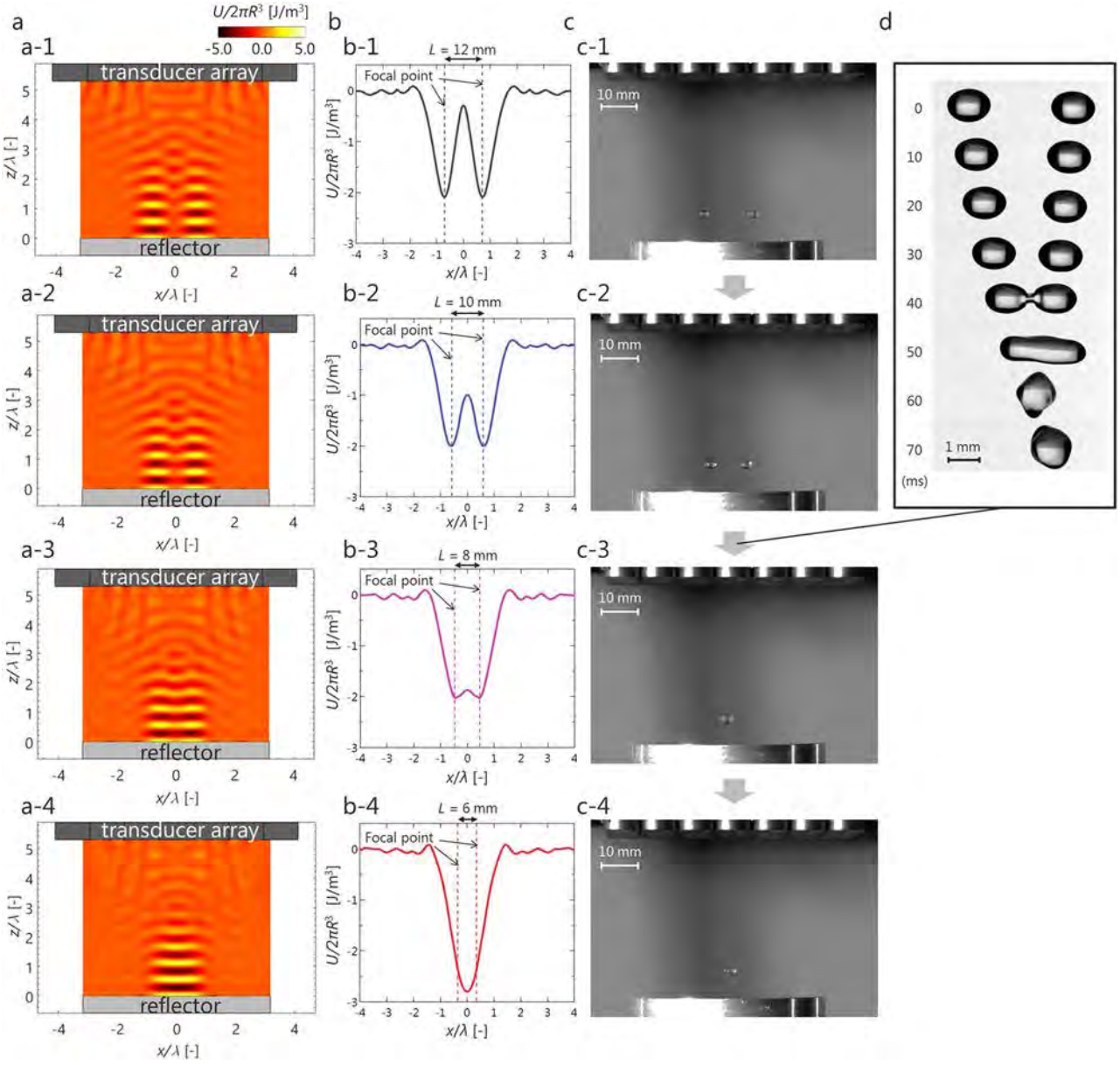

FIG. 6. Noncontact translation and coalescence is achieved using time variable acoustic fields. The acoustic potential of the transducer array and reflector combination can be seen in (a), while (b) shows the acoustic potential as a function of x. Photographs of the droplets within the focal points above the reflector can be seen in (c). A time series of the coalescence is shown in (d). The two focal points are moved toward the central position with each iteration. Reproduced with permission from A. Watanabe, K. Hasegawa, and Y. Abe, "Contactless fluid manipulation in air: Droplet coalescence and active mixing by acoustic levitation," Sci. Rep. **8**(1), 10221 (2018).[43]

In Ref. 44, a variation on the single axis levitator system was reported that saw each transducer "bowl" divided into two symmetric halves with an invertible phase to facilitate the emission of both vertical standing waves and twin-traps, where the confining force is also applied laterally. It was shown that the system could stop the rotation in the supplementary video of Ref. 44 showing the effect on solid objects and by way of example insects. There are no data presented within the manuscript for liquid levitation although it has been shown in the supplementary material of Ref. 44. This system provides the ability to trade-off the lateral stability for the levitation of denser materials. Thus, lower density samples, such as insects, may be held in a more stable position than samples such as acrylic or wooden cuboids.

FROM BASIC HARDWARE TO LIQUID DROP APPLICATIONS

In Ref. 45, a rectangular ultrasonic phased array was combined with a reflector surface to demonstrate contactless coalescence and mixing techniques for droplets in air. The array was designed to have two focal points, generated by switching at 500 Hz between the two (since all transducers are used to form the two traps). The distance between the two focal points could then be reduced to produce a single large standing wave resulting in coalescence of the droplets within a single trap. Figure 6(a) shows the estimation of the acoustic potentials, the resulting potentials at the pressure nodes, and images of two water drops being brought together and coalescing.

Shen *et al.*[46] had previously demonstrated oscillation modes in a "conventional" single-axis acoustic levitator forming a standing wave between the emitter and the curved reflector by modulating the amplitude by up to 10%. They swept the modulation frequency upward with increments of 0.5 Hz and observed different oscillation modes being excited. Watanabe[45] implemented a similar scheme in the phased array and compared mixing performance between cases with and without mode oscillation and showed that the flow induced by mode oscillation promotes droplet mixing (an example of which

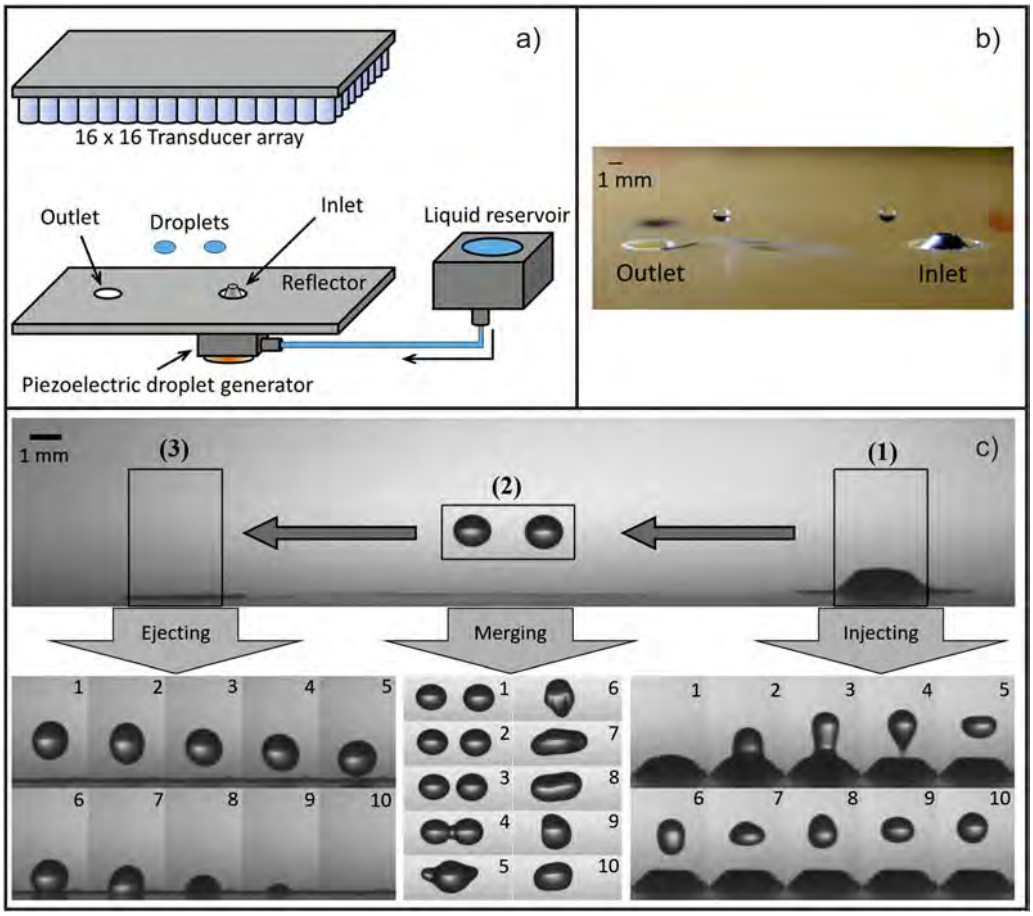

FIG. 7. (a) shows a diagram of the acoustic levitation system consisting of a 16 × 16 transducer array and a planar reflector. Liquid is drawn from the reservoir and into the system via a piezoelectric droplet generator. The droplets are ejected from the system by moving them to above the outlet and switching off the acoustic field. (b) shows a color photograph of the inlet and outlet with two droplets being transported between. (c) shows a series of images of the droplets being injected (1), merged (2), and ejected (3). Subfigures reproduced with permission from M. A. Andrade, T. S. Camargo, and A. Marzo, "Automatic contactless injection, transportation, merging, and ejection of droplets with a multifocal point acoustic levitator," Rev. Sci. Instrum. **89**(12), 125105 (2018). Copyright 2018 AIP Publishing LLC.

TABLE I. Comparison of the current state of the art for key parameters between Langevin and transducer arrays.

Parameter	Langevin	References	Transducer array best	References
Power	130 W	10	5 W	11
Frequency/wavelength	25 kHz	51	28 kHz, 40 kHz	Various
Wavelength step	n/a	n/a	2π/128	40
Maximum sample size	50 mm	51	16 mm	39
Acoustic force	12 mN	51	27 mN	35

is shown in Fig. 6) which effectively brings this technique into a useful tool for containerless chemistry.

In *Automatic contactless injection, transportation, merging, and ejection of droplets with a multifocal point acoustic levitator*,[46] Andrade *et al.* used a 16 × 16 array of 40 kHz ultrasonic transducers, a distance of 110 mm away from a plane reflector which along with the superposition of the incident and reflected waves formed a standing wave with a series of pressure nodes where liquid droplets could be trapped and moved in two dimensions above the surface. The reflectors' position was chosen by focusing the transducers to different positions and empirically determining which distance provided the largest pressure amplitude.[47] Their system had an integrated droplet injector inserted in the reflector including a piezoelectric buzzer and a 1 mm diameter nozzle. When a voltage pulse was applied, a droplet was injected and trapped at the bottom pressure node of the standing wave. The droplet outlet was a simple hole in the reflector, and switching off the acoustic field allowed the drop to pass through under gravity. Figure 7 shows the injection of two droplets followed by the merging and subsequent ejection.

NEW PERSPECTIVES—THE FUTURE OF ACOUSTIC LEVITATION OF LIQUIDS

There was a mention in the supplementary material of Ref. 44 of the levitation of liquids. This made important reference to the shape of the resulting confined droplet: it was found that the droplet formed an approximate ovoid and the boundary of the liquid appeared less smooth. In the move from levitation of solids such as polystyrene balls which have relatively fixed morphology, to fluids which conform to their confinement, the shape of the produced acoustic fields has become increasingly important. For many experimental systems, this is simply a feature of the acoustic field which limits the size of droplet that can be confined. In sample presentation scenarios, however, the shape of the droplet can be an important factor which directly impacts the results. Consequently, there is an increasing shift from awareness toward control of droplet shape by balancing the confinement potential of the acoustic field against the forces applied to the droplets to maximize sphericity; for example, in Ref. 48, the droplet sphericity as a function of voltage applied to the TinyLev system was determined and optimized to balance these key parameters.

In recent publications such as Ref. 48, this new era of low-cost phased array ultrasonic levitation devices are beginning to find use in sample presentation to noncontact measurement techniques in applications previously making use of Langevin horns.[49] This facilitates containerless, background free spectroscopy which ushers in a new wave of experimental techniques and brings with it significant advantages in terms of measurement resolution without imparting significant energy into the sample. Although further developments are required for these techniques to become universally applied, it is clear that sample presentation systems based on acoustic levitation are likely to become as ubiquitous as pipettes are now in fluidic analysis over the coming decade.

To our knowledge, there are currently no truly single sided systems which can reliably confine nonrigid samples such as fluid droplets, owing to the limited transverse acoustic forces. This represents one of the clear directions for future developments to produce complex acoustic fields which have improved transverse fields for fluid entrapment. Advances in microcontroller systems, capable of smaller wavelength fractions, will be a key enabler of such developments, allowing for realistic implementation of arbitrary acoustic fields. The final element which will provide scope for further improvement is the availability of acoustic transducers specifically engineered for such purposes. The limitations in absolute output power, frequency, and physical size are largely governed by mass production for other applications such as range finding. Recent developments toward customized transducers[50] will allow for better control of these parameters yielding better control of wavelength and permitting systems to be tailored to specific sample sizes of interest. In combination with sample manipulation processes such as those presented in Ref. 45, such developments will allow for sample preparation and presentation to almost all spectroscopic measurement techniques.

SUMMARY

In this review article, we have summarized the current state of the art of acoustic levitation of liquids using low cost transducer arrays. In Table I, we briefly summarize the current state of the art for each of the key parameters which dictate the levitation performance. The maximum sample size is for nonliquid samples and is presented as the size which may one day be achievable. These parameters are then compared to a traditional Langevin system.

CONCLUSION

The realization that low-cost transducers could be driven by an amplified logic signal has transformed the feasibility of phased arrays. Through field programmable gate arrays (FPGAs) or simple microcontrollers, a large number of transducers can have their signals tailored in a cost-effective way to produce a given pressure field

profile. Commercial companies such as Pixie Dust Technologies[52] and Ultrahaptics[53] offer customers bespoke phased array packages, primarily for midair tactile transducers. This review has focused on the development of ultrasonic phased arrays although alongside there have been developments in single transducer levitation through the use of acoustic hologram reflectors[54] and transmission "metamaterial bricks."[55] We have presented an expected future direction of the technology based on the current direction, but it is clear that we are witnessing the start of a new era of containerless sample preparation and presentation.

REFERENCES

[1] M. D. Simon and A. K. Geim, "Diamagnetic levitation: Flying frogs and floating magnets," J. Appl. Phys. **87**(9), 6200–6204 (2000).
[2] W. K. Rhim and S. K. Chung, "Containerless protein crystal growth method," J. Cryst. Growth **110**(1-2), 293–301 (1991).
[3] A. Ashkin and J. M. Dziedzic, "Optical levitation by radiation pressure," Appl. Phys. Lett. **19**(8), 283–285 (1971).
[4] D. A. Winborne, P. C. Nordine, D. E. Rosner, and N. F. Marley, "Aerodynamic levitation technique for containerless high temperature studies on liquid and solid samples," Metall. Trans. B **7**(4), 711–713 (1976).
[5] T. G. Wang, "Acoustic levitation and manipulation for space applications," NASA Technical Report No. 19810026300, 1979.
[6] E. H. Brandt, "Levitation in physics," Science **243**(4889), 349–355 (1989).
[7] M. A. Andrade, N. Pérez, and J. C. Adamowski, "Review of progress in acoustic levitation," Braz. J. Phys. **48**(2), 190–213 (2018).
[8] S. Santesson and S. Nilsson, "Airborne chemistry: Acoustic levitation in chemical analysis," Anal. Bioanal. Chem. **378**(7), 1704–1709 (2004).
[9] J. K. Weber, C. A. Rey, J. Neuefeind, and C. J. Benmore, "Acoustic levitator for structure measurements on low temperature liquid droplets," Rev. Sci. Instrum. **80**(8), 083904 (2009).
[10] G. K. Lewis, Jr. and W. L. Olbricht, "Design and characterization of a high-power ultrasound driver with ultralow-output impedance," Rev. Sci. Instrum. **80**(11), 114704 (2009).
[11] A. Marzo, A. Barnes, and B. W. Drinkwater, "TinyLev: A multi-emitter single-axis acoustic levitator," Rev. Sci. Instrum. **88**(8), 085105 (2017).
[12] Y. Cerenius, Å. Oskarsson, S. Santesson, S. Nilsson, and L. Kloo, "Preliminary tests on the use of an acoustic levitator for liquid X-ray diffraction experiments," J. Appl. Crystallogr. **36**(1), 163–164 (2003).
[13] J. Leiterer, F. Delissen, F. Emmerling, A. F. Thünemann, and U. Panne, "Structure analysis using acoustically levitated droplets," Anal. Bioanal. Chem. **391**(4), 1221–1228 (2008).
[14] J. Leiterer, F. Emmerling, U. Panne, W. Christen, and K. Rademann, "Tracing coffee tabletop traces," Langmuir **24**(15), 7970–7978 (2008).
[15] S. Tsujino and T. Tomizaki, "Ultrasonic acoustic levitation for fast frame rate X-ray protein crystallography at room temperature," Sci. Rep. **6**, 25558 (2016).
[16] J. Leiterer, W. Leitenberger, F. Emmerling, A. F. Thünemann, and U. Panne, "The use of an acoustic levitator to follow crystallization in small droplets by energy-dispersive X-ray diffraction," J. Appl. Crystallogr. **39**(5), 771–773 (2006).
[17] F. Deliß̈en, J. Leiterer, R. Bienert, F. Emmerling, and A. F. Thünemann, "Agglomeration of proteins in acoustically levitated droplets," Anal. Bioanal. Chem. **392**(1-2), 161–165 (2008).
[18] J. Radnik, U. Bentrup, J. Leiterer, A. Brückner, and F. Emmerling, "Levitated droplets as model system for spray drying of complex oxides: A simultaneous *in situ* X-ray diffraction/Raman study," Chem. Mater. **23**(24), 5425–5431 (2011).
[19] N. Leopold, M. Haberkorn, T. Laurell, J. Nilsson, J. R. Baena, J. Frank, and B. Lendl, "On-line monitoring of airborne chemistry in levitated nanodroplets: *In situ* synthesis and application of SERS-active Ag^{-} sols for trace analysis by FT-Raman spectroscopy," Anal. Chem. **75**(9), 2166–2171 (2003).
[20] B. R. Wood, P. Heraud, S. Stojkovic, D. Morrison, J. Beardall, and D. McNaughton, "A portable Raman acoustic levitation spectroscopic system for the identification and environmental monitoring of algal cells," Anal. Chem. **77**(15), 4955–4961 (2005).
[21] S. Biedasek, M. Abboud, H. U. Moritz, and A. Stammer, "Online-analysis on acoustically levitated droplets," in *Macromolecular Symposia, December* (Wiley-VCH Verlag, Weinheim, 2007), Vol. 259, No. 1, pp. 390–396.
[22] J. T. Cronin and T. B. Brill, "Acoustic levitation as an IR spectroscopy sampling technique," Appl. Spectrosc. **43**(2), 253–257 (1989).
[23] S. J. Brotton and R. I. Kaiser, "Novel high-temperature and pressure-compatible ultrasonic levitator apparatus coupled to Raman and Fourier transform infrared spectrometers," Rev. Sci. Instrum. **84**(5), 055114 (2013).
[24] S. J. Brotton, M. Lucas, T. N. Jensen, S. L. Anderson, and R. I. Kaiser, "Spectroscopic study on the intermediates and reaction rates in the oxidation of levitated droplets of energetic ionic liquids by nitrogen dioxide," J. Phys. Chem. A **122**(37), 7351–7377 (2018).
[25] S. J. Brotton and R. I. Kaiser, "Spectroscopic study on the polymer condensates formed via pyrolysis of levitated droplets of dicyanamide-containing ionic liquids," J. Phys. Chem. A **123**, 1153 (2019).
[26] S. J. Brotton, M. Lucas, S. D. Chambreau, G. L. Vaghjiani, J. Yu, S. L. Anderson, and R. I. Kaiser, "Spectroscopic investigation of the primary reaction intermediates in the oxidation of levitated droplets of energetic ionic liquids," J. Phys. Chem. Lett. **8**(24), 6053–6059 (2017).
[27] C. J. Benmore, J. K. Weber, A. N. Tailor, B. R. Cherry, J. L. Yarger, Q. Mou, W. Weber, J. Neuefeind, and S. R. Byrn, "Structural characterization and aging of glassy pharmaceuticals made using acoustic levitation," J. Pharm. Sci. **102**(4), 1290–1300 (2013).
[28] J. Leiterer, M. Grabolle, K. Rurack, U. Resch-Genger, J. Ziegler, T. Nann, and U. Panne, "Acoustically levitated droplets," Ann. N. Y. Acad. Sci. **1130**(1), 78–84 (2008).
[29] C. Warschat, A. Stindt, U. Panne, and J. Riedel, "Mass spectrometry of levitated droplets by thermally unconfined infrared-laser desorption," Anal. Chem. **87**(16), 8323–8327 (2015).
[30] M. S. Westphall, K. Jorabchi, and L. M. Smith, "Mass spectrometry of acoustically levitated droplets," Anal. Chem. **80**(15), 5847–5853 (2008).
[31] E. A. Crawford, C. Esen, and D. A. Volmer, "Real time monitoring of containerless microreactions in acoustically levitated droplets via ambient ionization mass spectrometry," Anal. Chem. **88**(17), 8396–8403 (2016).
[32] M. Barmatz and P. Collas, "Acoustic radiation potential on a sphere in plane, cylindrical, and spherical standing wave fields," J. Acoust. Soc. Am. **77**(3), 928–945 (1985).
[33] T. Hoshi, M. Takahashi, T. Iwamoto, and H. Shinoda, "Noncontact tactile display based on radiation pressure of airborne ultrasound," IEEE Trans. Haptics **3**(3), 155–165 (2010).
[34] T. Hoshi, Y. Ochiai, and J. Rekimoto, "Three-dimensional noncontact manipulation by opposite ultrasonic phased arrays," Jpn. J. Appl. Phys., Part 2 **53**(7S), 07KE07 (2014).
[35] Y. Ochiai, T. Hoshi, and J. Rekimoto, "Three-dimensional mid-air acoustic manipulation by ultrasonic phased arrays," PLoS One **9**(5), e97590 (2014).
[36] A. Marzo, S. A. Seah, B. W. Drinkwater, D. R. Sahoo, B. Long, and S. Subramanian, "Holographic acoustic elements for manipulation of levitated objects," Nat. Commun. **6**, 8661 (2015).
[37] A. Marzo, A. Ghobrial, L. Cox, M. Caleap, A. Croxford, and B. W. Drinkwater, "Realization of compact tractor beams using acoustic delay-lines," Appl. Phys. Lett. **110**(1), 014102 (2017).
[38] C. Andersson and J. Ahrens, "A method for simultaneous creation of an acoustic trap and a quiet zone," in *2018 IEEE 10th Sensor Array and Multichannel Signal Processing Workshop (SAM), July* (IEEE, 2018), pp. 622–626.
[39] A. Marzo, M. Caleap, and B. W. Drinkwater, "Acoustic virtual vortices with tunable orbital angular momentum for trapping of mie particles," Phys. Rev. Lett. **120**(4), 044301 (2018).
[40] T. Fushimi, A. Marzo, T. L. Hill, and B. W. Drinkwater, "Trajectory optimization of levitated particles in mid-air ultrasonic standing wave levitators," in *2018 IEEE International Ultrasonics Symposium (IUS), October 22* (IEEE, 2018), pp. 1–9.

[41] A. Marzo and B. W. Drinkwater, "Holographic acoustic tweezers," Proc. Natl. Acad. Sci. U. S. A. **116**(1), 84–89 (2019).
[42] UpnaLab, Acoustic Levitator, 2019, www.Instructables.com, available at https://www.instructables.com/id/Acoustic-Levitator/; accessed 27 June 2019.
[43] A. Marzo, T. Corkett, and B. W. Drinkwater, "Ultraino: An open phased-array system for narrowband airborne ultrasound transmission," IEEE Trans. Ultrason., Ferroelectr., Freq. Control **65**(1), 102–111 (2017).
[44] L. Cox, A. Croxford, B. W. Drinkwater, and A. Marzo, "Acoustic lock: Position and orientation trapping of non-spherical sub-wavelength particles in mid-air using a single-axis acoustic levitator," Appl. Phys. Lett. **113**(5), 054101 (2018).
[45] A. Watanabe, K. Hasegawa, and Y. Abe, "Contactless fluid manipulation in air: Droplet coalescence and active mixing by acoustic levitation," Sci. Rep. **8**(1), 10221 (2018).
[46] C. L. Shen, W. J. Xie, and B. Wei, "Parametrically excited sectorial oscillation of liquid drops floating in ultrasound," Phys. Rev. E **81**(4), 046305 (2010).
[47] M. A. Andrade, T. S. Camargo, and A. Marzo, "Automatic contactless injection, transportation, merging, and ejection of droplets with a multifocal point acoustic levitator," Rev. Sci. Instrum. **89**(12), 125105 (2018).
[48] R. H. Morris, E. R. Dye, D. A. Axford, M. I. Newton, J. Beale, and P. Docker, "Non-contact universal sample presentation for room temperature macromolecular crystallography using acoustic levitation," Scientific Reports **9**, 12431 (2019).
[49] S. Tsujino, A. Shinoda, and T. Tomizaki, "On-demand droplet loading of ultrasonic acoustic levitator and its application for protein crystallography experiments," Appl. Phys. Lett. **114**, 213702 (2019).
[50] S. Jackson, *Measurement and Simulation of an Open-Type Flexural Ultrasonic Transducer* (Acoustofluidics Forum & Olympics, Bristol, June 2019).
[51] M. A. Andrade, A. L. Bernassau, and J. C. Adamowski, "Acoustic levitation of a large solid sphere," Appl. Phys. Lett. **109**(4), 044101 (2016).
[52] Pixie Dust Technologies, Project, 2019, Pixy Dust Technologies Co., Ltd., available at https://pixiedusttech.com/project/, accessed 27 June 2019.
[53] Ultrahaptics, Ultrahaptics—Discover a new type of haptics, 2019, available at https://www.ultrahaptics.com/products-programs/stratos-explore-development-kit/; accessed 27 June 2019.
[54] K. Melde, A. G. Mark, T. Qiu, and P. Fischer, "Holograms for acoustics," Nature **537**(7621), 518 (2016).
[55] G. Memoli, M. Caleap, M. Asakawa, D. R. Sahoo, B. W. Drinkwater, and S. Subramanian, "Metamaterial bricks and quantization of meta-surfaces," Nat. Commun. **8**, 14608 (2017).